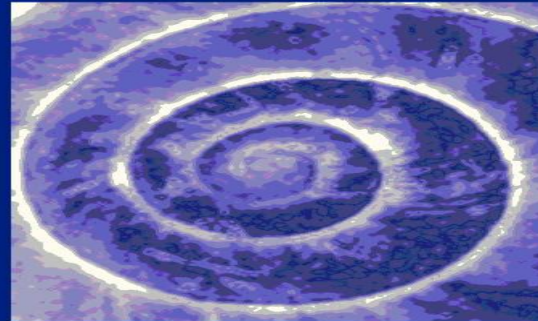


**Amplitude and phase
characteristics of
distortion product
otoacoustic emissions**



Sandra Schneider

Amplitude and phase characteristics of distortion product otoacoustic emissions Sandra Schneider

Uitnodiging

voor het bijwonen van
de openbare verdediging
van dit proefschrift

woensdag
21 januari 2004
om 14.15 uur

in de
Senaatskamer van het
Academiègebouw
Rapenburg 73
Leiden

Receptie ter plaatse na
afloop van de promotie

Wegens beperkte ruimte
is het bijwonen van de
promotie alleen mogelijk
op vertoon van een
plaatsbewijs,
aan te vragen
bij de promovenda:

Sandra Schneider
Van Exelstraat 27
3602 PE Maarssen
0346-240020
s.schneider@brokdede.nl

AMPLITUDE AND PHASE CHARACTERISTICS OF DISTORTION PRODUCT OTOACOUSTIC EMISSIONS

Cover: Marcel Peters and Bea Steenbergen

Amplitude and phase characteristics of distortion product
otoacoustic emissions / Sandra Schneider.

Thesis Universiteit Leiden. - Illustrated.

With references. - With summary in Dutch.

ISBN 90-9017534-2

NUR 927

AMPLITUDE AND PHASE CHARACTERISTICS OF DISTORTION PRODUCT OTOACOUSTIC EMISSIONS

PROEFSCHRIFT

TER VERKRIJGING VAN DE GRAAD VAN DOCTOR
AAN DE UNIVERSITEIT LEIDEN,
OP GEZAG VAN DE RECTOR MAGNIFICUS DR. D.D. BREIMER,
HOOGLEERAAR IN DE FACULTEIT DER WISKUNDE EN
NATUURWETENSCHAPPEN EN DIE DER GENEESKUNDE,
VOLGENS BESLUIT VAN HET COLLEGE VOOR PROMOTIES
TE VERDEDIGEN OP WOENSDAG 21 JANUARI 2004
TE KLOKKE 14.15 UUR

DOOR

SANDRA SCHNEIDER

GEBOREN TE TILBURG IN 1972

Promotiecommissie

Promotor:	Prof. Dr. J.J. Grote
Copromotores:	Dr. R. Schoonhoven (VU medisch centrum Amsterdam) Dr. V.F. Prijs (UMC Utrecht)
Referent:	Prof. Dr. Ir. H. Duifhuis (Rijksuniversiteit Groningen)
Overige leden:	Prof. Dr. J.W.M. Frenken Prof. Dr. D.L. Ypey

This research project was part of the NWO/ALW program ‘Biophysics of otoacoustic emissions and essential nonlinearities of the inner ear’ and was supported by the Heinsius Houbolt Fund.

Publication of this thesis was financially supported by Stichting Atze Spoor Fonds, Veenhuis Medical Audio B.V., GN ReSound bv, Beltone, and EMID.

voor Iwan en Boris

Contents

1	General introduction	11
1.1	The peripheral auditory system	12
1.1.1	Outer and middle ear	12
1.1.2	Cochlea	13
1.1.3	Organ of Corti	14
1.1.4	Outer hair cells	14
1.2	Distortion product otoacoustic emissions	16
1.2.1	Recording DPOAEs	16
1.2.2	Clinical application	18
1.2.3	DPOAE group delay	18
1.2.4	DPOAE amplitude as a function of primary frequency ratio	18
1.3	Theoretical concepts of delay measures	19
1.4	Outline	21
2	Group delays of distortion product otoacoustic emissions in the guinea pig	27
2.1	Introduction	28
2.2	Methods	29
2.2.1	Subjects	29
2.2.2	Material	30
2.2.3	DPOAE recording paradigms	30
2.2.4	Data analysis	30
2.3	Results	31
2.4	Discussion	36
2.4.1	Comparison of the two sweep paradigms for the lower sideband DPOAEs	39
2.4.2	Comparison of the two sweep paradigms for the upper sideband DPOAE $2f_2 - f_1$	40
2.4.3	Group delay differences between DPOAEs	41
2.4.4	Place- and wave-fixed DPOAE generation models	41
2.4.5	Contribution from the X_{dp} place to the generation of the $2f_1 - f_2$ DPOAE	42
2.5	Conclusions	43

3	Group delays of distortion product otoacoustic emissions: relating delays measured with f_1- and f_2-sweep paradigms	47
3.1	Introduction	48
3.2	Theory	50
3.2.1	Analysis with x_g related to X_2	53
3.2.2	Analysis for the USB DPOAEs with x_g related to X_{dp}	54
3.3	Results	55
3.4	Discussion	57
3.4.1	Assumptions and theoretical considerations	57
3.4.2	Comparison with earlier theoretical analyses of f_1 - and f_2 -sweep group delays	59
3.4.3	Validation against experimental data	59
3.5	Conclusions	60
3.6	Appendix	61
3.6.1	Frequency-shift invariance	61
3.6.2	The wave-fixed model	62
3.6.3	LSB DPOAEs with OAE coming from reflection site X_{dp}	64
4	DPOAE group delays from a nonlinear transmission line model of the cochlea	69
4.1	Introduction	70
4.2	Methods	70
4.2.1	Model description	70
4.2.2	Stimuli and data analysis	71
4.3	Results	72
4.4	Discussion	73
5	Amplitude versus frequency functions of distortion product otoacoustic emissions in the guinea pig	81
5.1	Introduction	82
5.2	Methods	83
5.3	Results	84
5.3.1	Amplitude versus frequency	84
5.3.2	Maximum amplitude	84
5.3.3	Optimum ratio	86
5.3.4	Alignment	87
5.3.5	Width of the amplitude functions	88
5.4	Discussion	90
5.4.1	Optimum ratio	90
5.4.2	Alignment	94
5.4.3	Width of the amplitude functions	94

5.4.4	Second filter	95
5.5	Conclusions	95
6	Amplitude and phase of distortion product otoacoustic emissions in the guinea pig in an (f_1, f_2) area study	101
6.1	Introduction	102
6.2	Theory	104
6.2.1	Distortion component	106
6.2.2	Reflection component	106
6.3	Methods	107
6.3.1	Animal care and preparation	107
6.3.2	Material	107
6.3.3	DPOAE recording paradigms	108
6.3.4	Data analysis	109
6.4	Results	110
6.4.1	Incidence of the different DPOAE orders	110
6.4.2	Amplitude and phase characteristics in the (f_1, f_2) plane	110
6.4.3	Group delays	114
6.4.4	Fine structure	116
6.5	Discussion	116
6.5.1	Incidence of the different DPOAE orders	116
6.5.2	Amplitude and phase characteristics in the (f_1, f_2) plane	118
6.5.3	Group delays	119
6.5.4	Fine structure	121
	Summary	127
	Samenvatting	131
	Curriculum Vitae	137
	Publications	139

Chapter 1

General introduction

Abstract

Apart from receiving and transducing sound, the ear is also capable of emitting weak sounds. Produced inside the inner ear as a by-product of the normal hearing process and detectable in the outer ear canal with a sensitive microphone, these sounds are called otoacoustic emissions (OAEs). Among several types of OAEs, distortion product otoacoustic emissions (DPOAEs) are the ones that are generated due to nonlinear properties of the inner ear upon stimulation with two pure tones of slightly different frequency. DPOAEs only arise in a healthy cochlea and can therefore be used as an objective clinical tool to assess the integrity of the inner ear. The aim of the research project, the results of which are presented in this thesis, was to increase the knowledge of the peripheral auditory mechanisms involved in the generation of DPOAEs. The amplitude and phase behavior of DPOAEs was studied both experimentally, in the guinea pig ear canal, and theoretically. Properties of the DPOAEs like their group delay, the place where they are generated, and the dependence of their amplitude on stimulus frequency ratio were studied. In this introductory chapter background information on the peripheral auditory system, cochlear mechanics, distortion product otoacoustic emissions, and group delay is provided. The chapter is concluded with an outline of the further content of this thesis.

1.1 The peripheral auditory system

The mammalian hearing system shows extreme sensitivity and frequency selectivity. For instance, normal hearing humans are able to detect a 1 kHz tone at a sound pressure of $20 \mu\text{Pa}$ (0 dB SPL), which is only $2 \cdot 10^{-10}$ times the normal air pressure. Equally amazing is the fact that they can discriminate between two tones having frequencies that differ by only 0.1%. Before an acoustic signal can be perceived, it needs to be transduced into an electrical signal and transmitted to the central nervous system. This is done by the peripheral auditory system comprising the outer, middle, and inner ear (figure 1.1). Obviously, the sensitivity and selectivity of the system require highly specialized structures.

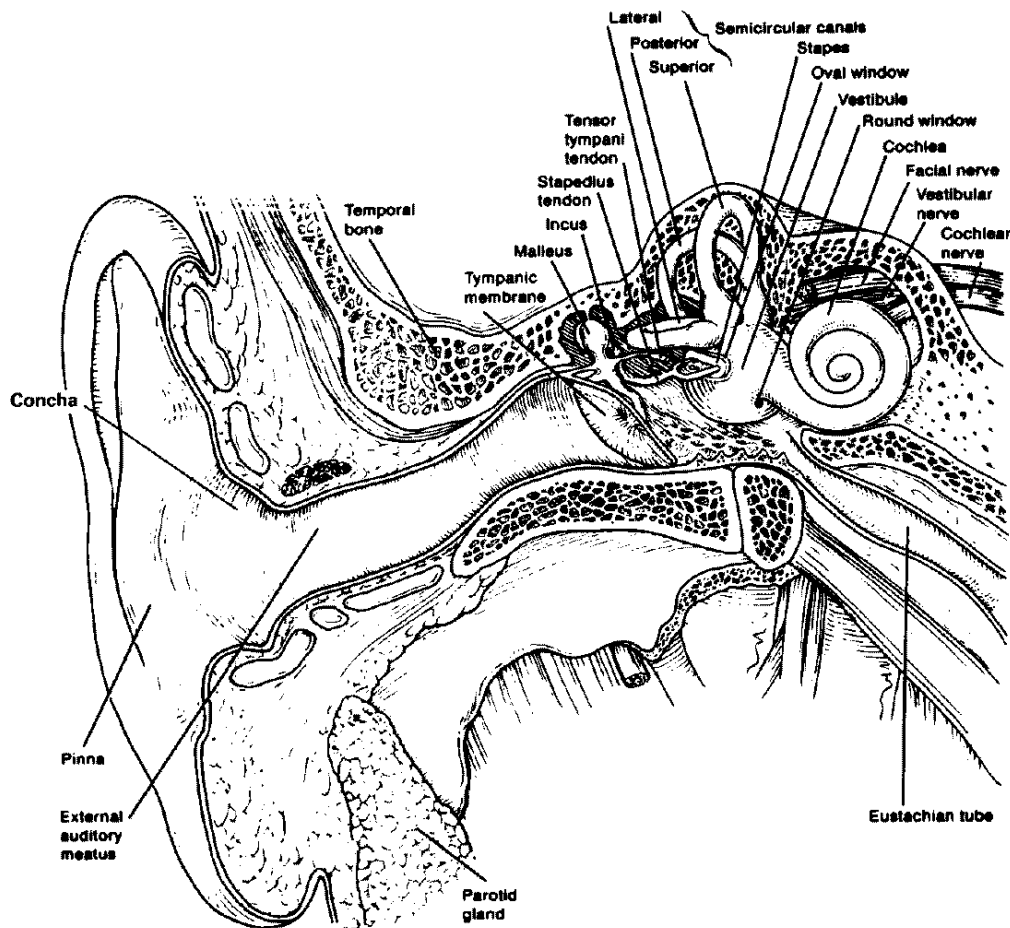


Figure 1.1: The peripheral auditory system (from Kessel and Kardon, 1979).

1.1.1 Outer and middle ear

Together the outer and middle ear form the conductive part of the peripheral auditory system. They transfer sound waves from outside to the fluid filled inner ear. Upon entering

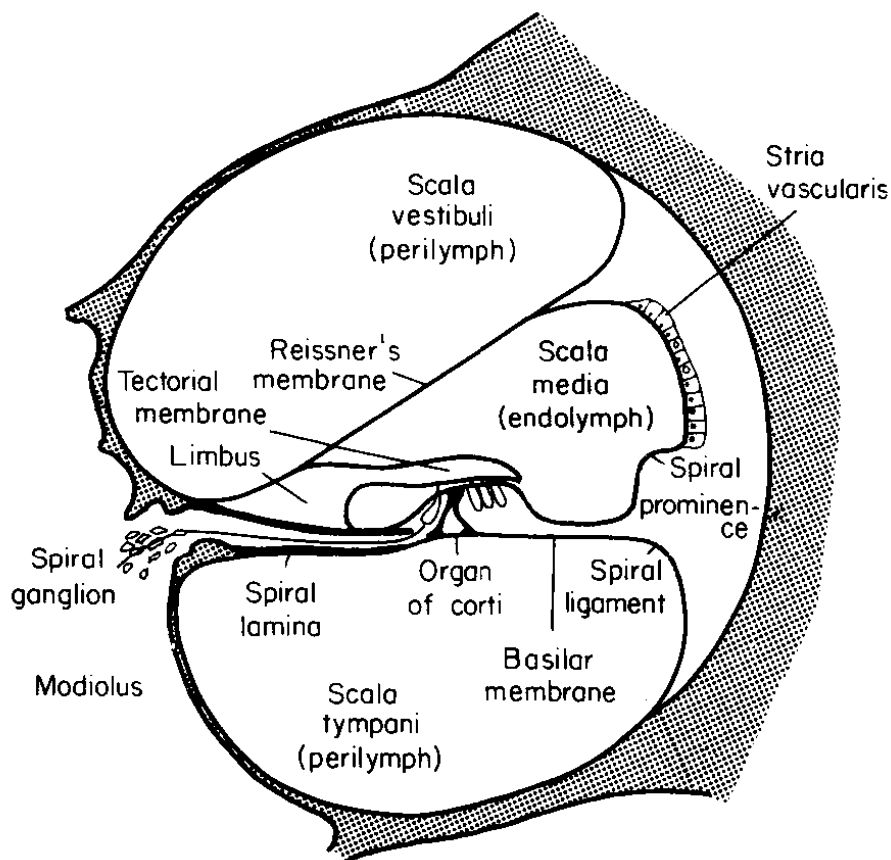


Figure 1.2: Cross-section of one cochlear duct (from Pickles, 1988).

the ear canal, sound waves cause the tympanic membrane to vibrate, at hearing threshold with an amplitude at only atomic scale. These vibrations are passed to the inner ear by the chain of three middle ear ossicles (malleus, incus, and stapes). The malleus is attached to the tympanic membrane, and the footplate of the stapes rests at the oval window, closing the fluid filled inner ear. A substantial acoustical energy loss is expected from the impedance difference between air and inner ear, but this is compensated by the lever function of the middle ear ossicles and the area ratio of tympanic membrane and oval window (Pickles, 1988).

1.1.2 Cochlea

The inner ear, a series of connected fluid filled canals in the temporal bone, has a vestibular part and an auditory part, the cochlea (figure 1.2). The latter is the sensory part of the peripheral auditory system, where the conversion of mechanical energy into electrical energy takes place. The electrical signals, coding the sound, are transferred to the brain by the auditory nerve. Figure 1.2 shows a schematic cross-section of the cochlea, a coiled tube with the shape of a snail shell. Two membranes running along the length

of the cochlea divide it into three compartments: scala vestibuli, scala media, and scala tympani. At the apex of the cochlea the two outer scalae are joined by an opening (the helicotrema). The scala media is filled with endolymph while the other two scalae contain perilymph with a different ionic composition. The very thin and acoustically transparent Reissner's membrane separates scala vestibuli from scala media. Its only known function is to keep the fluids in the scalae apart. Between scala media and scala tympani lies the basilar membrane, which has a much more complicated function than Reissner's membrane. Movement of the stapes footplate causes the oval window to vibrate and induces pressure changes in the cochlear fluids. Upon sinusoidal stimulation, the pressure differences above and below the basilar membrane result in a movement of the basilar membrane, which can be described as a traveling wave propagating from the base of the cochlea towards the apex. The propagation velocity of the traveling wave decreases and its amplitude increases until a point of maximum excitation is reached. The location of this point in the cochlea is called the characteristic place and depends on the frequency of the stimulus tone. High frequencies reach their maximum at a point close to the base of the cochlea while lower frequencies peak at a more apical location. The place-frequency map has a logarithmical distribution, implying that the distance between characteristic places is fixed for constant frequency ratio. Responsible for the place-dependent resonance frequency in the cochlea are the mechanical properties of the basilar membrane that vary systematically along the length of the cochlea, in particular its stiffness and damping.

1.1.3 Organ of Corti

On top of the basilar membrane lies the organ of Corti, the structure containing the sensory cells involved in the mechano-electrical transduction process (figure 1.3). There are two types of sensory cells in the organ of Corti, inner hair cells (IHCs) and outer hair cells (OHCs). The latter outnumber the former by a factor of three. The stereocilia (hairs) located on top of the IHCs and OHCs are covered by the tectorial membrane. Movement of the basilar membrane and the structures attached to it (together called the cochlear partition) causes a shear movement of the tectorial membrane relative to the organ of Corti, deflecting the stereocilia. Ion channels in the hair cells open upon deflection of the stereocilia, resulting in a change in the cell's potential. Inner hair cells, mostly innervated by afferent nerve fibers, subsequently generate action potentials in the afferent fibers, carrying the acoustical information to the brain.

1.1.4 Outer hair cells

Outer hair cells are mostly contacted by efferent nerve fibers, originating from the auditory brainstem, so they must have a completely different function than the inner hair cells. In 1985, Brownell *et al.* reported the first evidence of the role of outer hair cells as small motors. They found that isolated OHCs showed reversible length changes in response to electrical stimulation, a process called electromotility. The same effect was found for acoustical stimulation (Canlon *et al.*, 1988). Later Brundin *et al.* (1989) reported that

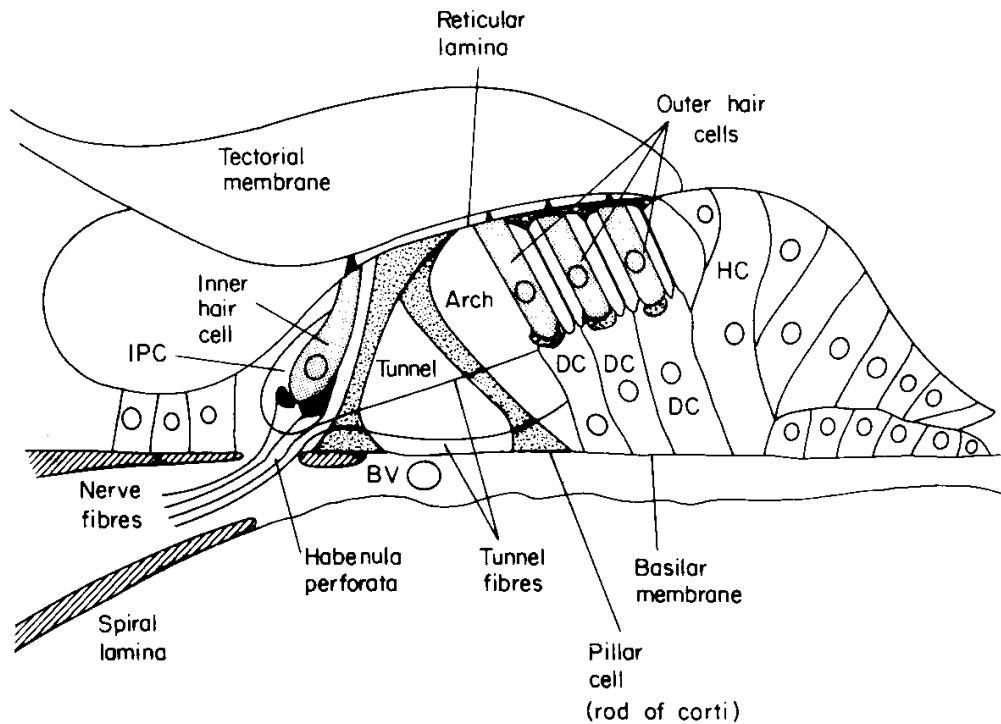


Figure 1.3: Cross-section of the organ of Corti (from Pickles, 1988).

the response of the OHCs to acoustical stimulation was highly frequency dependent. Short OHCs from the base of the cochlea responded best to high frequencies while long OHCs from the apical region were most sensitive to low frequencies. The outer hair cells thus act as tiny motors, locally altering the micromechanics and influencing the movement of the basilar membrane. From a number of theoretical and experimental considerations it is concluded that, at low stimulus levels and for frequencies near the characteristic frequency, the outer hair cells in fact enhance the vibration of the basilar membrane, and thus act as what has been called the cochlear amplifier (Davis, 1983). Thus, with the function of the outer hair cells intact, the cochlea is an active system, adding energy to the passively conducted acoustic energy to enhance the sensitivity and frequency selectivity (Dallos, 1992). This explains the inconsistency of von Békésy's traveling wave experiments in dead cochleae (von Békésy, 1960) with the extreme sensitivity and frequency selectivity in live cochleae (Kemp, 1997). Activity in the cochlea was already predicted in 1948 by Gold four decades before the discovery of electromotility in the OHCs, the basis of the active feedback system. He tried to convince auditory physiologists of his idea that the live cochlea must have a mechanism for energy loss reduction or undamping. Gold also predicted that some ears would be able to emit sounds. A period of 30 years passed by before he was proven right.

1.2 Distortion product otoacoustic emissions

In the late 1970s Kemp showed that ears could produce sounds that were detectable in the outer ear canal, both spontaneously and upon stimulation (Kemp, 1978; Kemp, 1979). These sounds were termed *otoacoustic emissions* after the Greek word *oto* for ear (OAEs, for a review see Probst *et al.*, 1991). One type of OAE is the distortion product otoacoustic emission (DPOAE), which is generated in a healthy cochlea upon stimulation with two tones at frequencies f_1 and f_2 ($f_1 < f_2$). Other than in the ear canal, distortion products have also been detected psychophysically and in neural recordings (e.g. Smoorenburg, 1972; Smoorenburg *et al.*, 1976; Wilson, 1980). The active mechanism, originating in the outer hair cell motility, is nonlinear. It is a frequency selective mechanism which only acts near the characteristic place of each frequency component present in the cochlea. The amplitude of the basilar membrane excitation saturates instead of increasing linearly with stimulus level as would be expected for a passive system (Nobili *et al.*, 1998). This compressive nonlinearity does not only occur at high sound levels, but also at low stimulus levels. It is therefore called an essential nonlinearity (Goldstein, 1967). The nonlinearity results in the generation of frequency components that are not present in the stimulus. The form of the nonlinearity is such that distortion products with frequencies $f_{dp} = a \cdot f_1 + b \cdot f_2$ arise, with a, b integers. Odd order components of the form $f_{dp} = (n + 1) \cdot f_1 - n \cdot f_2$ are most common. The order of the distortion product is defined as $2n + 1$. There are distortion products with a frequency smaller than the primaries ($n \geq 1$), called lower sideband or apical DPOAEs, and distortion products with frequencies higher than the primaries ($n \leq -2$), called upper sideband or basal DPOAEs. The terms apical and basal refer to the location of the characteristic place of the distortion product itself with respect to the characteristic places of the stimuli. The lower sideband DPOAEs are generated in the overlap region of the excitation pattern of the two stimulus tones f_1 and f_2 , more specific primarily at X_2 , the characteristic place of f_2 (e.g. Kim *et al.*, 1980). There is evidence from several studies that the distortion product reaches its own characteristic place X_{dp} apically from the generation region (Smoorenburg *et al.*, 1976; Kim *et al.*, 1980; Robles *et al.*, 1991), and that there is a contribution from this place to the DPOAE in the ear canal (Kummer *et al.*, 1995; Brown *et al.*, 1996; Heitmann *et al.*, 1998). In figure 1.4 a schematic of the generation of lower sideband DPOAEs inside the cochlea is given. The upper sideband distortion products are thought to be generated in the region basally from the characteristic places of the stimulus frequencies, with the largest contribution to the DPOAE in the ear canal probably coming from a place close to their own characteristic place (Martin *et al.*, 1987).

1.2.1 Recording DPOAEs

The basic components of a modern DPOAE measurement system are two loudspeakers to produce the stimulus tones, a microphone to record the sounds in the ear canal, and a digital signal processing board in a computer. The microphone is housed in a probe assembly, which must be sealed tightly into the ear canal. To reduce artificial distortion products the loudspeakers are usually located outside the probe and the stimulus tones are

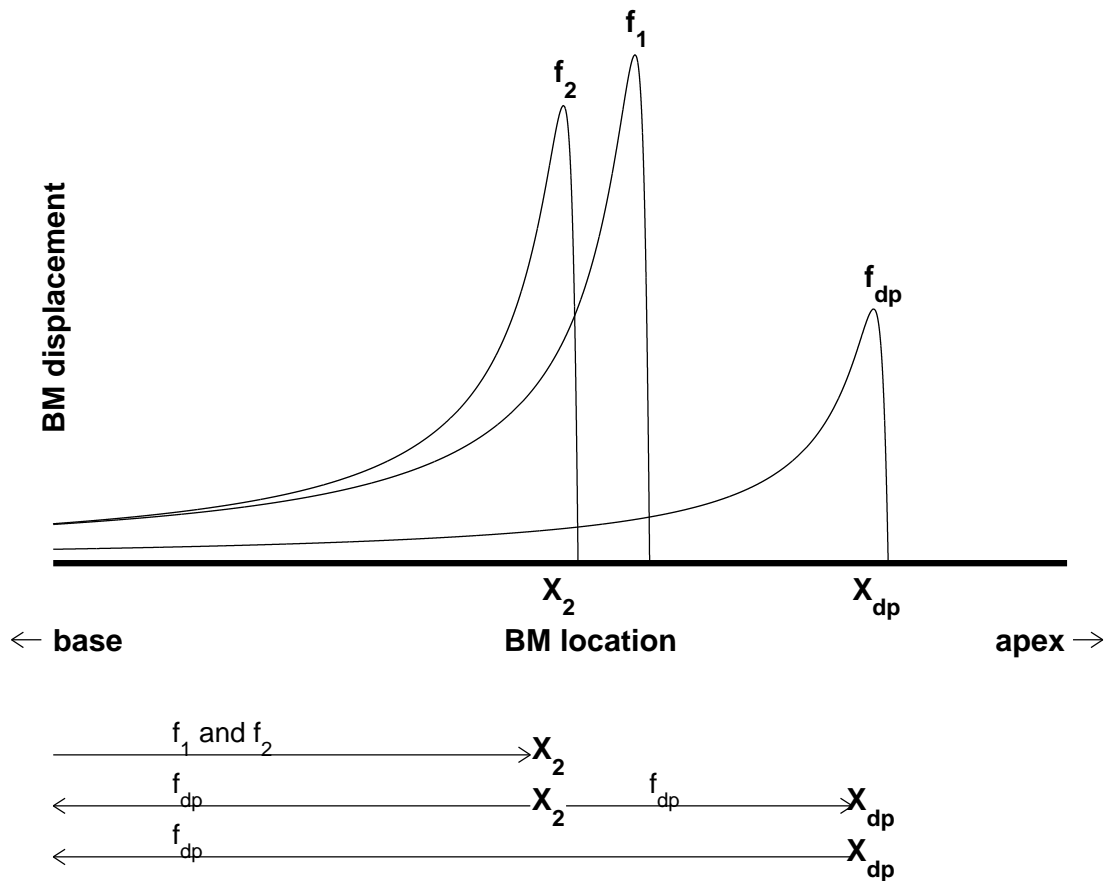


Figure 1.4: Schematic of lower sideband DPOAE generation. The maximum basilar membrane displacement for tones with frequencies f_1 , f_2 and f_{dp} is drawn. In the region of maximal interaction of f_1 and f_2 on the basilar membrane (around X_2) the distortion product is generated. It propagates both basally and apically to its characteristic place X_{dp} . From there, another DP component runs basally, contributing to the DPOAE in the ear canal.

delivered separately to the ear canal by tubes passing through the probe. The stimulus tones are digitally synthesized, converted to analog signals, and fed to the loudspeakers which deliver them as acoustical signals to the ear canal. While the stimulus tones are presented continuously, the cochlea generates distortion products. The microphone records the acoustical signal inside the ear canal, which contains the stimulus frequencies and the DPOAEs. The microphone signal is amplified, converted to a digital signal and processed further by the computer. The frequency components present in the ear canal are separated into their amplitude and phase components by Fourier analysis.

1.2.2 Clinical application

Since distortion product generation is based on normal functioning of outer hair cells, DPOAE amplitudes of patients with a cochlear hearing deficit are generally lower than those of normal hearing subjects, which makes the DPOAE a valuable clinical tool (Gorga *et al.*, 2002). DPOAEs are mostly used for screening. Generally, DPOAEs are only present when the hearing threshold is better than approximately 30 dB HL. So, with a DPOAE measurement the presence or absence of a hearing loss larger than 30 dB HL can be predicted, but the severity of the loss or the changes cannot be detected reliably. One advantage of a DPOAE measurement over a classical hearing test, like the pure-tone audiogram, is its objectiveness. Therefore it is also useful for patients incapable of giving a reliable response like neonates, infants, and mentally disabled. With DPOAEs only the functioning of the peripheral auditory system is tested. Of course it is the entire system including the neural processing that determines how well a subject can hear, but most hearing deficits have a cochlear origin and can be detected with a DPOAE test. An advantage of DPOAEs over click-evoked otoacoustic emissions is the frequency selectivity of the measurement. The primary frequencies f_1 and f_2 can be chosen in the frequency region of interest. The question is, however, whether the presence or absence of a DPOAE with frequency f_{dp} gives information about the cochlear area which is sensitive to f_1 , f_2 , f_{dp} or even some other frequency region.

1.2.3 DPOAE group delay

For the understanding of cochlear mechanics and for the interpretation of clinical DPOAE data it is necessary to know which cochlear regions are most involved in the generation process of the DPOAEs. Since due to the traveling wave there is a close relation between cochlear place and response delay, one way of studying generation places is to estimate cochlear delays. This is usually done with the phase-gradient method (Kimberley *et al.*, 1993; O'Mahoney and Kemp, 1995) in which the DPOAE frequency is slightly changed in successive measurements, either with fixed f_2 (the f_1 -sweep paradigm) or with fixed f_1 (the f_2 -sweep paradigm). This results in a DPOAE phase versus frequency curve, which is approximately linear for small frequency changes. The slope of this curve, often called group delay, is used as an estimate of the traveling wave delay of the stimulus tones to the generation place plus the traveling wave delay of the DP component traveling from generation place back to the ear canal. The interpretation of group delays is detailed in section 1.3. There appears to be a difference between group delays measured with the f_1 -sweep paradigm and group delays measured with the f_2 -sweep paradigm (O'Mahoney and Kemp, 1995). At the beginning of this research project, that difference was not well understood. This issue is dealt with in chapters 2 and 3.

1.2.4 DPOAE amplitude as a function of primary frequency ratio

The amplitude of DPOAEs depends on a number of factors, one of which is the frequency ratio f_2/f_1 . Measuring the amplitude as a function of frequency ratio results in a bandpass

structure (e.g. Wilson, 1980). For the $2f_1 - f_2$ distortion product measured in humans, the maximum amplitude is elicited by a frequency ratio of approximately 1.22 (Harris *et al.*, 1989). It is found that the optimum ratio is smaller for higher order DPOAEs. The amplitude functions of lower sideband DPOAEs like $2f_1 - f_2$ and $3f_1 - 2f_2$ peak at the same DPOAE frequency when measured with fixed f_2 and varying f_1 (Fahey and Allen, 1986; Brown and Gaskill, 1990a). The decrease of amplitude with increasing ratio f_2/f_1 is not only found in DPOAE recordings, but also in neural and psychophysical distortion product measurements. It can be explained by the decreasing overlap of the excitation patterns of the stimulus frequencies f_1 and f_2 . The amplitude decrease for decreasing frequency ratio (f_1 and f_2 closer) is harder to explain. This decrease in amplitude is only found in DPOAE recordings, not in psychophysical and neural distortion product measurements (Goldstein, 1967; Smoorenburg *et al.*, 1976; Wilson, 1980). Together with the fact that the DPOAEs peak at the same frequency independent of order, this has led Brown and Gaskill (1990a) and Allen and Fahey (1993) to the assumption that there is a filter mechanism at the characteristic place of f_2 in the cochlea (the so-called "second filter"). In models of cochlear mechanics, however, no additional filter mechanism is needed to produce a bandpass structure (e.g. Matthews and Molnar, 1986).

1.3 Theoretical concepts of delay measures

Throughout this thesis the concept of phase slope delay plays an important role. Therefore, the theoretical framework of this delay measure is given here. The DPOAE phase slope delay, resulting from f_1 - or f_2 -sweep measurements, is defined as

$$\tau_\varphi \equiv -\frac{d\varphi_{\text{dp}}}{d\omega_{\text{dp}}}, \quad (1.1)$$

with φ_{dp} the DPOAE phase and ω_{dp} the DPOAE angular frequency. This delay is often used as an estimate of the traveling wave delay of the stimulus tones to the generation place plus the traveling wave delay of the DP component traveling from generation place back to the ear canal. Forward traveling wave delay, previously measured both psychoacoustically and electrophysiologically (e.g. Anderson *et al.*, 1971), is of considerable interest to the field of cochlear mechanics. With the DPOAE technique to estimate traveling wave delay only the cochlea is involved, which eliminates neural or synaptic delays that need to be subtracted from the other delay measures. However, with DPOAEs an estimate of a roundtrip delay is made, which cannot be simply divided by two to yield the forward delay. In addition, there are other reasons why we should be careful interpreting the DPOAE phase slope delays as true time delays and relating them to the other measures of cochlear delay. The DPOAE phase slope delay depends for instance on the sweep paradigm, and can even be negative under certain experimental conditions. The DPOAE phase is not only based on pure time delays, but also on the behavior of the generation place during the sweep paradigm and on interference in the cochlea. The phase slope delay is often termed "group delay", while other investigators prefer not to use that term and speak of for instance "DPOAE latency", "phase gradient latency", or "roundtrip delay". The

mathematical background of these issues is given below (Talmadge, 1999; Lighthill, 1978).

In the cochlea, as in many other media, waves of low frequency travel faster than waves of high frequency. This phenomenon is called dispersion; a variation of wave velocity with frequency. Fortunately, sound waves in air are approximately nondispersive, so that waves of different frequency all take the same time to travel a distance x . The relation between frequency ω ($2\pi f$) and wavenumber k ($2\pi/\lambda$) is called the dispersion relation. The phase velocity is defined as

$$v_{\text{phase}} = \omega/k, \quad (1.2)$$

this is the velocity at which the crest of a wave moves along. The group velocity is the velocity of the wave envelope, the center of energy of the wave package. It is defined as

$$v_{\text{group}} = \partial\omega/\partial k. \quad (1.3)$$

When a wave package, consisting of several frequency components, travels in a nondispersive medium, the phase velocity and the group velocity are equal. However, in a dispersive medium they differ. Each individual wave crest moves at a different (phase) velocity, and the group velocity is dominated by the frequency component having the largest amplitude. Due to the different speeds of the individual frequency components in the wave package, the form of the wave envelope changes as time prolongs. The time delay of a wave, traveling a distance x at a constant speed v (in a nondispersive medium) is $t(x) = x/v$, independent of frequency. In a dispersive medium, where velocity depends on frequency, the time delay is $t(x; \omega) = x/v(\omega)$. In the cochlea, velocity not only depends on frequency, but also on place x . Then, the time delay of the wave envelope (group delay) propagating from place 0 to x is defined as

$$t(x; \omega) = \int_0^x \frac{dx'}{v(x'; \omega)}. \quad (1.4)$$

With the group velocity being $v(x; \omega) = \partial\omega/\partial k$, this results in

$$t(x; \omega) = \int_0^x \frac{\partial k(x'; \omega)}{\partial \omega} dx'. \quad (1.5)$$

This is a true time delay, of a wave package with center frequency ω traveling from 0 to x .

The negative slope of the phase versus frequency relation, often called “group delay” can be written as

$$\tau_\varphi(x; \omega) = -\frac{d\varphi(x; \omega)}{d\omega}, \quad (1.6)$$

with the accumulated phase lag of the traveling wave being

$$\varphi(x; \omega) = -\int_0^x k(x'; \omega) dx'. \quad (1.7)$$

For a fixed place x , combining equations 1.6 and 1.7 gives

$$\tau_\varphi(x; \omega) = \int_0^x \frac{\partial k(x'; \omega)}{\partial \omega} dx', \quad (1.8)$$

which equals the real group delay as defined by equation 1.5. In DPOAE phase slope delay measurements, especially with f_2 -sweep, the place x (generation place) is changed when the frequency ω is changed. In addition to the mathematical group delay, the phase-frequency derivative, a second component which is a phase-place derivative is introduced. The phase-slope delay that is measured is

$$\tau_\varphi(x; \omega) = -\frac{d\varphi(x; \omega)}{d\omega} \equiv -\frac{\partial\varphi(x; \omega)}{\partial\omega} - \frac{\partial\varphi(x; \omega)}{\partial x} \cdot \frac{dx}{d\omega}, \quad (1.9)$$

of which only the first term equals the mathematical group delay. In the scaling-invariant cochlea (see chapter 3), the phase of a frequency component ω at its characteristic place $X(\omega)$ is constant with frequency, so

$$\tau_\varphi(X; \omega) = -\frac{d\varphi(X; \omega)}{d\omega} = 0. \quad (1.10)$$

In this case, the phase slope delay would be zero which is definitely not the same as the real travel time (group delay) of a frequency component to its characteristic place. Another thing to keep in mind with DPOAE group delays is that there can be more than one component with frequency ω_{dp} in the cochlea, so the phase of the distortion product in the cochlea is the result of interference of these components. This also obscures the phase slope delay and makes it harder to interpret it as a true time delay. Although the interpretation of phase slope delays is not straightforward, they can be informative about some essential properties of DPOAEs if all the above mentioned aspects are taken into account. In fact, by studying the phase slope delays of different DPOAE components and different sweep paradigms, we can even learn about the behavior of generation sites (see chapter 3). In the following chapters, the phase slope delays are termed group delay in accordance with other studies, although this term is not theoretically correct under all experimental conditions.

1.4 Outline

In chapter 2 experimental results of group delays of DPOAEs measured in the guinea pig are presented. Two different methods, f_1 - and f_2 -sweep, were used to measure the phase of the distortion products $2f_1 - f_2$, $3f_1 - 2f_2$, $4f_1 - 3f_2$, and $2f_2 - f_1$ as a function of DPOAE frequency, yielding the associated group delays. It was already known from the literature that the two methods give different group delays. However, proper understanding of this phenomenon was lacking. By measuring the delays of several DPOAE orders with the two methods in the same subjects, we could make an adequate comparison. The results of this study together with the place- and wave-fixed description of DPOAE generation were the basis for the theoretical analysis relating f_1 - and f_2 -sweep group delays as presented in chapter 3. The shifting of the assumed generation place X_2 with f_2 -sweep in the wave-fixed model was incorporated by using a local approximation of the scaling symmetry of the cochlea. This resulted in a simple analytical expression for the relation between f_1 - and f_2 -sweep group delays which could be compared directly with the experimental results. The research project described in this thesis was part of a collaboration with the

Department of Biophysics of the University of Groningen. At this department a previously developed one-dimensional model of the cochlea was used to simulate guinea pig group delays. The results of the simulations are compared with the experimental group delay data in chapter 4. In chapter 5 several properties concerning the amplitude of DPOAEs measured in the guinea pig are described. The amplitude versus frequency functions of the lower sideband DPOAEs show a bandpass shape. The primary frequency ratio yielding the maximum DPOAE amplitude is measured, which shows a pattern as a function of f_2 different from that known in humans and several other species. The width of the amplitude versus frequency functions is studied as well as the alignment of the maxima of three different lower sideband DPOAEs. Differences in these features between DPOAE order and between the two sweep paradigms showed that the DPOAE amplitude is best described as a function of f_{dp}/f_2 . Chapter 6 reports on a detailed (f_1, f_2) area study in the guinea pig. At many combinations of f_1 and f_2 , within the ranges $f_2 = 7 - 9$ kHz and $f_2/f_1 = 1.01 - 1.50$, the amplitude and phase of several distortion products were measured. Phase-frequency slopes in the directions of constant f_1 , constant f_2 , and constant f_2/f_1 could be calculated for all (f_1, f_2) combinations, representing the f_2 -sweep group delay, f_1 -sweep group delay, and constant f_2/f_1 -sweep group delay. Comparing these experimental delay values with the predictions from the place- and wave-fixed theories, we were able to determine at which frequency ratios (distance between the stimulus tone characteristic places) the phase behavior of the DPOAE was wave-fixed, indicating that the DPOAE component arising directly from the generation region near X_2 was dominant.

References

- Allen, J. B., and Fahey, P. F. (1993). “A second cochlear-frequency map that correlates distortion product and neural tuning measurements,” *J. Acoust. Soc. Am.* **94**, 809–816.
- Anderson, D. J., Rose, J. E., Hind, J. E., and Brugge, J. F. (1971). “Temporal position of discharges in single auditory nerve fibers within the cycle of a sine-wave stimulus: frequency and intensity effects,” *J. Acoust. Soc. Am.* **49**, 1131–1139.
- Békésy, G. von (1960). *Experiments in Hearing* (McGraw-Hill, New-York).
- Brown, A. M., and Gaskill, S. A. (1990a). “Can basilar membrane tuning be inferred from distortion product measurement?” in *The mechanics and biophysics of hearing*, edited by P. Dallos, C. D. Geisler, J. W. Matthews, M. A. Ruggero, and C. R. Steele (Springer-Verlag, New York), pp. 164–169.
- Brown, A. M., Harris, F. P., and Beveridge, H. A. (1996). “Two sources of acoustic distortion products from the human cochlea,” *J. Acoust. Soc. Am.* **100**, 3260–3267.
- Brownell, W. E., Bader, C. R., Bertran, D., and de Ribaupierre, Y. (1985). “Evoked mechanical responses of isolated cochlear hair cells,” *Science* **227**, 194–196.
- Brundin, L., Flock, A., and Canlon, B. (1989). “Sound-induced motility of isolated cochlear outer hair cells is frequency specific,” *Nature* **342**, 814–816.
- Dallos, P. (1992). “The active cochlea,” *J. Neurosci.* **12**, 4575–4585.
- Davis, H. (1983). “An active process in cochlear mechanics,” *Hear. Res.* **9**, 79–90.
- Fahey, P. F. and Allen, J. B. (1986). “Characterization of cubic intermodulation distortion products in the cat external auditory meatus,” in *Peripheral Auditory Mechanisms*, edited by J. B. Allen, J. L. Hall, A. E. Hubbard, S. T. Neely, and A. Tubis (Springer-Verlag, Berlin) pp. 314–321.
- Gold, T. (1948). “Hearing II: The physical basis of the action of the cochlea,” *Proceedings of the Royal Society of London, Series B: Biological Sciences* **135**, 492–498.
- Goldstein, J. L. (1967). “Auditory nonlinearity,” *J. Acoust. Soc. Am.* **41**, 676–689.
- Gorga, M. P., Neely, S. T., and Dorn, P. A. (2002). “Distortion product otoacoustic emissions in relation to hearing loss,” in *Otoacoustic Emissions - Clinical Applications*, 2nd ed., edited by R. M. Robinette and T. Glatcke (Thieme, New York) pp. 243–272.

- Harris, F. P., Lonsbury-Martin, B. L., Stagner, B. B., Coats, A. C., and Martin, G. K. (1989). "Acoustic distortion products in humans: Systematic changes in amplitude as a function of f_2/f_1 ratio," J. Acoust. Soc. Am. **85**, 220–229.
- Heitmann, J., Waldmann, B., Schnitzler, H.-U., Plinkert, P. K., and Zenner, H.-P. (1998). "Suppression of distortion product otoacoustic emissions (DPOAE) near $2f_1 - f_2$ removes DP-gram fine structure -Evidence for a secondary generator," J. Acoust. Soc. Am. **103**, 1527–1531.
- Kemp, D. T. (1978). "Stimulated acoustic emissions from within the human auditory system," J. Acoust. Soc. Am. **64**, 1386–1391.
- Kemp, D. T. (1979). "Evidence of mechanical nonlinearity and frequency selective wave amplification in the cochlea," Archives of Otorhinolaryngology **224**, 37–45.
- Kemp, D. T. (1997). "Otoacoustic emissions in perspective," in *Otoacoustic emissions, Clinical applications*, edited by M. S. Robinette and T. J. Glatcke (Thieme, New York), pp. 1–21.
- Kessel, R. G. and Kardon, R. H. (1979). *Tissues and organs: A Text-Atlas of Scanning Electron Microscopy* (W. H. Freeman and Company, San Francisco).
- Kim, D. O., Molnar, C. E., and Matthews, J. W. (1980). "Cochlear mechanics: Nonlinear behavior in two-tone responses as reflected in cochlear-nerve-fiber responses and in ear-canal sound pressure," J. Acoust. Soc. Am. **67**, 1704–1721.
- Kimberley, B. P., Brown, D. K., and Eggermont, J. J. (1993). "Measuring human cochlear traveling wave delay using distortion product otoacoustic emission phase responses," J. Acoust. Soc. Am. **94**, 1343–1350.
- Kummer, P., Janssen, T., and Arnold, W. (1995). "Suppression tuning characteristics of the $2f_1 - f_2$ distortion product otoacoustic emission in humans," J. Acoust. Soc. Am. **98**, 197–210.
- Lighthill, J. (1978). *Waves in fluids* (Cambridge University Press).
- Martin, G. K., Lonsbury-Martin, B. L., Probst, R., Scheinin, S. A., and Coats, A. C. (1987). "Acoustic distortion products in rabbit ear canal. II. Sites of origin revealed by suppression contours and pure-tone exposures," Hearing Res. **28**, 191–208.
- Matthews, J. W., and Molnar, C. E. (1986). "Modeling intracochlear and ear canal distortion product ($2f_1 - f_2$)," in *Peripheral auditory mechanisms*, edited by J. B. Allen, J. L. Hall, A. E. Hubbard, S. T. Neely, and A. Tubis (Springer-Verlag, Berlin), pp. 258–265.
- Nobili, R., Mammano, F., and Ashmore, J. (1998). "How well do we understand the cochlea," TINS **21**, 159–167.

- O'Mahoney, C. F., and Kemp, D. T. (1995). "Distortion product otoacoustic emission delay measurement in human ears," *J. Acoust. Soc. Am.* **97**, 3721–3735.
- Pickles, J. O. (1988). *An introduction to the physiology of hearing* (Academic Press, London).
- Probst, R., Lonsbury-Martin, B. L., and Martin, G. K. (1991). "A review of otoacoustic emissions," *J. Acoust. Soc. Am.* **89**, 2027–2067.
- Robles, L., Ruggero, M. A., and Rich, N. C. (1991). "Two-tone distortion in the basilar membrane of the cochlea," *Nature (London)* **349**, 413–414.
- Smooenburg, G. F. (1972). "Combination tones and their origin," *J. Acoust. Soc. Am.* **52**, 615–631.
- Smooenburg, G. F., Morton Gibson, M., Kitzes, L. M., Rose, J. E., and Hind, J. E. (1976). "Correlates of combination tones observed in the response of neurons in the anteroventral cochlear nucleus of the cat," *J. Acoust. Soc. Am.* **59**, 945–962.
- Talmadge, C. L. (1999). "Some notes on group delay," personal communication.
- Wilson, J. P. (1980). "The combination tone, $2f_1 - f_2$, in psychophysics and ear-canal recording," in *Psychophysical, physiological, and behavioral studies in hearing*, edited by G. van den Brink, and F. A. Bilsen (Delft U.P., Delft, The Netherlands), pp. 43–50.

Chapter 2

Group delays of distortion product otoacoustic emissions in the guinea pig

Abstract

This chapter presents a comprehensive set of experimental data on group delays of distortion product otoacoustic emissions (DPOAEs) in the guinea pig. Group delays of the DPOAEs with frequencies $2f_1 - f_2$, $3f_1 - 2f_2$, $4f_1 - 3f_2$ and $2f_2 - f_1$ were measured with the phase-gradient method. Both the f_1 - and the f_2 -sweep paradigms were used. Differences between the two sweep paradigms were investigated for the four DPOAEs, as well as the group delay differences between the DPOAEs. Analysis revealed larger group delays with the f_2 -sweep paradigm, but only for the lower sideband DPOAEs (with $f_{dp} < f_1, f_2$). For the lower sideband cubic distortion product $2f_1 - f_2$, the f_2 -sweep delays were a factor of 1.17 - 1.54 larger than the f_1 -sweep delays, depending on frequency. The upper sideband DPOAE $2f_2 - f_1$ showed no significant difference between f_1 - and f_2 -sweep group delays, except for the highest and lowest f_2 frequencies. Comparing the group delays of the DPOAEs for each sweep paradigm separately, equal group delays were found for all four DPOAEs measured with the f_1 -sweep. With the f_2 -sweep paradigm on the other hand, the group delays of the three lower sideband DPOAEs occurred to be larger than the group delays of the upper sideband DPOAE $2f_2 - f_1$. A tentative interpretation of the data in the context of proposed explanatory hypotheses on DPOAE group delays is given.

2.1 Introduction

Distortion product otoacoustic emissions (DPOAEs) are a product of nonlinear processes in the inner ear and form an important tool to study cochlear mechanics. Upon stimulating the ear with two pure tones of slightly different frequency f_1 and f_2 (the primaries), combination tones are generated in the cochlea with frequencies $f_{dp} = mf_1 + nf_2$ (given that $f_1 < f_2$ and m, n integers). Only the strongest combination tones are measurable in the outer ear canal as DPOAEs (Kemp, 1979). The emission with frequency $2f_1 - f_2$, known as the cubic distortion product, usually has the highest amplitude and therefore is the one most frequently studied (Probst *et al.*, 1991). The definitions lower sideband (LSB) and upper sideband (USB) DPOAE are used to indicate whether the DP frequency is lower or higher than the primary frequencies, respectively.

The distortion products are assumed to be generated in the region where the f_1 and f_2 excitation patterns show substantial overlap (Kim, 1980; Kim *et al.*, 1980; Siegel *et al.*, 1982). Within that region, the place where f_2 reaches its maximum basilar membrane displacement (X_2) is supposedly the largest contributor to the generation of a DPOAE. Suppression experiments support this view by showing that the amplitude of the cubic distortion product $2f_1 - f_2$ is most effectively decreased by a tone close to f_2 (Brown and Kemp, 1984; Kummer *et al.*, 1995) or between f_1 and f_2 (Martin *et al.*, 1987).

There is evidence from neural recordings in cats (Smoorenburg *et al.*, 1976; Kim *et al.*, 1980) and basilar membrane velocity measurements (Robles *et al.*, 1991) that the $2f_1 - f_2$ distortion product reaches its own characteristic place X_{dp} apically from the generation site X_2 . Recently, several studies showed that there is a contribution from this characteristic place to the $2f_1 - f_2$ DPOAE in the ear canal of human subjects (Kummer *et al.*, 1995; Brown *et al.*, 1996; Heitmann *et al.*, 1998).

The upper sideband DPOAE with frequency $2f_2 - f_1$ differs from the lower sideband DPOAEs ($2f_1 - f_2$, $3f_1 - 2f_2$, $4f_1 - 3f_2$, etc.) in several ways. Its amplitude is considerably smaller than the amplitude of the $2f_1 - f_2$ DPOAE, and its characteristic frequency place is located basally from the primary frequency regions. Therefore, a distortion product with frequency $2f_2 - f_1$ generated close to X_2 is not likely to reach the ear canal. Suppression experiments have shown that the $2f_2 - f_1$ level is best suppressed by a tone with a frequency close to $2f_2 - f_1$, not to f_2 (Martin *et al.*, 1987, 1998). This supports the idea that the contribution of the $2f_2 - f_1$ characteristic frequency place is larger than that of X_2 . While early studies mostly focused on DPOAE amplitude under various stimulus conditions, more recently several authors have also considered the phase of the ear canal response. The interest here is that a measure of the mechanical delay in the cochlea can be obtained by determining the group delay of the DPOAEs with the phase-gradient method (Kimberley *et al.*, 1993, O'Mahoney and Kemp, 1995), fixing one of the primaries while varying the other. The f_1 -sweep paradigm refers to varying the f_1 frequency at fixed values of f_2 , while the f_2 -sweep paradigm refers to the opposite situation. Under the assumption that the DPOAEs are generated at X_2 , the first is easier to interpret, since the generation site will not move during the f_1 -sweep. Several studies reported larger group delays when determined with the f_2 -sweep method as opposed to the f_1 -sweep in humans (O'Mahoney

and Kemp, 1995; Moulin and Kemp, 1996b; (Bowman et al., 1997); Bowman *et al.*, 1997) and in rabbits (Whitehead *et al.*, 1996). Moulin and Kemp (1996b) have shown that this only holds true for the lower sideband DPOAEs. They reported no significant difference between f_1 - and f_2 -sweep for the $2f_2 - f_1$ group delays in human subjects. In the attempts to explain the differences found between the group delays obtained with f_1 - and f_2 -sweeps, two hypotheses have been proposed, concerning the way the DPOAE generation site moves with the changing primary frequencies: the place- and the wave-fixed model (Kemp, 1986; O'Mahoney and Kemp, 1995; Moulin and Kemp, 1996a,b). The place-fixed model for the generation of DPOAEs is based on the assumption that the generation place does not move during the f_1 - or f_2 -sweep. In the wave-fixed description, however, the generation place X_2 is fixed to the peak of the traveling wave, which means that it shifts in the f_2 -sweep paradigm. Bowman *et al.* (1997, 1998) ascribed the differences between f_1 - and f_2 -sweep group delays to the level-dependent filter build-up time. In their view, which is based on the place-fixed model, the f_2 -sweep paradigm includes a larger portion of the filter build-up time in the group delay than does the f_1 -sweep.

In this chapter we present a comprehensive set of DPOAE group delay data for the guinea pig. In this animal, as well as in other rodents, DPOAE amplitudes are substantially higher than in human subjects (Brown, 1987; Brown and Gaskill, 1990). This gives the possibility to measure several DPOAE components with a good signal-to-noise ratio. As part of a larger study of distortion products in the guinea pig, we measured the amplitudes and phases of the four DPOAEs with frequencies $2f_1 - f_2$, $3f_1 - 2f_2$, $4f_1 - 3f_2$, and $2f_2 - f_1$, with both the f_1 - and the f_2 -sweep paradigms. In this chapter we focus on the phase data, from which the group delays were calculated. A comparative evaluation is presented of group delays of different DP components when measured with the same sweep paradigm, and of group delays obtained with the f_1 -sweep versus the f_2 -sweep paradigm. Finally, a tentative analysis is made of the interpretation of the data in terms of the place-fixed and wave-fixed models, proposed to explain the differences of DPOAE group delays in different paradigms (Kemp, 1986; O'Mahoney and Kemp, 1995; Moulin and Kemp, 1996a,b).

2.2 Methods

2.2.1 Subjects

Five pigmented female guinea pigs, weighing between 500 and 700 g, were tested. Otoscopic inspection revealed no abnormalities in any of the ears. The animals were anesthetized with an intramuscular injection of ketamine hydrochloride (Ketalar, 20 mg/kg) and xylazine (Rompun, 15 mg/kg). Their body temperature was maintained at 38°C with a heating blanket. During each experimental session, lasting between 1 and 2 hours, one ear was tested. Each ear was measured twice, on different days, except one ear, which was only tested once. This resulted in a total of 19 sessions.

2.2.2 Material

The stimulus tones were generated on a DSP board (Ariel DSP 16+) and delivered to the ear canal via two ER2 transducers (Etymotic Research). These were connected to an ER10B probe system (Etymotic Research), housing a low noise miniature microphone for the recording of ear canal sound pressure levels. The microphone signal was amplified 40 dB. The probe system was sealed into the external auditory meatus with a plastic earplug. All recordings were made in a sound-treated booth. We used modified versions of CUBDIS[®] software, which enabled us to record several other distortion products in addition to the $2f_1 - f_2$ component, over a wide range of f_2/f_1 values, with both the f_1 - and the f_2 -sweep paradigms.

2.2.3 DPOAE recording paradigms

Ear canal calibration

Prior to each f_1 - or f_2 -sweep measurement, an ear canal calibration was performed to set the level and starting phase of the primaries. The responses to 50 swept tones (“chirps”), generated at a constant voltage and presented in a continuous mode, were averaged and the amplitude and phase spectra were computed. From these spectra, the voltage and the starting phase of each frequency, necessary to obtain the desired primary level and zero phase at the place of the microphone, were calculated. The amplitude spectra of the ear canal calibrations were also used to check the probe fit. Whenever the spectrum showed signs that the probe was no longer sealing the ear canal, the probe was replaced and calibration was done again.

f_1 - and f_2 -sweeps

Amplitudes and phases of the following DPOAE components were recorded as a function of DPOAE frequency: $2f_1 - f_2$, $3f_1 - 2f_2$, $4f_1 - 3f_2$, and $2f_2 - f_1$. Two different methods were used to modify the DPOAE frequency: the f_1 -sweep paradigm, with frequency f_2 fixed and f_1 varied, and the f_2 -sweep paradigm, with f_1 fixed and f_2 varied. The fixed f_2 frequencies were between 1.5 and 11 kHz, the fixed f_1 values a factor of 1.25 lower. The step-size of the varying primary frequency was 24.4 or 48.8 Hz. During each sweep, the f_2/f_1 ratio varied over a broad range of at most 1.01 - 1.70. Primary levels in all sweep experiments were constant at $L_1, L_2 = 65, 55$ dB SPL. Noise levels were determined from the average amplitudes of the six frequency bins closest to the DPOAE frequency bin.

2.2.4 Data analysis

The phase-frequency relations were unwrapped to eliminate 2π discontinuities. Group delays were calculated from the slope of the unwrapped phase curves according to the following equation:

$$D = -\frac{1}{2\pi} \frac{d\varphi_{dp}}{df_{dp}} \quad (2.1)$$

with D , the group delay, in ms; φ_{dp} , the DPOAE phase, in radians; and f_{dp} , the DPOAE frequency, in kHz. Since the phase-frequency curve is linear only over a small range of f_2/f_1 (Moulin and Kemp, 1996a), the slope was determined from a regression line fitted through a small part of the curve, consisting of 11 points. Those points corresponded to the frequencies centered on the maximum in the DPOAE amplitude versus frequency relation. This implies that for each f_1 - or f_2 -sweep measurement, the group delay is determined at the primary frequency separation that yields the maximum DPOAE level, which can be different for all four DP components. All group delays in this study are referenced to f_2 frequency. In case of f_1 -sweeps this is the fixed primary, but group delays measured with the f_2 -sweep method are given as a function of the f_2 belonging to the maximum in DPOAE level, where the phase-frequency gradient was computed. Group delays were excluded from further analysis when one or more of the data points used for group delay calculation had a signal-to-noise ratio smaller than 10 dB.

Using the method as described above, the group delay was not determined when there was no clear maximum in the DPOAE level. Together with the 10 dB noise criterion, this resulted in unequal numbers of group delay data points for the different DP components and for the two sweep paradigms. Since the group delays were determined at the primary frequencies yielding the maximum DPOAE level, we found f_2 -sweep group delays in each individual ear at many slightly different f_2 values instead of at a few fixed values (as for the f_1 -sweep paradigm). Therefore, instead of paired statistical tests, an alternative test was used to compare the f_1 - and f_2 -sweep group delay values, which consists of comparing the linear fits through the pooled data.

The group delay versus f_2 curves were fitted with the following regression equation:

$$\log(D) = a + b \cdot \log(f_2) + c \cdot S + d \cdot \log(f_2) \cdot S, \quad (2.2)$$

with S as the “dummy” variable, which is 0 or 1 in case of f_1 -sweep and f_2 -sweep, respectively. This results in the two regression lines $\log(D_1) = a + b \cdot \log(f_2)$ and $\log(D_2) = (a + c) + (b + d) \cdot \log(f_2)$ for the two sweep paradigms, which are exactly the same lines as two separate linear fits would have given (Draper and Smith, 1981). Subtracting these lines yields $\log(D_2/D_1) = c + d \cdot \log(f_2)$. Plotting D_2/D_1 as a function of f_2 , with the 95% confidence interval, shows the frequency areas where D_1 is significantly different from D_2 ($p < 0.05$).

2.3 Results

As an illustrative example of the raw data, the amplitude and phase-frequency relations of a representative measurement, obtained with the f_1 -sweep paradigm and f_2 fixed at 8 kHz, are shown in figure 2.1. The f_2 -sweep results, at $f_1 = 6$ kHz, of the same ear are plotted in figure 2.2. The upper panels show the levels of the four DPOAEs with frequencies $2f_1 - f_2$, $3f_1 - 2f_2$, $4f_1 - 3f_2$, and $2f_2 - f_1$ as a function of the distortion product frequency f_{dp} . Only data points with signal-to-noise ratio > 10 dB are plotted. The three lower sideband DPOAEs all peak at approximately the same f_{dp} , which implies that the ratio f_2/f_1 at

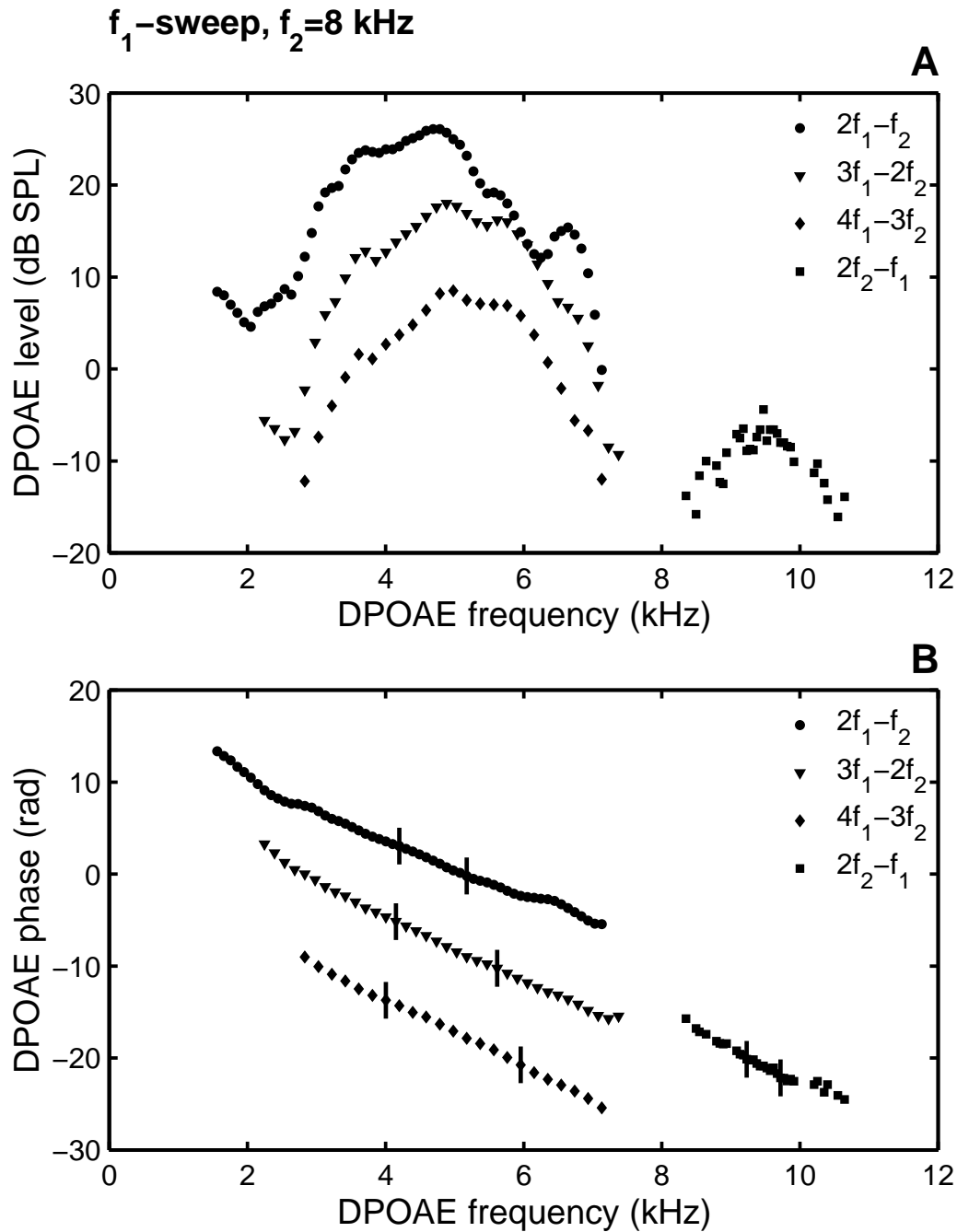


Figure 2.1: DPOAEs measured in an individual guinea pig ear, with the f_1 -sweep paradigm at $f_2 = 8$ kHz. (A) DPOAE level as a function of DPOAE frequency ($\bullet = 2f_1 - f_2$, $\blacktriangledown = 3f_1 - 2f_2$, $\blacklozenge = 4f_1 - 3f_2$, $\blacksquare = 2f_2 - f_1$). All data points shown have signal-to-noise ratio > 10 dB. (B) Corresponding DPOAE phase as a function of DPOAE frequency. The region from which the group delays are calculated, consisting of 11 points around the maximum in DPOAE level, is indicated with vertical lines.

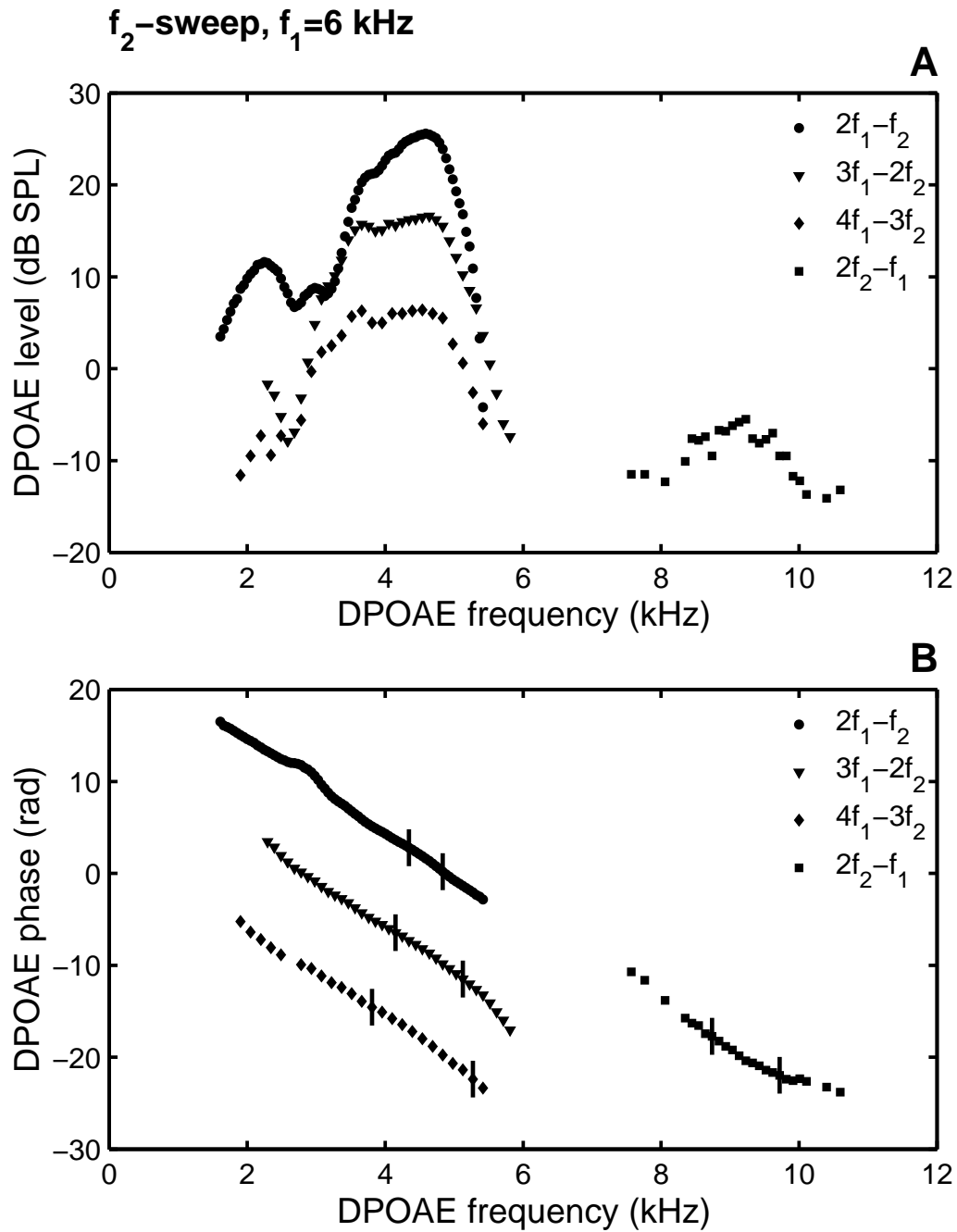


Figure 2.2: DPOAEs measured in an individual guinea pig ear (the same ear as in figure 2.1), with the f_2 -sweep paradigm at $f_1 = 6$ kHz. See caption for figure 2.1.

maximum DP level decreases with increasing DP order. The $2f_2 - f_1$ DPOAE has its maximum at a higher f_{dp} . The lower panels of figures 2.1 and 2.2 show the corresponding DPOAE phases. The curves are shifted arbitrarily with a multiple of 2π . The region where the regression line was fitted to determine the slope is indicated in each phase curve.

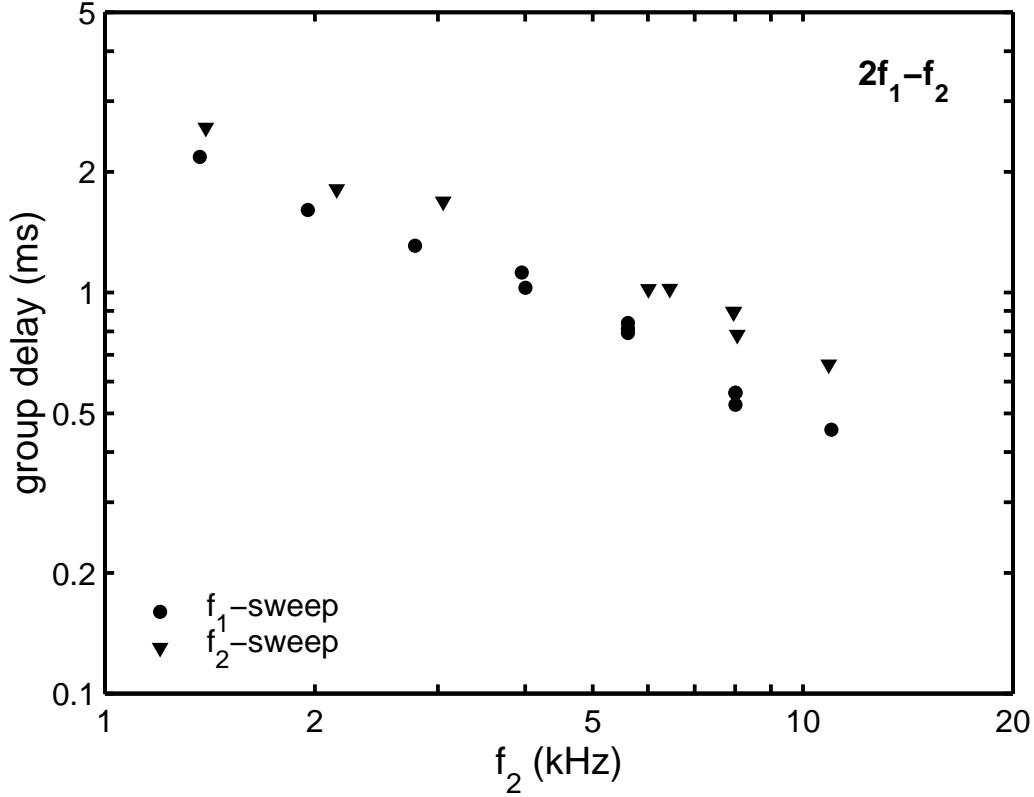


Figure 2.3: Group delays of the $2f_1 - f_2$ DPOAE as a function of f_2 frequency, measured in one individual ear (\bullet = f_1 -sweep group delays, \blacktriangledown = f_2 -sweep group delays).

All group delays of the $2f_1 - f_2$ DPOAE from one measurement (one ear) are plotted on a double-logarithmic scale in figure 2.3, as a function of the f_2 frequency. For the f_1 -sweep group delays, this is the fixed f_2 frequency, and for the f_2 -sweep group delays this is the f_2 frequency belonging to the maximum in DPOAE level, at which the group delay was determined. The f_1 - and f_2 -sweep group delays (D_1 and D_2 , respectively) are indicated with different symbols. The group delay decreases as a function of frequency, and the f_2 -sweep group delays are larger than those obtained with the f_1 -sweep paradigm.

Figure 2.4 shows the pooled group delay data from all measurements, for the DPOAEs with frequency $2f_1 - f_2$, $3f_1 - 2f_2$, $4f_1 - 3f_2$, and $2f_2 - f_1$. The data are fitted with regression lines according to equation 2.2. The dashed and solid lines represent the fits through the f_1 -sweep and the f_2 -sweep group delays, respectively. The lower sideband DPOAEs all show the same effect: f_2 -sweep group delays are larger than the group delays determined with the f_1 -sweep paradigm. The DPOAE with frequency $2f_2 - f_1$, in the lower right panel, behaves differently. At the lowest frequencies, the f_1 -sweep delays seem to be larger, while in the higher frequency region the f_2 -sweep method gives larger group delays. In table 2.1, the coefficients are given of the regression lines that were plotted in figure 2.4, together with the goodness of fit R^2 .

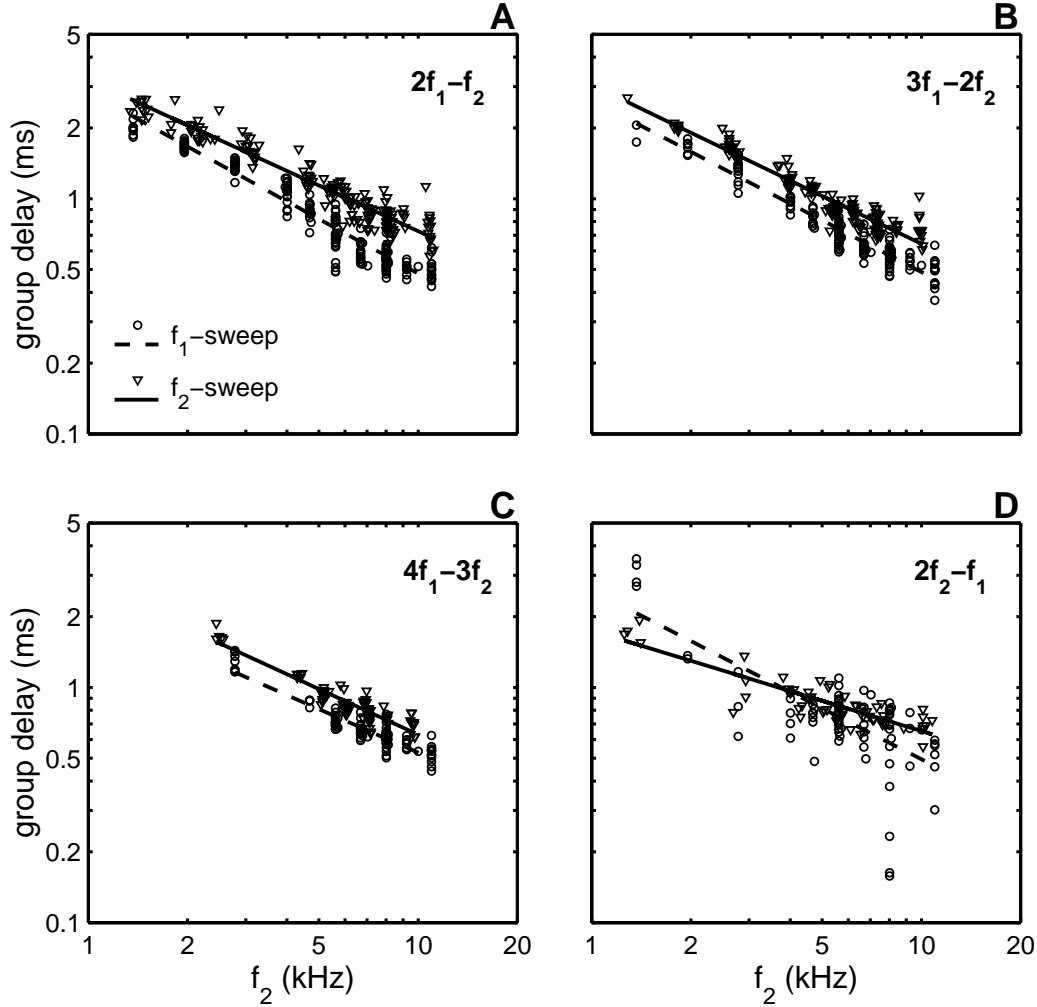


Figure 2.4: Pooled group delay data from all measurements. Group delays are plotted as a function of f_2 frequency, for both sweep paradigms. For each sweep paradigm and DPOAE component, the regression line is fitted (equation 2.2) and plotted with a dashed line (f_1 -sweep, \circ) or a solid line (f_2 -sweep, ∇). (A) Group delays of the $2f_1 - f_2$ DPOAE. (B) Group delays of the $3f_1 - 2f_2$ DPOAE. (C) Group delays of the $4f_1 - 3f_2$ DPOAE. (D) Group delays of the $2f_2 - f_1$ DPOAE.

In order to evaluate whether, and in which frequency range, the f_1 - and f_2 -sweep group delays are significantly different, the regression lines were compared as described in section 2.2.4. This method is illustrated in figure 2.5, for the $2f_1 - f_2$ DPOAE. The upper panel shows again the two logarithmic regression lines for the f_1 - and f_2 -sweep group delays as a function of f_2 (the same as in figure 2.4A). Subtracting these, results in the ratio of f_1 - and f_2 -sweep group delays D_2/D_1 . This ratio is plotted in the lower panel, as a function of f_2 with the 95% confidence interval. From figure 2.5B it is clear that the group delays of the $2f_1 - f_2$ DPOAE measured with f_2 -sweeps are significantly larger than the f_1 -sweep

Table 2.1: Coefficients of the regression lines $\log(D) = a + b \cdot \log(f_2)$, for the four DPOAEs and the two sweep paradigms.

	f_1 -sweep			f_2 -sweep		
	a	b	R^2	a	b	R^2
$2f_1 - f_2$	0.45	-0.77	0.93	0.51	-0.64	0.91
$3f_1 - 2f_2$	0.42	-0.73	0.91	0.48	-0.68	0.91
$4f_1 - 3f_2$	0.34	-0.61	0.85	0.44	-0.64	0.85
$2f_2 - f_1$	0.41	-0.72	0.52	0.24	-0.43	0.76

group delays, at all frequencies.

The same procedure was followed with the group delays of the other DPOAEs. Figure 2.6 shows the ratio between f_1 - and f_2 -sweep group delays for all four DPOAEs. For the lower sideband DPOAEs $2f_1 - f_2$, $3f_1 - 2f_2$ and $4f_1 - 3f_2$, the delays obtained with the f_2 -sweep method are significantly larger than those measured with an f_1 -sweep, at all measured frequencies (figure 2.6A, B, and C). The $2f_2 - f_1$ group delays show no significant difference between f_1 - and f_2 -sweep for f_2 in the range 1.8 - 5.4 kHz (the confidence interval overlaps the $D_2/D_1 = 1$ line, area II in figure 2.6D). For $f_2 < 1.8$ kHz, the f_1 -sweep paradigm produces the largest group delays (area I), while at $f_2 > 5.4$ kHz, the f_2 -sweep group delays are larger (area III).

In figure 2.7, the same group delay data from figure 2.4 are plotted again, although grouped differently. In this case not the sweep paradigms are compared, but the DPOAE components. This is done for the f_1 - and the f_2 -sweep method separately. Again, these are pooled data from all measurements. In figure 2.7A, the group delays of the lower sideband DPOAEs obtained with f_1 -sweeps are plotted, together with the regression lines (see table 2.1). The same method of comparing regression lines was used to determine whether the fits differ significantly. There appear to be no significant differences between the group delays of the three lower sideband DPOAEs obtained with the f_1 -sweep, in the observed frequency region. Figure 2.7B shows the group delays of the same lower sideband DPOAEs, obtained with the f_2 -sweep method. The only significant difference is found between the $2f_1 - f_2$ and the $4f_1 - 3f_2$ group delays. The latter are slightly smaller. A comparison between the $2f_1 - f_2$ and the $2f_2 - f_1$ group delays is shown in figure 2.7C, for the f_1 -sweep data. There is no significant difference. However, when the f_2 -sweep data of the same DPOAEs are compared (figure 2.7D), there appears to be a large significant difference for all measured frequencies. The group delays of the $2f_2 - f_1$ DPOAE are smaller than of the $2f_1 - f_2$ DPOAE, when obtained with the f_2 -sweep paradigm.

2.4 Discussion

The amplitudes of DPOAEs are larger in guinea pigs than in human subjects, which made it possible to measure several DP components with a good signal-to-noise ratio, in order

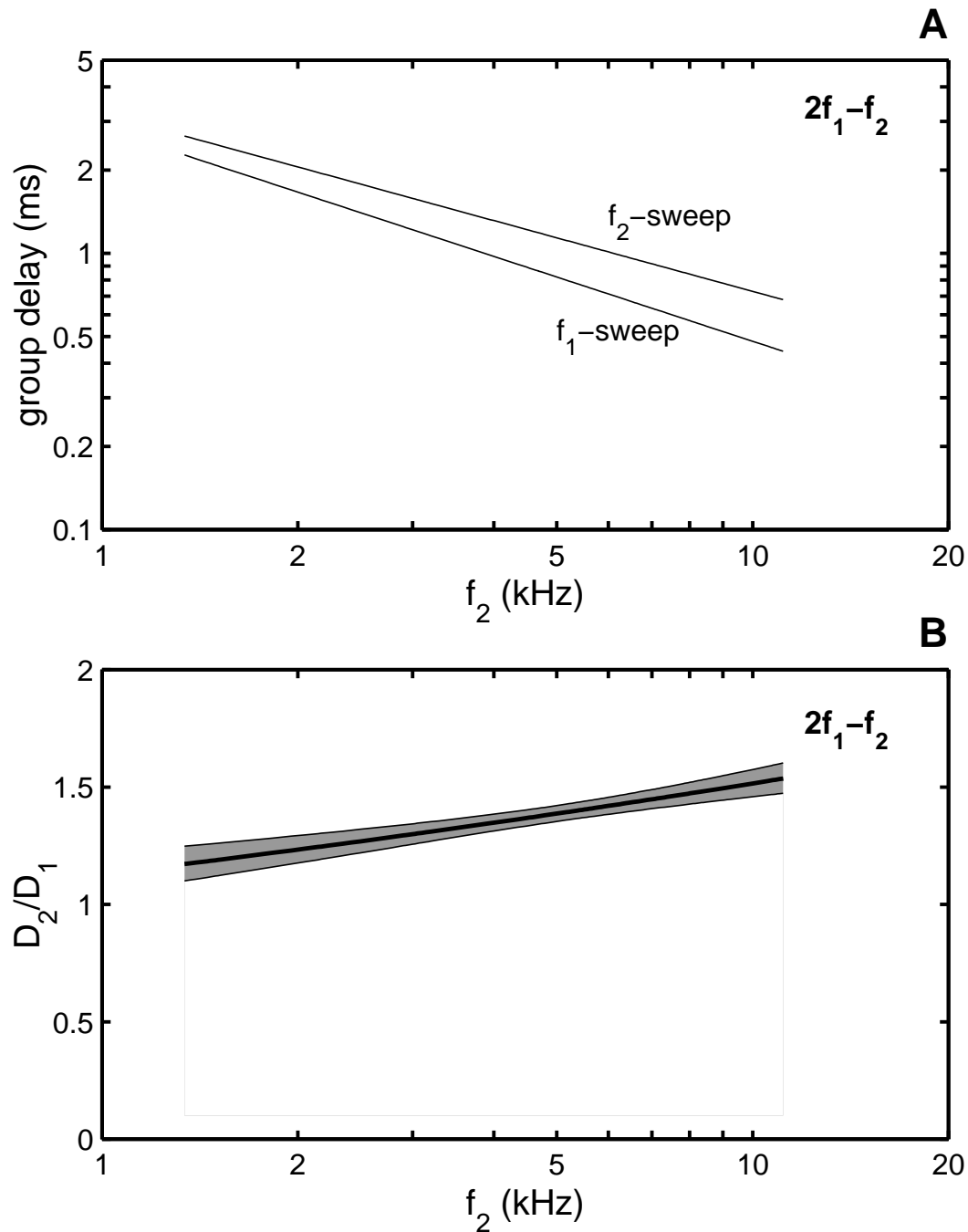


Figure 2.5: Comparison of the f_1 -sweep group delays (D_1) and the f_2 -sweep group delays (D_2). (A) Regression lines of the f_1 - and f_2 -sweep group delays for the $2f_1 - f_2$ DPOAE, as in figure 2.4A. (B) Subtracting the lines of (A) results in the ratio D_2/D_1 as a function of f_2 . The 95% confidence interval of the group delay ratio is indicated by the shaded area.

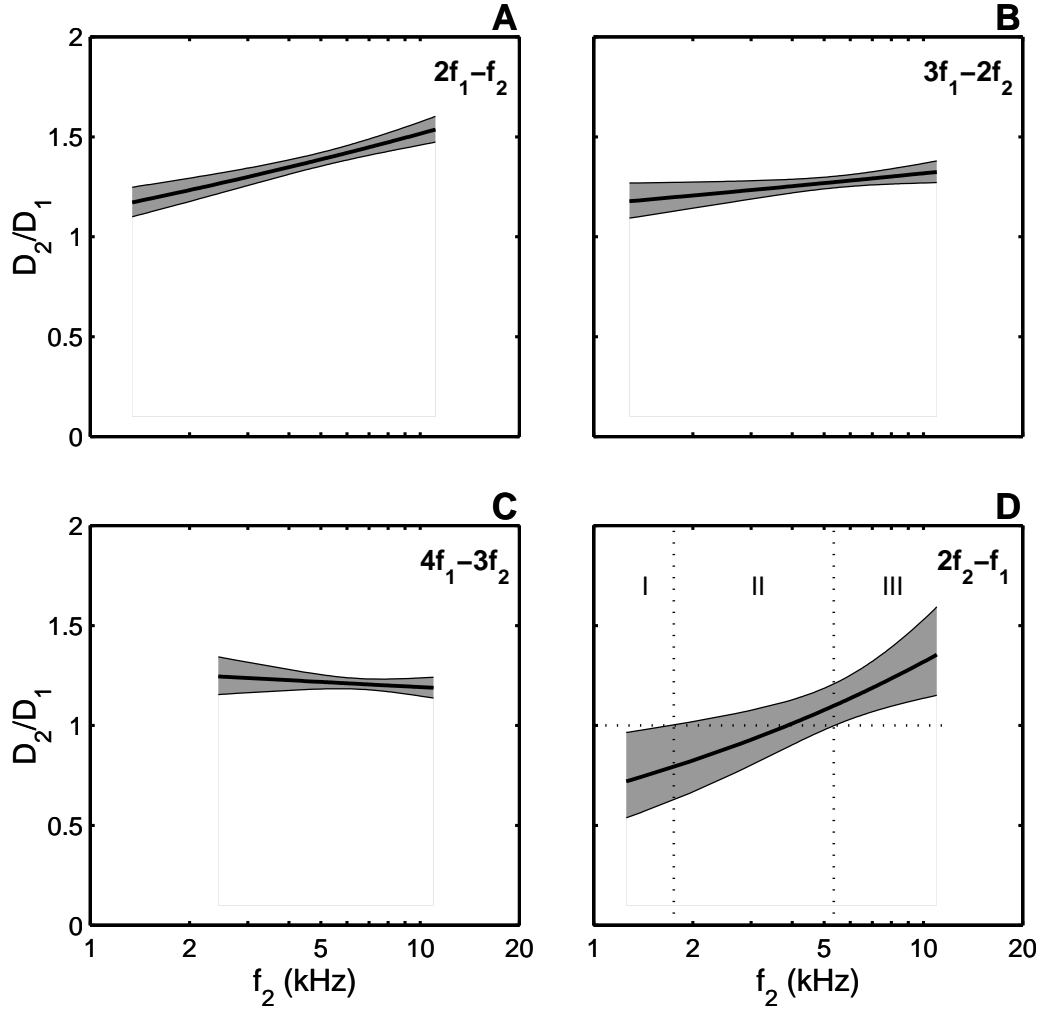


Figure 2.6: Ratio of f_1 -sweep and f_2 -sweep group delays D_2/D_1 as a function of f_2 with 95% confidence interval. Results for the three lower sideband DPOAEs $2f_1 - f_2$ (A), $3f_1 - 2f_2$ (B), $4f_1 - 3f_2$ (C), and for the upper sideband DPOAE $2f_2 - f_1$ (D). Area I indicates the frequency region below 1.8 kHz, where $D_2 > D_1$, in area II D_1 and D_2 are not significantly different and in area III, above 5.4 kHz, $D_2 > D_1$.

to compare their group delays. We have shown that the group delays of the distortion products $2f_1 - f_2$, $3f_1 - 2f_2$, $4f_1 - 3f_2$, and $2f_2 - f_1$ can be successfully recorded in the guinea pig, with both the f_1 - and the f_2 -sweep paradigms. Comparing the group delays of the two sweep paradigms, and in addition of the four different DP components in one study, can add to the discussion about the generation sites of the DPOAEs and the difference between the sweep paradigms. Note that in this study one pair of stimulus levels was used ($L_1, L_2 = 65, 55$ dB SPL) due to limited measurement time in each session. General validity of the given interpretation of the data is not proved here.

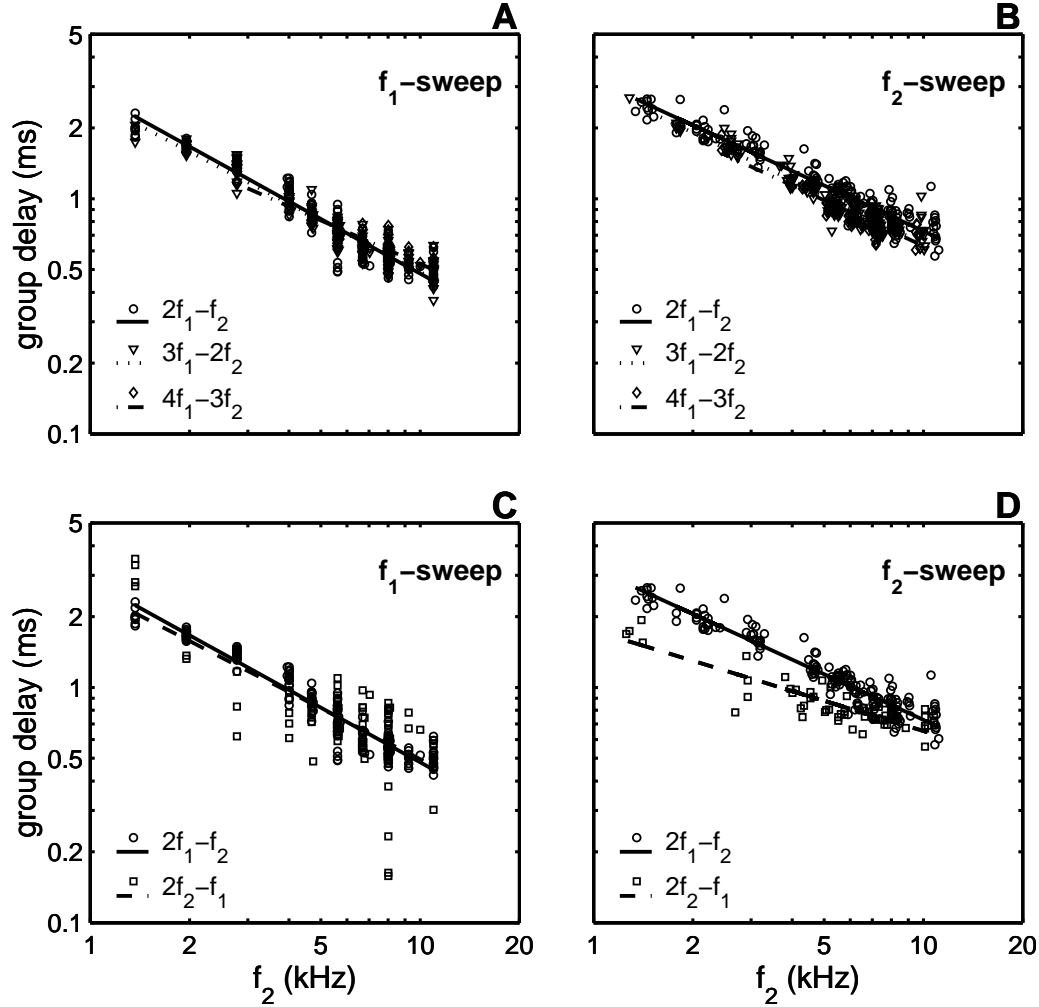


Figure 2.7: Pooled group delay data as a function of f_2 frequency. Same data points as in figure 2.4. (A) f_1 -sweep group delays of the three lower sideband DPOAEs with regression lines (\circ solid, $2f_1 - f_2$; ∇ dotted, $3f_1 - 2f_2$; \diamond dashed-dotted, $4f_1 - 3f_2$). (B) f_2 -sweep group delays of the three lower sideband DPOAEs. (C) f_1 -sweep group delays of $2f_1 - f_2$ (\circ , solid) and $2f_2 - f_1$ (\square , dashed). (D) f_2 -sweep group delays of $2f_1 - f_2$ and $2f_2 - f_1$.

2.4.1 Comparison of the two sweep paradigms for the lower sideband DPOAEs

The fact that the f_2 -sweep paradigm gives larger group delays than the f_1 -sweep paradigm for the lower sideband DPOAEs is in agreement with other studies. O'Mahoney and Kemp (1995) reported f_1 -sweep group delays that were on average 21.5% smaller than the f_2 -sweep group delays for the $2f_1 - f_2$ DPOAE in humans (with $L_1, L_2 = 70, 60$ dB SPL). This corresponds to a D_2/D_1 of 1.27, which is in the range of the values we found for the guinea pig (figure 2.6A). Whitehead *et al.* (1996) reported an average D_2/D_1 of 1.6 in

humans (with $L_1=L_2=75$ dB SPL). In the same study, the ratio of the f_1 - and f_2 -sweep group delays of the $2f_1 - f_2$ DPOAE in rabbits appeared to depend on the stimulus levels. At high levels (75 dB SPL) D_2/D_1 was close to one. Bowman *et al.* (1997) reported group delay values for f_1 - and f_2 -sweep measurements of the $2f_1 - f_2$ DPOAE in humans, which correspond to values for D_2/D_1 between 1.30 and 1.93. They reported a dependence of $D_2 - D_1$ on stimulus level. This has led them to conclude that the f_2 -sweep delay consists of a larger part of the filter build-up time, which is level dependent, than the f_1 -sweep delay. The ratio D_2/D_1 based on the fits of the group delays that Moulin and Kemp (1996a,b) found for the $2f_1 - f_2$ DPOAE in humans, ranges from 1.28 to 1.62, for f_2 from 1 to 6 kHz, which is close to our values for the guinea pig. For the next lower sideband DPOAE $3f_1 - 2f_2$, Moulin and Kemp (1996b) reported fits that correspond to D_2/D_1 of 1.23 to 1.37, for f_2 from 1 to 6 kHz. Results for the $4f_1 - 3f_2$ group delays have not been reported so far. We conclude that the ratios of f_1 - versus f_2 -sweep group delays we have found for the lower sideband DPOAEs in the guinea pig are in the same range as those found in other species. Additionally, our data show that the ratio D_2/D_1 decreases with increasing order of the lower sideband distortion product.

2.4.2 Comparison of the two sweep paradigms for the upper sideband DPOAE $2f_2 - f_1$

With respect to group delay differences between the f_1 - and the f_2 -sweep paradigm, the upper sideband DPOAE with frequency $2f_2 - f_1$ does not behave like the lower sideband DPOAEs. We found no significant difference between D_1 and D_2 for frequencies in the range 1.8 - 5.4 kHz. For $f_2 < 1.8$ kHz, the f_1 -sweep group delays were larger than the f_2 -sweep group delays, and for $f_2 > 5.4$ kHz the group delays obtained with an f_2 -sweep were larger. Other studies report similar results. Whitehead *et al.* (1996) found “little difference” between f_1 - and f_2 -sweep group delays for the $2f_2 - f_1$ DPOAE in humans and in rabbits. Moulin and Kemp (1996a,b) saw no significant difference between f_1 - and f_2 -sweep group delays for the $2f_2 - f_1$ DPOAE in humans, except at 4 kHz, where the f_2 -sweep group delay was larger. So, the results of our study in the guinea pig are similar to those reported for humans and rabbits, regarding the dependence of the group delays of the upper sideband DPOAE $2f_2 - f_1$ on sweep paradigm.

The fact that the group delays of the upper sideband DPOAE do not depend on which primary is swept, at least in the mid-frequency range, while the group delays of the lower sidebands do, indicates that there is no common generation site for upper and lower sideband DPOAEs. The same conclusion can be drawn from the results of suppression experiments (Martin *et al.*, 1987, 1998). In addition, onset latencies and amplitude correlation functions also strongly suggest that the $2f_2 - f_1$ DPOAE is generated basal to the primary frequency region on the basilar membrane (Martin *et al.*, 1998).

2.4.3 Group delay differences between DPOAEs

The group delay differences between the four DP components appear to depend on the sweep paradigm that is used. The f_1 -sweep method gives the same group delay values for all DP components. In contrast, the group delays that were measured with f_2 -sweeps show a small but significant difference between $2f_1 - f_2$ and $4f_1 - 3f_2$, and in particular a large disparity between the two cubic distortion products $2f_1 - f_2$ and $2f_2 - f_1$. The latter upper sideband DPOAE has 12% (at 11 kHz) to 46% (at 1.5 kHz) smaller group delays than the lower sideband DPOAE $2f_1 - f_2$. Several other studies showed the same effect of the $2f_2 - f_1$ group delays being smaller than the $2f_1 - f_2$ group delays, when measured with the f_2 -sweep, in humans (Wable *et al.*, 1996; Moulin and Kemp, 1996b; Whitehead *et al.*, 1996). Moulin and Kemp (1996b) reported values corresponding to an average percentage of 27%, which is in the same range as our values. In addition, Whitehead *et al.* (1996) and Martin *et al.* (1998) reported onset latencies that were shorter for $2f_2 - f_1$ than for $2f_1 - f_2$ in rabbits and humans. In gerbils, $2f_2 - f_1$ group delays were shorter than $2f_1 - f_2$ group delays when measured with the f_1 -sweep paradigm at an f_2 of 4 kHz and stimulus levels of 50 dB and higher (Brown and Kemp, 1985). This is in contrast with our f_1 -sweep data for the guinea pig. We conclude that our findings for the two cubic distortion products are qualitatively similar to those reported in man and rabbit.

2.4.4 Place- and wave-fixed DPOAE generation models

So far, two hypotheses have been proposed in literature that link the changing frequency of the primaries with the presumed DPOAE generation site: the place-fixed and the wave-fixed model (Kemp, 1986; O'Mahoney and Kemp, 1995; Moulin and Kemp, 1996b). Both models assume a common generation site for all distortion products. This site is fixed to a place near X_2 at the cochlear partition in the place-fixed model, for small changes in the primary frequencies. In the wave-fixed model, the generation site is assumed to be fixed to the f_2 traveling wave, the amplitude and phase profile of which are invariant apart from a translation along the basilar membrane. Considering the f_1 -sweep, both the place- and wave-fixed models represent the same situation, where the DPOAE generation site X_2 is place-fixed even for the wave-fixed model since the f_2 frequency is constant. In this case, the group delay will only depend on the change in the phase of the changing f_1 primary, at the fixed generation site. For the f_2 -sweep paradigm, the place- and wave-fixed models describe two different situations. In the place-fixed model, the group delay will depend on the phase change of the changing f_2 primary at the fixed generation site. In the wave-fixed model, the place of generation X_2 will move along with the changing f_2 in case of an f_2 -sweep, and the group delay only depends on the phase change of the fixed f_1 primary at the generation place, due to the movement of X_2 . The phase of f_2 will have no influence, since it is constant at its own characteristic frequency place (Kemp, 1986).

Both the place- and the wave-fixed models predict the group delays of the lower sideband DPOAEs measured with the f_2 -sweep paradigm to be larger than the f_1 -sweep group delays (Moulin and Kemp, 1996b). So here our data are in accordance with both the place- and the wave-fixed hypotheses. When the comparison of the group delays of the different

lower sideband DPOAEs is considered, we can distinguish between place- and wave-fixed. The place-fixed model predicts the group delays of all lower sideband DPOAEs to be equal, with either sweep paradigm. The wave-fixed model, on the other hand, predicts a difference between group delays of the lower sideband DPOAEs, depending on the order of the distortion product, only for the f_2 -sweep paradigm: the higher the order of the distortion product, the smaller the f_2 -sweep group delay would be (Moulin and Kemp, 1996b). Our data agree with this concept, since the group delay measured with f_2 -sweep decreases with increasing DPOAE order, although the effect was only small. The only significant difference is between the $2f_1 - f_2$ and $4f_1 - 3f_2$ group delays. We conclude that our lower sideband group delay data are in favor of the wave-fixed model.

Our results for the upper sideband DPOAE $2f_2 - f_1$, as well as those of Moulin and Kemp (1996b), disagree with the place-fixed model. When X_2 is the assumed generation site, the place-fixed model predicts a difference in $2f_2 - f_1$ group delay between the two sweep paradigms, for all frequencies. This is not observed in the present data, which show no significant difference between the two sweep paradigms for the $2f_2 - f_1$ group delay, in the frequency range 1.8 - 5.4 kHz. Again, this suggests that the hypothesis that the $2f_2 - f_1$ has the same generation place as the lower sideband DPOAEs is not valid, as also suggested by, e.g., Moulin and Kemp (1996b).

2.4.5 Contribution from the X_{dp} place to the generation of the $2f_1 - f_2$ DPOAE

Several studies have suggested a second place contributing to the cubic distortion product $2f_1 - f_2$ measured in the ear canal, namely its characteristic frequency place X_{dp} which is located apically from the primary frequency region (Gaskill and Brown, 1996; Brown *et al.*, 1996; Heitmann *et al.*, 1998). In a study by Stover *et al.* (1996), indications were found for the existence of multiple DPOAE generators. Brown *et al.* (1996) have shown that the cubic distortion product measured in the human ear canal can be described as a vector summation of two components originating from X_2 and X_{dp} . They suggest that the component from X_{dp} gives rise to the fine structure observed in the DPOAE amplitude. Heitmann *et al.* (1998) found additional proof for this view in the results of suppression experiments, which showed a decrease in the fine structure when the suppressor tone had a frequency close to $2f_1 - f_2$. However, the amplitude versus frequency characteristics of guinea pig DPOAEs do not show fine structure (Brown and Gaskill, 1990). This could indicate that the contribution of the X_{dp} place to the generation of the lower sideband DPOAEs is relatively small in the guinea pig. As a result, we can conclude that the assumption made in the place- and wave-fixed model, of a place (close to) X_2 being the only contributor to the generation of the lower sideband DPOAEs, is probably closer to the truth in guinea pig than in human.

2.5 Conclusions

For the lower sideband DPOAEs measured in the guinea pig, the f_2 -sweep gave larger group delays than the f_1 -sweep paradigm. The ratio between f_2 -sweep and f_1 -sweep group delay D_2/D_1 decreases with increasing order of the lower sideband DPOAE. In contrast with the lower sideband DPOAEs, the upper sideband DPOAE $2f_2 - f_1$ showed no difference in group delay measured with f_1 - or f_2 -sweep between 1.8 and 5.4 kHz. This indicates that, at least below 5.4 kHz, there is no common generation site for upper and lower sideband DPOAEs.

The f_1 -sweep method gives the same group delay values for all DPOAE components with our stimulus conditions. Group delays measured with the f_2 -sweep method, however, show a small but significant difference between the $2f_1 - f_2$ and the $4f_1 - 3f_2$ DPOAE, and a large difference between $2f_1 - f_2$ and $2f_2 - f_1$, with the group delays of the latter being the smallest. Most aspects of these results are better described by the wave-fixed than by the place-fixed model for DPOAE generation.

References

- Bowman, D. M., Brown, D. K., Eggermont, J. J., and Kimberley, B. P. (1997). “The effect of sound intensity on f_1 -sweep and f_2 -sweep distortion product otoacoustic emissions phase delay estimates in human adults,” *J. Acoust. Soc. Am.* **101**, 1550–1559.
- Bowman, D. M., Eggermont, J. J., Brown, D. K., and Kimberley, B. P. (1998). “Estimating cochlear filter response properties from distortion product otoacoustic emission (DPOAE) phase delay measurements in normal hearing adults,” *Hearing Res.* **119**, 14–26.
- Brown, A. M. (1987). “Acoustic distortion from rodent ears: A comparison of responses from rats, guinea pigs and gerbils,” *Hearing Res.* **31**, 25–38.
- Brown, A. M., and Gaskill, S. A. (1990). “Measurement of acoustic distortion reveals underlying similarities between human and rodent mechanical responses,” *J. Acoust. Soc. Am.* **88**, 840–849.
- Brown, A. M., and Kemp, D. T. (1984). “Suppressibility of the $2f_1 - f_2$ stimulated acoustic emissions in gerbil and man,” *Hearing Res.* **13**, 29–37.
- Brown, A. M., and Kemp, D. T. (1985). “Intermodulation distortion in the cochlea: Could basal vibration be the major cause of round window CM distortion?,” *Hearing Res.* **19**, 191–198.
- Brown, A. M., Harris, F. P., and Beveridge, H. A. (1996). “Two sources of acoustic distortion products from the human cochlea,” *J. Acoust. Soc. Am.* **100**, 3260–3267.
- Draper, N. R., and Smith, H. (1981). *Applied Regression Analysis*, 2nd ed. (Wiley, New York).
- Gaskill, S. A., and Brown, A. M. (1996). “Suppression of human acoustic distortion product: Dual origin of $2f_1 - f_2$,” *J. Acoust. Soc. Am.* **100**, 3268–3274.
- Heitmann, J., Waldmann, B., Schnitzler, H.-U., Plinkert, P. K., and Zenner, H.-P. (1998). “Suppression of distortion product otoacoustic emissions (DPOAE) near $2f_1 - f_2$ removes DP-gram fine structure -Evidence for a secondary generator,” *J. Acoust. Soc. Am.* **103**, 1527–1531.

- Kemp, D. T. (1979). "Evidence of mechanical nonlinearity and frequency selective wave amplification in the cochlea," *Arch. Otorhinolaryngol.* **224**, 37–45.
- Kemp, D. T. (1986). "Otoacoustic emissions, travelling waves and cochlear mechanisms," *Hearing Res.* **22**, 95–104.
- Kim, D. O. (1980). "Cochlear mechanics: Implications of electrophysiological and acoustical observations," *Hearing Res.* **2**, 297–317.
- Kim, D. O., Molnar, C. E., and Matthews, J. W. (1980). "Cochlear mechanics: Nonlinear behavior in two-tone responses as reflected in cochlear-nerve-fiber responses and in ear-canal sound pressure," *J. Acoust. Soc. Am.* **67**, 1704–1721.
- Kimberley, B. P., Brown, D. K., and Eggermont, J. J. (1993). "Measuring human cochlear traveling wave delay using distortion product otoacoustic emission phase responses," *J. Acoust. Soc. Am.* **94**, 1343–1350.
- Kummer, P., Janssen, T., and Arnold, W. (1995). "Suppression tuning characteristics of the $2f_1 - f_2$ distortion product otoacoustic emission in humans," *J. Acoust. Soc. Am.* **98**, 197–210.
- Martin, G. K., Jassir, D., Stagner, B. B., Whitehead, M. L., and Lonsbury-Martin, B. L. (1998). "Locus of generation for the $2f_1 - f_2$ vs $2f_2 - f_1$ distortion-product otoacoustic emissions in normal-hearing humans revealed by suppression tuning, onset latencies, and amplitude correlations," *J. Acoust. Soc. Am.* **103**, 1957–1971.
- Martin, G. K., Lonsbury-Martin, B. L., Probst, R., Scheinin, S. A., and Coats, A. C. (1987). "Acoustic distortion products in rabbit ear canal. II. Sites of origin revealed by suppression contours and pure-tone exposures," *Hearing Res.* **28**, 191–208.
- Moulin, A., and Kemp, D. T. (1996a). "Multicomponent acoustic distortion product otoacoustic emission phase in humans. I. General characteristics," *J. Acoust. Soc. Am.* **100**, 1617–1639.
- Moulin, A., and Kemp, D. T. (1996b). "Multicomponent acoustic distortion product otoacoustic emission phase in humans. II. Implications for distortion product otoacoustic emissions generation," *J. Acoust. Soc. Am.* **100**, 1640–1662.
- O'Mahoney, C. F., and Kemp, D. T. (1995). "Distortion product otoacoustic emission delay measurement in human ears," *J. Acoust. Soc. Am.* **97**, 3721–3735.
- Probst, R., Lonsbury-Martin, B. L., and Martin, G. K. (1991). "A review of otoacoustic emissions," *J. Acoust. Soc. Am.* **89**, 2027–2067.
- Robles, L., Ruggero, M. A., and Rich, N. C. (1991). "Two-tone distortion in the basilar membrane of the cochlea," *Nature (London)* **349**, 413–414.

- Siegel, J. H., Kim, D. O., and Molnar, C. E. (1982). “Effects of altering organ of Corti on cochlear distortion products $f_2 - f_1$ and $2f_1 - f_2$,” J. Neurophysiol. **47**, 303–328.
- Smooenburg, G. F., Morton Gibson, M., Kitzes, L. M., Rose, J. E., and Hind, J. E. (1976). “Correlates of combination tones observed in the response of neurons in the anteroventral cochlear nucleus of the cat,” J. Acoust. Soc. Am. **59**, 945–962.
- Stover, L. J., Neely, S. T., and Gorga, M. P. (1996). “Latency and multiple sources of distortion product otoacoustic emissions,” J. Acoust. Soc. Am. **99**, 1016–1024.
- Wable, J., Collet, L., and Chéry-Croze, S. (1996). “Phase delay measurements of distortion product otoacoustic emissions at $2f_1 - f_2$ and $2f_2 - f_1$ in human ears,” J. Acoust. Soc. Am. **100**, 2228–2235.
- Whitehead, M. L., Stagner, B. B., Martin, G. K., and Lonsbury-Martin, B. L. (1996). “Visualization of the onset of distortion-product otoacoustic emissions, and measurement of their latency,” J. Acoust. Soc. Am. **100**, 1663–1679.

Chapter 3

Group delays of distortion product otoacoustic emissions: relating delays measured with f_1 - and f_2 -sweep paradigms

Abstract

A theoretical analysis is presented of group delays of distortion product otoacoustic emissions (DPOAEs) measured with the phase-gradient method. The aim of the analysis is to clarify the differences in group delays D_1 and D_2 , obtained using the f_1 - and the f_2 -sweep paradigms, respectively, and the dependence of group delays on the order of the DPOAE. Two models are considered, the place-fixed and the wave-fixed model. While in the former model the generation place is assumed to be invariant with both f_1 - and f_2 -sweeps, in the latter model the shift of generation place is fully accounted for. By making a simple local approximation of the cochlear scale invariance, a mathematical conversion from phase-place to phase-frequency gradients is incorporated in the wave-fixed model. Under the assumption that the DPOAE (as recorded at the best f_2/f_1 ratio) is dominated by the contribution from the generation site and not by, e.g., reflection components, the analysis leads to simple expressions for the ratio and difference between D_1 and D_2 . Validation of the models against experimental data indicates that lower sideband DPOAEs ($2f_1 - f_2$, $3f_1 - 2f_2$, $4f_1 - 3f_2$) are most consistent with the wave-fixed model. Upper sideband components ($2f_2 - f_1$), in contrast, are not properly described by either the place-fixed or the wave-fixed model, independent whether DPOAE generation is assumed to originate at the f_2 or at the more basally located f_{dp} characteristic place.

List of symbols

f_i	frequency of component i ; $i = 1, 2, \text{dp}$
f_1, f_2	primary frequencies; $f_2 > f_1$
f_{dp}	distortion product frequency, $f_{\text{dp}} = (n + 1)f_1 - nf_2$; n integer, where $n \geq 1$ for the lower sideband DPOAEs: $f_{\text{dp}} < f_1, f_2$ and $n \leq -2$ for the upper sideband DPOAEs: $f_{\text{dp}} > f_1, f_2$
x	place along the basilar membrane
X_i	characteristic place of component i
x_g	place of maximal DPOAE generation
L_i	level of component i in the ear canal
$\varphi(x; \omega_i)$	phase at place x of component i with $\omega_i = 2\pi f_i$
$\vec{\varphi}(x; \omega)$	forward phase change
$\overleftarrow{\varphi}(x; \omega)$	retrograde phase change
D_i	DPOAE group delay for f_i -sweep
\vec{D}	forward delay
\overleftarrow{D}	backward delay

3.1 Introduction

Distortion product otoacoustic emissions (DPOAEs) are generated in the cochlea when the ear is stimulated with two primaries having slightly different frequencies f_1 and f_2 ($f_1 < f_2$). The group delay of a DPOAE can be determined using the phase-gradient method, i.e., from the slope of the DPOAE phase-frequency function. Thereto, variation of DPOAE frequency is accomplished by keeping one of the primaries fixed while changing the other (Kimberley *et al.*, 1993). In the f_1 -sweep paradigm f_1 is varied at fixed values of f_2 , while in the f_2 -sweep paradigm f_2 is varied at fixed f_1 .

For the lower sideband (LSB) DPOAEs (with f_{dp} smaller than the primaries f_1 and f_2 , i.e., $2f_1 - f_2$, $3f_1 - 2f_2$, and $4f_1 - 3f_2$), these two methods give different group delay values. The group delays determined with f_2 -sweep appear to be systematically larger (chapter 2; O'Mahoney and Kemp, 1995; Moulin and Kemp, 1996a,b; Whitehead *et al.*, 1996; Bowman *et al.*, 1997). However, for the upper sideband (USB) DPOAE $2f_2 - f_1$ the delays measured with the two methods are basically equal (chapter 2; Moulin and Kemp, 1996b). Additionally, f_1 -sweep group delays do not depend on the order of the DPOAE, while the f_2 -sweep group delays show a small but significant dependence on order for the lower sidebands. Furthermore, in contrast with f_1 -sweep delays, f_2 -sweep delays demonstrate a large difference between lower and upper sidebands (chapter 2; Wable *et al.*, 1996; Moulin and Kemp, 1996b; Whitehead *et al.*, 1996).

The origin of the differences between upper and lower sideband DPOAEs is sought in different generation sites. Suppression experiments, onset latencies and amplitude correlations have shown that the main source of the lower sideband DPOAEs is close to the f_2 characteristic place X_2 , while the upper sideband DPOAE $2f_2 - f_1$ originates from a

more basal region, close to X_{dp} (Brown and Kemp, 1984; Kummer *et al.*, 1995; Martin *et al.* 1987, 1998).

With regard to LSB DPOAEs the notion is now accepted that two sources contribute to the acoustic ear canal response. The region of nonlinear interaction near X_2 generates distortion products f_{dp} . Propagation takes place in two directions, basally towards the ear canal, and apically towards the DPOAE characteristic place. There, the apically traveling component is partially reflected by the mechanism of linear coherent reflection, resulting in a backward traveling wave. In the ear canal, the DPOAE is a combination of a component generated at X_2 , and a component reflected at X_{dp} (Shera and Guinan, 1999; Talmadge *et al.*, 1998). Interference of both components is held responsible for the fine structure in DPOAE amplitude and the corresponding irregularities in the phase-frequency profiles (Brown *et al.*, 1996; Heitmann *et al.*, 1998; Talmadge *et al.*, 1999). The relative strength of the two contributions depends, among others, on the primary levels and the primary frequency regions (Fahey and Allen, 1997; Knight and Kemp, 2000). Near the f_2/f_1 ratio producing maximal DPOAE amplitudes, where the aforementioned DPOAE group delay studies were performed, the DPOAE is thought to be dominated by the contribution from the generation place X_2 (Knight and Kemp, 2000). The present study concentrates on the same condition and therefore focuses on an analysis of the consequences of sweeping either f_1 or f_2 for the phase variation of the DPOAE generated at X_2 .

The difference between f_1 - and f_2 -sweep group delays for the LSB components is thought to originate from a difference in shift of the generation place with swept f_1 or f_2 . Two models have been proposed in this context: the place- and the wave-fixed models (Kemp, 1986; O'Mahoney and Kemp, 1995; Moulin and Kemp, 1996b). In the place-fixed model, the generation place is thought to be unchanged during both the f_1 - and the f_2 -sweep paradigms. The generation place is fixed to the cochlear partition, close to X_2 . It is tentatively associated with an anatomical irregularity in the cochlea. The wave-fixed model assumes a generation place which is fixed to the maximum in the traveling wave envelope of f_2 , i.e., to X_2 . As a consequence, in this model the generation place shifts along with a swept f_2 . Based on general assumptions, Moulin and Kemp (1996b) were able to give several qualitative and some quantitative predictions regarding the relations between f_1 -sweep and f_2 -sweep group delays and their dependence on the order of the DPOAE. A full quantitative description of the wave-fixed model was not feasible due to the lack of an appropriate description of the spatial phase changes of the f_1 -wave read out by a moving X_2 in the f_2 -sweep paradigm. The intermediate model, introduced by Moulin and Kemp (1996b), is in fact place-fixed for small changes in frequency, but for larger changes it accounts for "jumps" of the generation site to another "place-fixed" site. A different approach was taken by Bowman *et al.* (1997,1998), who assign the difference in f_1 - and f_2 -sweep group delays to the build-up time of the cochlear filter, which they consider to make up a larger part of the f_2 -sweep group delay than of the f_1 -sweep group delay. They do not explicitly take possible spatial shifts of the generation place into consideration.

The aim of the present study is to elaborate on a mathematical analysis for the place- and the wave-fixed hypotheses, yielding relations between the group delays determined with f_1 - and with f_2 -sweeps (D_1 and D_2 , respectively). The problem in giving a theo-

retical description of the wave-fixed model that allows verification against experimental data is the shifting of the presumed generation place X_2 when sweeping f_2 . This generates phase-place gradients which therefore need to be translated into phase-frequency gradients. This conversion is achieved by using the scale invariance of the cochlea (Zweig and Shera, 1995; Talmadge *et al.*, 1998, 1999). Additionally, the place- and wave-fixed models will be elaborated for the upper sideband DPOAEs under the assumption that these components originate from a place basal to X_2 , near the DP characteristic place X_{dp} . The analytical results of the theory will be compared to the guinea pig data presented in chapter 2 (see also Schneider *et al.*, 2000). A tentative extension of the theory to LSB DPOAE reflection components from the X_{dp} characteristic place is discussed briefly.

3.2 Theory

Given any combination of primary frequencies (f_1, f_2) (with $f_2 > f_1$) that produces a measurable DPOAE, group delays can be obtained by applying small frequency changes of either of the two primaries around (f_1, f_2) and determining the DPOAE's phase-frequency gradient. The DPOAE group delays derived with f_1 - and f_2 -sweep measurement paradigms will be denoted as D_1 and D_2 , respectively. The goal of the present analysis is to derive descriptions of D_1 and D_2 in both the place-fixed and the wave-fixed models that allow for interpretation of properties, mutual relations, and dependence on the order of the DPOAE.

In this section the assumptions are given, followed by the main steps of reasoning and the resulting expressions for D_1 , D_2 and their relations. For further mathematical details the reader is referred to the Appendix. The first part of this section is dedicated to the basic conventions and assumptions. Then the situation is elaborated where the main DPOAE contribution originates from the region where the cochlear waves associated with f_1 and f_2 show maximal overlap, i.e., where the generation site x_g is assumed to be close to X_2 , the characteristic place of f_2 . Finally, the condition for the upper sideband components where the dominant generation site is likely to be near X_{dp} , i.e., basal to X_1 and X_2 , is treated separately.

The following general assumptions are made:

- I. DPOAE-generation is thought to be concentrated at a single generation site x_g . In the place-fixed model changes in x_g during a primary sweep are neglected: $dx_g = 0$. In the wave-fixed model changes in x_g are accounted for.
- II. Contributions to the DPOAE in the ear canal from sites other than the generation site x_g are neglected.

The DPOAE group delay is defined as

$$D \equiv -\frac{d\varphi_{dp}}{d\omega_{dp}}, \quad (3.1)$$

where φ_{dp} is the phase of the DPOAE in the ear canal and ω_{dp} is $2\pi f_{\text{dp}}$. The frequencies of the DPs are related to the primary frequencies as

$$\omega_{\text{dp}} = (n + 1)\omega_1 - n\omega_2, \quad (3.2)$$

with $n \geq 1$ for the lower sideband DPOAEs and $n \leq -2$ for the upper sideband DPOAEs. The phase of the DPOAE (φ_{dp}) in the ear canal is thought to consist of a forward component ($\vec{\varphi}(x_g; \omega_{\text{dp}})$), related to the phases of the primaries at x_g according to the relation of the ω_i 's as given in equation 3.2, and a retrograde component ($\overleftarrow{\varphi}(x_g; \omega_{\text{dp}})$). The same applies to the group delay D which can thus be written as the sum of \vec{D} and \overleftarrow{D} , respectively. Since φ_{dp} depends on both x_g and ω_{dp} , partial derivatives have to be used. The forward delay can be written as

$$\vec{D} = - \left(\frac{\partial \vec{\varphi}(x_g; \omega_{\text{dp}})}{\partial \omega_{\text{dp}}} + \frac{\partial \vec{\varphi}(x_g; \omega_{\text{dp}})}{\partial x_g} \frac{dx_g}{d\omega_{\text{dp}}} \right). \quad (3.3)$$

Combination of equations 3.2 and 3.3 results in

$$\begin{aligned} \vec{D} = & -(n + 1) \left(\frac{\partial \varphi(x_g; \omega_1)}{\partial \omega_1} \frac{d\omega_1}{d\omega_{\text{dp}}} + \frac{\partial \varphi(x_g; \omega_1)}{\partial x_g} \frac{dx_g}{d\omega_{\text{dp}}} \right) \\ & + n \left(\frac{\partial \varphi(x_g; \omega_2)}{\partial \omega_2} \frac{d\omega_2}{d\omega_{\text{dp}}} + \frac{\partial \varphi(x_g; \omega_2)}{\partial x_g} \frac{dx_g}{d\omega_{\text{dp}}} \right), \end{aligned} \quad (3.4)$$

where $\frac{\partial \varphi(x_g; \omega_i)}{\partial \omega_i}$ is the phase-frequency gradient for primary i at x_g , and $\frac{\partial \varphi(x_g; \omega_i)}{\partial x_g}$ is the phase-place gradient for primary i at x_g . Accordingly, the backward delay can be written as

$$\overleftarrow{D} = - \left(\frac{\partial \overleftarrow{\varphi}(x_g; \omega_{\text{dp}})}{\partial \omega_{\text{dp}}} + \frac{\partial \overleftarrow{\varphi}(x_g; \omega_{\text{dp}})}{\partial x_g} \frac{dx_g}{d\omega_{\text{dp}}} \right). \quad (3.5)$$

According to the relation of the ω_i 's, the gradients $\frac{d\omega_i}{d\omega_{\text{dp}}}$ depend on which primary is swept:

$$d\omega_{\text{dp}} = (n + 1)d\omega_1 \quad \text{and} \quad d\omega_2 = 0 \quad \text{for } f_1\text{-sweeps} \quad (3.6)$$

and

$$d\omega_{\text{dp}} = -nd\omega_2 \quad \text{and} \quad d\omega_1 = 0 \quad \text{for } f_2\text{-sweeps.} \quad (3.7)$$

The various phases in equations 3.4 and 3.5 are a function of the ω_i 's and of the DPOAE generation place x_g . Since x_g is assumed constant in the place-fixed hypothesis, only the frequency dependence will remain. The same consideration applies for the wave-fixed hypothesis during an f_1 -sweep when x_g equals the constant X_2 . However, in the wave-fixed hypothesis, where, e.g., $x_g = X_2$ changes during an f_2 -sweep, the DPOAE group delay is not only determined by phase-frequency gradients at one place but also by phase-place gradients at one frequency. To that end we will translate each phase-place gradient into a phase-frequency gradient so that all phase changes can be described as phase-frequency gradients. In addition, the original wave-fixed model has to be extended with a description of the characteristic frequency-place relation. We therefore make the following assumptions:

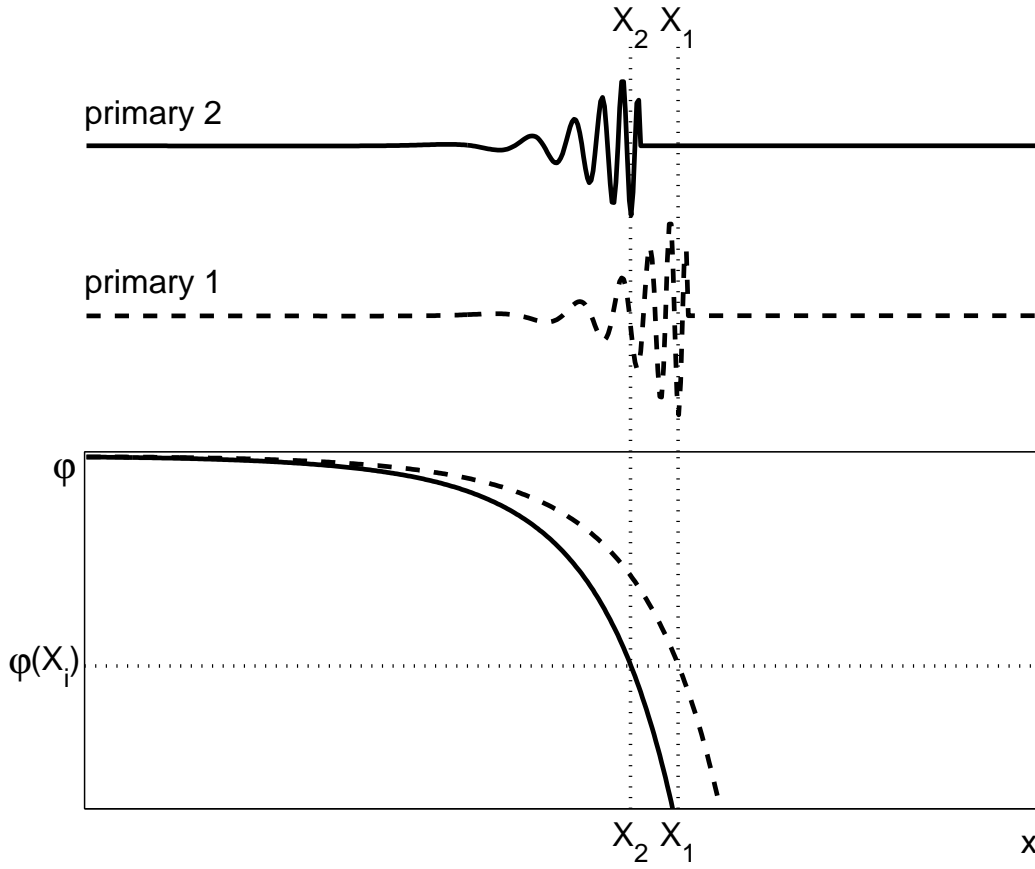


Figure 3.1: Schematic representation of the mechanical response of the basilar membrane in response to primaries with frequencies f_1 and f_2 ($f_1 < f_2$). The figure demonstrates the principal consequence of cochlear scale invariance, i.e., that the phase of the response at the characteristic place is independent of frequency.

- III.** In a restricted region near x_g the phase distribution of a primary along the basilar membrane is frequency invariant, apart from a shift along the membrane that corresponds to the shift in frequency.
- IV.** The characteristic frequencies are logarithmically distributed along the basilar membrane.

Assumption III, the “frequency-shift invariance”, is a local approximation of the scale invariance of the cochlea (Zweig and Shera, 1995; Talmadge *et al.*, 1999, 2000) that was also used in the present context by, e.g., Moulin and Kemp (1996a,b). A visualization of this concept is given in figure 3.1, which also illustrates that, as a consequence, the phase at the characteristic place is independent of frequency. Assumption IV implies that

$$\frac{d\omega_i}{dX_i} = -\frac{\omega_i}{C}, \quad (3.8)$$

where C is a positive constant. Combination of assumptions III and IV results in the relation of the phase-place and phase-frequency gradients that takes an essential part in the analysis (see the Appendix):

$$\frac{\partial\varphi(x_g; \omega_i)}{\partial x_g} = \frac{\partial\varphi(x_g; \omega_i)}{\partial \omega_i} \frac{\omega_i}{C}. \quad (3.9)$$

Equations 3.1-3.9 form the base of the further analysis. In the original place- and wave-fixed hypotheses x_g is identified with the X_2 of the primary pair (f_1, f_2) . This concept is elaborated in the next section. Since several studies suggest that for the USB DPOAEs x_g is basally from X_2 , close to X_{dp} , a second section is dedicated to the assumption that for these DPOAEs $x_g = X_{dp}$.

3.2.1 Analysis with x_g related to X_2

The place-fixed model

In this model $dx_g = 0$, during both f_1 - and f_2 -sweeps. Therefore, only phase-frequency gradients are left in equations 3.4 and 3.5. With implementation of the $d\omega_i$ relations (equations 3.6 and 3.7) the following descriptions of the f_1 - and f_2 -sweep group delays are found:

$$D_1 = -\frac{\partial\varphi(X_2; \omega_1)}{\partial \omega_1} - \frac{\partial\bar{\varphi}(X_2; \omega_{dp})}{\partial \omega_{dp}}, \quad (3.10)$$

$$D_2 = -\frac{\partial\varphi(X_2; \omega_2)}{\partial \omega_2} - \frac{\partial\bar{\varphi}(X_2; \omega_{dp})}{\partial \omega_{dp}}. \quad (3.11)$$

Both delays are the sum of the forward delay of the sweeping primary and the retrograde delay of the DP, which is equal in both expressions. Relations between D_1 and D_2 are

$$D_2 - D_1 = -\frac{\partial\varphi(X_2; \omega_2)}{\partial \omega_2} + \frac{\partial\varphi(X_2; \omega_1)}{\partial \omega_1} \quad (3.12)$$

and

$$\frac{D_2}{D_1} = \frac{-\frac{\partial\varphi(X_2; \omega_2)}{\partial \omega_2} - \frac{\partial\bar{\varphi}(X_2; \omega_{dp})}{\partial \omega_{dp}}}{-\frac{\partial\varphi(X_2; \omega_1)}{\partial \omega_1} - \frac{\partial\bar{\varphi}(X_2; \omega_{dp})}{\partial \omega_{dp}}}. \quad (3.13)$$

Equation 3.12 means that, in the place-fixed model, the difference of the DPOAE group delay as measured with f_1 - and f_2 -sweeps is equal to the difference in forward group delay of the respective primaries at the place of maximal DP generation, here X_2 . This difference is independent of the order of the DPOAE. Since the forward delay of f_2 to X_2 is larger than that of the smaller frequency f_1 (see figure 3.1), D_2 is larger than D_1 .

The wave-fixed model

In this model $x_g = X_2$ is constant during f_1 -sweep and changes with frequency during f_2 -sweep. Hence, during the f_1 -sweep the hypotheses of place- and wave-fixed models are equal and D_1 in the wave-fixed model is identical to the expression given in equation 3.10 for the place-fixed model. During an f_2 -sweep the first primary is constant, and as a result of the frequency-shift invariance the phase of the second primary at the moving generation site X_2 does not change either (cf. figure 3.1). Therefore, \vec{D}_2 is affected only by X_2 moving through the f_1 -wave, as induced by the f_2 -sweep. The retrograde delay is affected by both the change in generation site and in DP frequency. Here we use the translation of phase-place gradients into phase-frequency gradients (see the Appendix). Combining the forward and retrograde delays we can describe D_2 as

$$D_2 = \frac{(n+1)}{n} \frac{\omega_1}{\omega_2} \left(-\frac{\partial \varphi(X_2; \omega_1)}{\partial \omega_1} - \frac{\partial \bar{\varphi}(X_2; \omega_{dp})}{\partial \omega_{dp}} \right). \quad (3.14)$$

Clearly, D_2 depends on the order of the DPOAE. The relations of D_1 and D_2 are

$$D_2 - D_1 = \frac{(n+1)\omega_1 - n\omega_2}{n\omega_2} \left(-\frac{\partial \varphi(X_2; \omega_1)}{\partial \omega_1} - \frac{\partial \bar{\varphi}(X_2; \omega_{dp})}{\partial \omega_{dp}} \right) \quad (3.15)$$

and

$$\frac{D_2}{D_1} = \frac{(n+1)}{n} \frac{\omega_1}{\omega_2}. \quad (3.16)$$

Thus, in the wave-fixed model, the ratio of the delays D_2 and D_1 depends only on the order of the DPOAE and on the frequency ratio of the primaries at which the phase gradients are taken.

3.2.2 Analysis for the USB DPOAEs with x_g related to X_{dp}

In order to investigate the implication of a more basal generation site for the upper sideband DPOAEs in both the place- and wave-fixed models we calculated D_1 and D_2 using the assumption that this site is at the characteristic place of the DP: $x_g = X_{dp}$.

The place-fixed model

When the DPOAE generation site is at X_{dp} this location changes when either f_1 or f_2 is swept. In the place-fixed model this variation is neglected and consequently $dx_g = 0$. The delays thus depend only on the changes in the ω_i 's so that equations 3.4 and 3.5 can be reduced and D_1 and D_2 can be expressed as (cf. equations 3.10 and 3.11):

$$D_1 = -\frac{\partial \varphi(X_{dp}; \omega_1)}{\partial \omega_1} - \frac{\partial \bar{\varphi}(X_{dp}; \omega_{dp})}{\partial \omega_{dp}}, \quad (3.17)$$

$$D_2 = -\frac{\partial \varphi(X_{dp}; \omega_2)}{\partial \omega_2} - \frac{\partial \bar{\varphi}(X_{dp}; \omega_{dp})}{\partial \omega_{dp}}. \quad (3.18)$$

The second term in equations 3.17 and 3.18 represents the retrograde group delay of the DP from X_{dp} back to the ear canal, which is identical in D_1 and D_2 . Therefore, the difference of D_2 and D_1 equals the difference in the forward group delays of both primaries at the generation site:

$$D_2 - D_1 = -\frac{\partial\varphi(X_{dp};\omega_2)}{\partial\omega_2} + \frac{\partial\varphi(X_{dp};\omega_1)}{\partial\omega_1}. \quad (3.19)$$

The ratio of both delays can be expressed as

$$\frac{D_2}{D_1} = \frac{-\frac{\partial\varphi(X_{dp};\omega_2)}{\partial\omega_2} - \frac{\partial\bar{\varphi}(X_{dp};\omega_{dp})}{\partial\omega_{dp}}}{-\frac{\partial\varphi(X_{dp};\omega_1)}{\partial\omega_1} - \frac{\partial\bar{\varphi}(X_{dp};\omega_{dp})}{\partial\omega_{dp}}}. \quad (3.20)$$

The wave-fixed model

In the wave-fixed model the generation place x_g ($= X_{dp}$) changes both when f_1 and when f_2 is swept. The frequency-shift invariance implies that the retrograde delays from X_{dp} are zero. Using the relations between DP and primary frequencies, the logarithmical frequency map, and the transformation of phase-place into phase-frequency gradients (see the Appendix), we can write D_1 and D_2 as

$$D_1 = -n \frac{\omega_2}{\omega_{dp}} \left(\frac{\partial\varphi(X_{dp};\omega_2)}{\partial\omega_2} - \frac{\partial\varphi(X_{dp};\omega_1)}{\partial\omega_1} \right), \quad (3.21)$$

$$D_2 = -(n+1) \frac{\omega_1}{\omega_{dp}} \left(\frac{\partial\varphi(X_{dp};\omega_2)}{\partial\omega_2} - \frac{\partial\varphi(X_{dp};\omega_1)}{\partial\omega_1} \right). \quad (3.22)$$

Note that both D_1 and D_2 are proportional to the difference of the $-\frac{\partial\varphi(X_{dp};\omega_i)}{\partial\omega_i}$ for $i = 1, 2$, i.e., of the group delays of the primaries at X_{dp} . The difference between D_1 and D_2 reads

$$D_2 - D_1 = -\frac{\partial\varphi(X_{dp};\omega_2)}{\partial\omega_2} + \frac{\partial\varphi(X_{dp};\omega_1)}{\partial\omega_1}, \quad (3.23)$$

which is equal to the expression for the place-fixed model (equation 3.19). The ratio of D_2 and D_1 is

$$\frac{D_2}{D_1} = \frac{(n+1)}{n} \frac{\omega_1}{\omega_2}, \quad (3.24)$$

which is equal to the expression found for the lower sideband DPOAEs using the wave-fixed hypothesis with $x_g = X_2$ (equation 3.16).

3.3 Results

In figure 3.2 the ratio D_2/D_1 , predicted by the wave-fixed hypothesis (equations 3.16 and 3.24), is compared with experimental data from the guinea pig (chapter 2). The DPOAEs

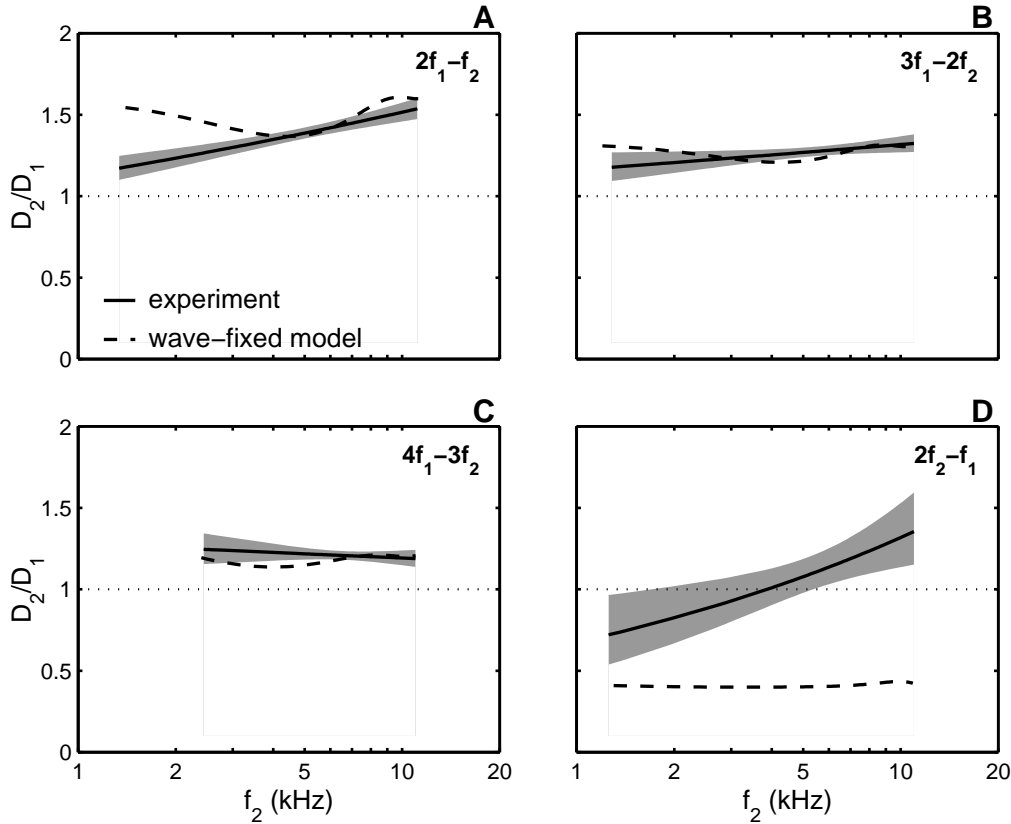


Figure 3.2: Validation of the wave-fixed model against experimental data for the guinea pig (chapter 2). The ratio of group delays measured with f_2 - and f_1 -sweep paradigms, D_2/D_1 , is plotted as a function of f_2 . Solid line and shaded area represent mean and 95% confidence interval for the experimental data; the dashed lines give the predictions from the wave-fixed model (equation 3.16).

with frequencies $2f_1 - f_2$, $3f_1 - 2f_2$, $4f_1 - 3f_2$, and $2f_2 - f_1$ were measured, with both the f_1 - and the f_2 -sweep paradigms. Group delays D_1 and D_2 were determined at the primary frequency ratio f_2/f_1 that yielded the maximum DPOAE level. The group delay versus f_2 curves were fitted with a double-logarithmic regression line. The f_1 - and f_2 -sweep fits were subtracted which resulted in the fits for D_2/D_1 as a function of f_2 as presented in this figure (solid lines, with 95% confidence interval; for details see chapter 2). For the prediction of the wave-fixed hypothesis, the experimental ratios f_2/f_1 that yielded the maximum DPOAE levels were substituted in equation 3.16. This resulted in the dashed lines in figure 3.2. For the lower sideband DPOAEs $2f_1 - f_2$, $3f_1 - 2f_2$, and $4f_1 - 3f_2$, there is good agreement between the experimental group delay ratio D_2/D_1 and the ratio predicted by the wave-fixed theory (figure 3.2A, B, C), except for the lower frequencies of the $2f_1 - f_2$ (figure 3.2A). The experimental results of the upper sideband DPOAE $2f_2 - f_1$ are not consistent with the wave-fixed theory with the assumptions made in our theoretical analysis (figure 3.2D).

3.4 Discussion

Distortion product otoacoustic emissions provide a simple and powerful technique to study fundamental properties of cochlear filter processes. After many studies had focused on DPOAE amplitudes, the analysis of DPOAE phase to derive measures of group delay was introduced by Kimberley *et al.* (1993). While these and other authors primarily used the f_1 -sweep paradigm, others advocated the f_2 -sweep paradigm (O'Mahoney and Kemp, 1995; Moulin and Kemp, 1996a; Wable *et al.*, 1996). The origin of the difference between the two sweep paradigms and between the delays of upper and lower sideband DPOAEs has not been fully understood. Such understanding is required before f_1 - and f_2 -sweep group delays can be interpreted in terms of other measures of delay in the cochlea (e.g., Anderson *et al.*, 1971; Goldstein *et al.*, 1971; Eggermont, 1979; Versnel *et al.*, 1992; Kimberley *et al.*, 1993; Whitehead *et al.*, 1996; Talmadge *et al.*, 2000). Similarly, a better comprehension of DPOAE group delays may contribute to our knowledge of fundamental properties of the cochlear filter process. The lack of understanding of DPOAE group delays is due to incomplete knowledge of (1) retrograde phase delays, (2) the generation site of USB versus LSB DPOAEs, (3) group delays of possible contributions from the f_{dp} characteristic place for LSB components, and (4) spatial phase changes of one primary read out when sweeping the other. The principal aim of the present chapter was to give a comprehensive description of particularly the last issue. Based on several assumptions, mathematical descriptions of D_1 and D_2 could be derived for both the place-fixed and the wave-fixed model, several of which could be tested against experimental data.

3.4.1 Assumptions and theoretical considerations

The analysis is based on four main assumptions. The assumed frequency-shift invariance of the frequency-place relation (assumption III) is a local approximation of the generally accepted concept of cochlear scale invariance (Sondhi, 1978; Viergever, 1980; Zweig and Shera, 1995), incorporated in the analysis of DPOAE group delays by several authors (Moulin and Kemp, 1996b; Talmadge *et al.*, 1998, 1999, 2000). The assumed logarithmic tonotopic map (assumption IV) finds similarly general application.

The neglect of contributions to the DPOAE recorded in the ear canal other than from the generation site (assumption II) is not self-evident. For LSB DPOAEs contributions from particularly the DP characteristic place have been identified (Kummer *et al.*, 1995; Brown *et al.*, 1996; Martin *et al.*, 1987, 1998). In the two-source model, recently described by Shera and Guinan (1999) and Talmadge *et al.* (1998; 1999), the DPOAE in the ear canal is a combination of the component generated by nonlinear interaction of the primaries around X_2 , and a component arising from linear coherent reflection of the apically traveling wave close to X_{dp} . The relative strength of those two components depends among others on the primary levels and the primary frequency ratio (Fahey and Allen, 1997; Knight and Kemp, 2000). The interference of the reflection component with the generation component is thought to be responsible for the fine structure in the DPOAE amplitude and for irregularities in the phase-frequency profile (Brown *et al.*, 1996; Heitmann *et al.*, 1998; Talmadge *et al.*, 1999). In this study, we have mainly focused at the

X_2 generation site component since all group delay studies referred to in the present context were performed at the best f_2/f_1 ratio where that component presumably dominates the response (Knight and Kemp, 2000). Possible effects of residual reflection components on measured phase-frequency profiles, and therefore on DPOAE group delays, are further averaged out when considering group average data as was done, e.g., in figure 3.2. Yet, some extension of the theory to the reflection component is feasible. As a corollary the last section of the Appendix indicates (assuming that both the generation and the reflection processes obey wave-fixed mechanisms) that the D_2/D_1 relation derived for the wave-fixed model applies also for the reflection component itself. Therefore the results regarding the D_2/D_1 ratio hold also if the measured DPOAE is dominated by the reflection component. The intermediate situation, where both components are approximately equal, is more difficult to interpret. More fundamentally, while DP generation at X_2 is likely to obey wave-fixed mechanisms, reflection at X_{dp} is thought to be due to local anatomical irregularities and therefore must have an essentially place-fixed character, a notion supported by recent experimental data (Talmadge *et al.*, 1999). An extension of the analysis for the wave-fixed generation component with a place-fixed reflection component greatly complicates the analysis and prohibits the formulation of transparent expressions for either $D_2 - D_1$ or D_2/D_1 .

Finally, the assumption was made that DP generation is concentrated on a single place x_g (assumption I). In the real situation the generation of nonlinear distortion is obviously distributed over a certain range along the cochlear partition where f_1 and f_2 activation patterns overlap. The assumption is thus based on a “center of mass” representation of this distributed source. The model, in fact, does not require x_g to be equal to, e.g., the place X_2 with characteristic frequency f_2 as defined, e.g., with a neural frequency threshold curve, but merely states that x_g is fixed to (and shifting with) the envelope of the f_2 response. This also means that, for example, x_g may depend on the level of the primaries.

After application of these assumptions the analysis leads to expressions for D_1 and D_2 fully in terms of phase-frequency gradients, in both the place-fixed and the wave-fixed models. Several aspects of these expressions are noteworthy. First, in the comparisons of D_1 and D_2 no explicit assumptions were made regarding (in)equality of forward and retrograde group delays. The expressions for $D_2 - D_1$ in the place-fixed model and for D_2/D_1 in the wave-fixed model (equations 3.12 and 3.16) are independent of the absolute values of the retrograde delay. In contrast, the retrograde delay term is explicitly included in the other expressions, equations 3.13 and 3.15. Second, the D_2/D_1 ratio in the wave-fixed model (equation 3.16) depends only on the order of the DPOAE and on the frequency ratio of the primaries. Thus, D_2/D_1 does not depend on parameters such as stimulus level, the absolute primary frequencies, and, e.g., a possible pathological condition of the cochlea, as long as the assumptions are, not violated. Several of these predictions can be subjected to experimental verification. Both the place-fixed and the wave-fixed models lead to the conclusion that $D_2 > D_1$, as can be seen from equations 3.12 and 3.16. Finally, since the predicted D_2/D_1 for the USB component in the wave-fixed model is identical whether X_2 or X_{dp} is the assumed generation place (equations 3.16 and 3.24), no distinction between those two alternatives can be made on the basis of the present analysis.

3.4.2 Comparison with earlier theoretical analyses of f_1 - and f_2 -sweep group delays

Several general properties of f_1 - and f_2 -sweep group delays were already indicated by Moulin and Kemp (1996b). The present analysis reconfirms and extends several of their results, and particularly gives a more thorough theoretical foundation to others. In their analysis of the place-fixed model forward delays were predicted to be larger for the f_2 - than for the f_1 -sweep paradigm; retrograde delays were implicitly assumed to be equal, making $D_2 > D_1$; their mathematical expressions were partly identical to those in the present chapter. The same authors elaborated the wave-fixed model on the basis of additional qualitative assumptions, and also predicted forward delays larger with the f_2 - than with the f_1 -sweep. A quantitative expression could not be given, since no explicit expression for the spatial phase changes of the f_1 -wave, read out by the moving X_2 , was available. No explicit indication was given of the difference of retrograde delays in the wave-fixed model. Similarly, Moulin and Kemp (1996b) derived predictions regarding the relative group delays of different order DPOAEs. The predicted equality of forward delays in the place-fixed model, irrespective of the order of the DPOAE or the choice of sweep paradigm, was more formally reproduced in the present theory. For the wave-fixed model, forward delays were predicted to depend on DPOAE order in a qualitatively very similar way as in the present theory. Again, however, since no explicit expression could be given regarding the spatial phase changes of the f_1 -wave, no definite quantitative results could be formulated by Moulin and Kemp (1996b).

In a different approach, Bowman *et al.* (1997, 1998) developed a description of DPOAE delays in which the build-up time of the cochlear filter plays an important role. They posed that, since generation takes place in the X_2 -region where rapid phase changes of f_2 occur, the filter build-up time is included in the DPOAE delay for the f_2 -sweep, but not for the f_1 -sweep. In their view, DPOAE delays are the sum of a forward delay of the primaries to the generation place, a filter response time, and a backward delay of the DP component. A possible link between that approach and the place-fixed and wave-fixed models is not evident at the present stage. Yet, given that the concept of a change of generation place in the f_2 -sweep paradigm was not explicitly accounted for by these authors, their approach is essentially place-fixed. The observation of Bowman *et al.* (1997) that $D_2 - D_1$ decreases with increasing stimulus levels is at least qualitatively consistent with a stimulus-independent D_2/D_1 ratio predicted by the present theory, given the decrease of both D_2 and D_1 with intensity demonstrated by Bowman *et al.* (1997). Recently, the expression for the D_2/D_1 ratio in the wave-fixed model (equation 3.16) was simultaneously presented in preliminary form by ourselves (Schneider *et al.*, 2000) and (for $n = 1$) by Talmadge *et al.* (2000).

3.4.3 Validation against experimental data

The formal mathematical character of the expressions for D_1 and D_2 does not allow a direct quantitative validation of the theory against experimental data. The only simple expression allowing such validation is the D_2/D_1 ratio in the wave-fixed model (equation

3.16). From the other expressions the difference $D_2 - D_1$ in the place-fixed model (equation 3.12) allows some qualitative interpretation that can be compared to experimental data.

The results shown in figure 3.2A, B, and C indicate that the theoretically predicted D_2/D_1 ratio quantitatively matches the experimental data for each LSB DPOAE component, and that it shows the appropriate dependence on the order of the DPOAE. The experimental data used for this comparison are consistent with other published data on D_2/D_1 (Moulin and Kemp, 1996b; Whitehead *et al.*, 1996). Regarding the values of D_1 and D_2 themselves, for the LSB components, D_1 was found to be invariant with the order of the DPOAE, while D_2 decreases with increasing order (chapter 2; Moulin and Kemp, 1996b). This dependence is theoretically predicted in the wave-fixed model but not in the place-fixed model, where the delay difference $D_2 - D_1$ should be order independent (equations 3.12 and 3.15). Therefore we conclude that, for the above-mentioned data, the variation with f_1 - versus f_2 -sweep of LSB DPOAE group delays and their dependence on DPOAE order are consistent with the wave-fixed model, and not with the place-fixed model.

The theoretical prediction of the group delay ratio D_2/D_1 for the $2f_2 - f_1$ upper sideband component shows a large discrepancy with the experimental data (figure 3.2D). Apparently, the wave-fixed model combined with the further assumptions made is not appropriate for this component, independent whether X_2 or X_{dp} is assumed to be the dominant generation site; this may be due to inappropriate description of the shift of the generation site with changing primaries, and therefore does not necessarily conflict with the notion that for the USB components x_g is probably close to X_{dp} . Some further quantitative validation in terms of a comparison of USB versus LSB components is possible if both would obey the place-fixed model. From the theory the difference $D_2 - D_1$ is larger for the LSB generated at X_2 than for the USB generated at X_{dp} (equation 3.12 versus 3.19), because particularly the first term in equation 3.12 is dominant (cf. figure 3.1). Our experimental data are consistent with this prediction when a comparison is made, e.g., between $2f_1 - f_2$ and $2f_2 - f_1$ components (chapter 2). This comparison, however, is precarious since the place-fixed model had already appeared inappropriate for the LSB components. As far as the present analysis reaches, the place-fixed model cannot be rejected for the USB components if generated basally from the primary region.

3.5 Conclusions

A theoretical analysis was presented of the phase behavior of distortion product otoacoustic emissions, which aims at elucidating the differences between delays observed in the f_1 - and in the f_2 -sweep paradigm, D_1 and D_2 , respectively. By making a local approximation of the cochlear scale invariance, a mathematical conversion from phase-place to phase-frequency gradients could be formulated. This allows incorporating the effects of a spatial shift of the X_2 generation place in the f_2 -sweep paradigm in the wave-fixed model. In this way expressions could be derived for D_1 , D_2 , and their ratios and differences in either of the two models, under the condition where the DPOAE recorded in the ear canal is dominated by the contribution from the generation site, and not, e.g., by reflection components.

Experimental validation of these expressions indicates that group delays of lower sideband DPOAEs ($2f_1 - f_2$, $3f_1 - 2f_2$, $4f_1 - 3f_2$) are most consistent with the wave-fixed model. In particular, the difference between the group delays obtained with f_1 - and f_2 -sweeps could be fully explained by the shift of the X_2 generation site in the f_2 -sweep paradigm. Group delays of the upper sideband DPOAE ($2f_2 - f_1$) are inconsistent with both wave-fixed and place-fixed models, independent of whether DP generation is assumed to take place at the f_2 characteristic place or at the f_{dp} characteristic place. Apparently, the assumptions made regarding the location of the generation site combined with its shift when sweeping either of the two primaries are inappropriate.

3.6 Appendix

3.6.1 Frequency-shift invariance

As a consequence of assumption III the phase $\varphi(X_i; \omega_i)$ of a particular frequency ω_i at its characteristic place X_i is equal for all frequencies (see figure 3.1):

$$\frac{d\varphi(X_i; \omega_i)}{d\omega_i} = \frac{\partial\varphi(X_i; \omega_i)}{\partial\omega_i} + \frac{\partial\varphi(X_i; \omega_i)}{\partial X_i} \frac{dX_i}{d\omega_i} = 0. \quad (3.25)$$

The frequency-shift invariance prescribes that when the radial frequency is changed from ω_i to ω'_i the new phase at x_g can be found from the original phase distribution for ω_i at place x'_g (figure 3.3):

$$\varphi(x_g; \omega'_i) = \varphi(x'_g; \omega_i), \quad (3.26)$$

where $x'_g = x_g + \Delta x_g$, and $(-\Delta x_g)$ corresponds to the change in characteristic place from X_i to X'_i : $\Delta x_g = -\Delta X_i = -(X'_i - X_i)$. Therefore, we can write

$$\frac{\varphi(x'_g; \omega_i) - \varphi(x_g; \omega_i)}{\Delta x_g} = \frac{\varphi(x_g; \omega'_i) - \varphi(x_g; \omega_i)}{\Delta x_g} = -\frac{\varphi(x_g; \omega'_i) - \varphi(x_g; \omega_i)}{\Delta X_i}. \quad (3.27)$$

Now we can formulate the desired relation of a phase-place gradient and a phase-frequency gradient:

$$\frac{\partial\varphi(x_g; \omega_i)}{\partial x_g} = -\frac{\partial\varphi(x_g; \omega_i)}{\partial\omega_i} \frac{d\omega_i}{dX_i}, \quad (3.28)$$

where $\frac{d\omega_i}{dX_i}$ can be found from assumption IV expressed as

$$\frac{d\omega_i}{dX_i} = -\frac{\omega_i}{C}, \quad (3.29)$$

where C is a constant. Combination of equations 3.28 and 3.29 results in

$$\frac{\partial\varphi(x_g; \omega_i)}{\partial x_g} = \frac{\partial\varphi(x_g; \omega_i)}{\partial\omega_i} \frac{\omega_i}{C}. \quad (3.30)$$

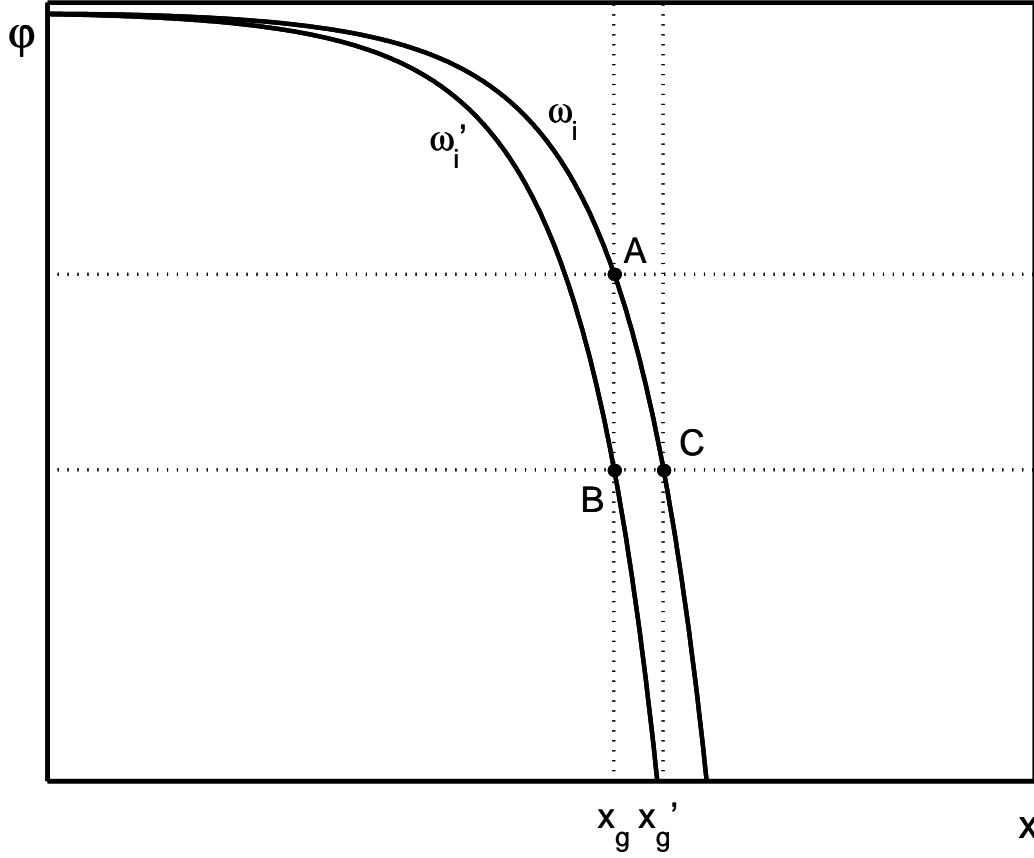


Figure 3.3: Illustration of the conversion from phase-place to phase-frequency gradients (equation 3.30). The phase of ω_i at place x_g is given by $\varphi(x_g; \omega_i)$ (point A). When the frequency is changed from ω_i to ω'_i , the new phase $\varphi(x_g; \omega'_i)$ of ω'_i at place x_g (point B) can be found from the original phase distribution of ω_i at place x'_g ($\varphi(x'_g; \omega_i)$; point C), with $x'_g = x_g + \Delta x_g$ and $\Delta x_g = X_i - X'_i$, the difference between the characteristic places of the frequencies ω_i and ω'_i .

3.6.2 The wave-fixed model

x_g related to X_2

Since in the wave-fixed model for the f_2 -sweep the DP generation place is thought to shift according to the X_2 , the forward DPOAE group delay (equation 3.4) can be expressed in relation to the primary parameters X_2 , ω_1 , and ω_2 :

$$\begin{aligned} \vec{D}_2 = & -(n+1) \left(\frac{\partial \varphi(X_2; \omega_1)}{\partial \omega_1} \frac{d\omega_1}{d\omega_{dp}} + \frac{\partial \varphi(X_2; \omega_1)}{\partial X_2} \frac{dX_2}{d\omega_2} \frac{d\omega_2}{d\omega_{dp}} \right) \\ & + n \frac{d\omega_2}{d\omega_{dp}} \left(\frac{\partial \varphi(X_2; \omega_2)}{\partial \omega_2} + \frac{\partial \varphi(X_2; \omega_2)}{\partial X_2} \frac{dX_2}{d\omega_2} \right), \end{aligned} \quad (3.31)$$

in which the first term is zero because ω_1 is constant ($d\omega_1 = 0$) and the last two terms together are zero as a direct consequence of the frequency-shift invariance (equation 3.25). This means that when using the f_2 -sweep paradigm the forward delay is affected by a change in phase of the f_1 component at the generation site caused by the variation of this site. The phase-place gradient can be translated into a phase-frequency gradient (equation 3.30):

$$\vec{D}_2 = -(n+1) \left(\frac{\partial \varphi(X_2; \omega_1)}{\partial \omega_1} \frac{\omega_1}{C} \frac{dX_2}{d\omega_2} \frac{d\omega_2}{d\omega_{dp}} \right). \quad (3.32)$$

When equations 3.7 and 3.29 are applied, the expression of this forward delay becomes

$$\vec{D}_2 = \frac{(n+1)}{n} \frac{\omega_1}{\omega_2} \left(-\frac{\partial \varphi(X_2; \omega_1)}{\partial \omega_1} \right). \quad (3.33)$$

Similarly, the backward delay is written as

$$\overleftarrow{D}_2 = -\frac{\partial \overleftarrow{\varphi}(X_2; \omega_{dp})}{\partial \omega_{dp}} - \frac{\partial \overleftarrow{\varphi}(X_2; \omega_{dp})}{\partial X_2} \frac{dX_2}{d\omega_2} \frac{d\omega_2}{d\omega_{dp}}. \quad (3.34)$$

Again applying the relation between the changes in ω_2 and ω_{dp} (equation 3.7), using the frequency-shift invariance and the logarithmic distribution of the characteristic frequencies (equations 3.29 and 3.30) \overleftarrow{D}_2 is written as

$$\overleftarrow{D}_2 = -\frac{\partial \overleftarrow{\varphi}(X_2; \omega_{dp})}{\partial \omega_{dp}} - \left(\frac{\partial \overleftarrow{\varphi}(X_2; \omega_{dp})}{\partial \omega_{dp}} \frac{\omega_{dp}}{C} \right) \frac{dX_2}{d\omega_2} \frac{(-1)}{n} = -\frac{\partial \overleftarrow{\varphi}(X_2; \omega_{dp})}{\partial \omega_{dp}} \left(1 + \frac{\omega_{dp}}{n\omega_2} \right). \quad (3.35)$$

With use of the relation between ω_1 , ω_2 , and ω_{dp} (equation 3.2) the backward delay \overleftarrow{D}_2 can be rewritten as

$$\overleftarrow{D}_2 = \frac{(n+1)}{n} \frac{\omega_1}{\omega_2} \left(-\frac{\partial \overleftarrow{\varphi}(X_2; \omega_{dp})}{\partial \omega_{dp}} \right). \quad (3.36)$$

Combination of the forward and the backward delay (equations 3.33 and 3.36) yields

$$D_2 = \frac{(n+1)}{n} \frac{\omega_1}{\omega_2} \left(-\frac{\partial \varphi(X_2; \omega_1)}{\partial \omega_1} - \frac{\partial \overleftarrow{\varphi}(X_2; \omega_{dp})}{\partial \omega_{dp}} \right). \quad (3.37)$$

USB DPOAEs with x_g related to X_{dp}

Here we assume the prominent contribution to the upper sideband DPOAEs to come from $x_g = X_{dp}$ that changes for both the f_1 - and f_2 -sweep paradigms.

$$\begin{aligned} \vec{D} = & -(n+1) \left(\frac{\partial \varphi(X_{dp}; \omega_1)}{\partial X_{dp}} \frac{dX_{dp}}{d\omega_{dp}} + \frac{\partial \varphi(X_{dp}; \omega_1)}{\partial \omega_1} \frac{d\omega_1}{d\omega_{dp}} \right) \\ & + n \left(\frac{\partial \varphi(X_{dp}; \omega_2)}{\partial X_{dp}} \frac{dX_{dp}}{d\omega_{dp}} + \frac{\partial \varphi(X_{dp}; \omega_2)}{\partial \omega_2} \frac{d\omega_2}{d\omega_{dp}} \right), \end{aligned} \quad (3.38)$$

$$\overleftarrow{D} = -\frac{\partial \overleftarrow{\varphi}(X_{dp}; \omega_{dp})}{\partial \omega_{dp}} - \frac{\partial \overleftarrow{\varphi}(X_{dp}; \omega_{dp})}{\partial X_{dp}} \frac{dX_{dp}}{d\omega_{dp}}. \quad (3.39)$$

Using the relation of relative changes in the ω_i 's (equations 3.6 and 3.7) in equation 3.38 we can describe the forward delays as

$$\vec{D}_1 = -(n+1) \frac{\partial \varphi(X_{dp}; \omega_1)}{\partial X_{dp}} \frac{dX_{dp}}{d\omega_{dp}} - \frac{\partial \varphi(X_{dp}; \omega_1)}{\partial \omega_1} + n \frac{\partial \varphi(X_{dp}; \omega_2)}{\partial X_{dp}} \frac{dX_{dp}}{d\omega_{dp}}, \quad (3.40)$$

$$\vec{D}_2 = -(n+1) \frac{\partial \varphi(X_{dp}; \omega_1)}{\partial X_{dp}} \frac{dX_{dp}}{d\omega_{dp}} - \frac{\partial \varphi(X_{dp}; \omega_2)}{\partial \omega_2} + n \frac{\partial \varphi(X_{dp}; \omega_2)}{\partial X_{dp}} \frac{dX_{dp}}{d\omega_{dp}}. \quad (3.41)$$

For simplification of these relations we used the frequency-shift invariance in combination with the logarithmic distribution of the characteristic frequencies over the basilar membrane (equations 3.29 and 3.30) as well as the relation between the $d\omega_i$'s (equations 3.6 and 3.7):

$$\vec{D}_1 = (n+1) \frac{\omega_1}{\omega_{dp}} \frac{\partial \varphi(X_{dp}; \omega_1)}{\partial \omega_1} - \frac{\partial \varphi(X_{dp}; \omega_1)}{\partial \omega_1} - n \frac{\omega_2}{\omega_{dp}} \frac{\partial \varphi(X_{dp}; \omega_2)}{\partial \omega_2}, \quad (3.42)$$

$$\vec{D}_2 = (n+1) \frac{\omega_1}{\omega_{dp}} \frac{\partial \varphi(X_{dp}; \omega_1)}{\partial \omega_1} - \frac{\partial \varphi(X_{dp}; \omega_2)}{\partial \omega_2} - n \frac{\omega_2}{\omega_{dp}} \frac{\partial \varphi(X_{dp}; \omega_2)}{\partial \omega_2}, \quad (3.43)$$

which can be reduced to

$$\vec{D}_1 = -n \frac{\omega_2}{\omega_{dp}} \left(\frac{\partial \varphi(X_{dp}; \omega_2)}{\partial \omega_2} - \frac{\partial \varphi(X_{dp}; \omega_1)}{\partial \omega_1} \right), \quad (3.44)$$

$$\vec{D}_2 = -(n+1) \frac{\omega_1}{\omega_{dp}} \left(\frac{\partial \varphi(X_{dp}; \omega_2)}{\partial \omega_2} - \frac{\partial \varphi(X_{dp}; \omega_1)}{\partial \omega_1} \right). \quad (3.45)$$

Both the backward delays, which are expressed by equation 3.39, are zero according to the frequency-shift invariance expressed by equation 3.25:

$$\bar{D}_1 = \bar{D}_2 = 0. \quad (3.46)$$

Therefore, the total group delays are equal to the forward delays:

$$D_1 = -n \frac{\omega_2}{\omega_{dp}} \left(\frac{\partial \varphi(X_{dp}; \omega_2)}{\partial \omega_2} - \frac{\partial \varphi(X_{dp}; \omega_1)}{\partial \omega_1} \right), \quad (3.47)$$

$$D_2 = -(n+1) \frac{\omega_1}{\omega_{dp}} \left(\frac{\partial \varphi(X_{dp}; \omega_2)}{\partial \omega_2} - \frac{\partial \varphi(X_{dp}; \omega_1)}{\partial \omega_1} \right). \quad (3.48)$$

3.6.3 LSB DPOAEs with OAE coming from reflection site X_{dp}

Here we assume the DP to be generated at $x_g = X_2$ from which a retrograde wave towards the base and a forward wave towards the apex starts. The latter wave is reflected at X_{dp} from where a retrograde wave starts. The contribution of this wave to the DPOAE has the group delay

$$D_i^r = \vec{D}_i(X_2; \omega_1, \omega_2) + \vec{D}_i(X_2 \rightarrow X_{dp}; \omega_{dp}) + \bar{D}_i(X_{dp}; \omega_{dp}), \quad (3.49)$$

where $\vec{D}_i(X_2; \omega_1, \omega_2)$ is the forward delay formulated earlier as \vec{D}_i , $\vec{D}_i(X_2 \rightarrow X_{\text{dp}}; \omega_{\text{dp}})$ is the forward delay for the generated DP traveling from X_2 to X_{dp} , and $\overleftarrow{D}_i(X_{\text{dp}}; \omega_{\text{dp}})$ is the retrograde delay of the reflected wave. The second term of equation 3.49 is written as

$$\vec{D}_i(X_2 \rightarrow X_{\text{dp}}; \omega_{\text{dp}}) = \vec{D}_i(X_{\text{dp}}; \omega_{\text{dp}}) - \vec{D}_i(X_2; \omega_{\text{dp}}), \quad (3.50)$$

so that equation 3.49 becomes

$$D_i^r = \vec{D}_i(X_2; \omega_1, \omega_2) + \vec{D}_i(X_{\text{dp}}; \omega_{\text{dp}}) + \overleftarrow{D}_i(X_{\text{dp}}; \omega_{\text{dp}}) - \vec{D}_i(X_2; \omega_{\text{dp}}). \quad (3.51)$$

According to assumption III or equation 3.25 the second and third component are zero. The resulting terms, for f_1 -sweep, give

$$D_1^r = \vec{D}_1(X_2; \omega_1, \omega_2) - \vec{D}_1(X_2; \omega_{\text{dp}}) = -\frac{\partial \varphi(X_2; \omega_1)}{\partial \omega_1} - \frac{\partial \varphi(X_2; \omega_{\text{dp}})}{\partial \omega_{\text{dp}}}, \quad (3.52)$$

and for f_2 -sweep

$$D_2^r = \vec{D}_2(X_2; \omega_1, \omega_2) - \vec{D}_2(X_2; \omega_{\text{dp}}) = \frac{(n+1)\omega_1}{n\omega_2} \left(-\frac{\partial \varphi(X_2; \omega_1)}{\partial \omega_1} - \frac{\partial \varphi(X_2; \omega_{\text{dp}})}{\partial \omega_{\text{dp}}} \right), \quad (3.53)$$

so that also for the DPOAE reflection component holds

$$\frac{D_2^r}{D_1^r} = \frac{(n+1)\omega_1}{n\omega_2}. \quad (3.54)$$

References

- Anderson, D. J., Rose, J. E., Hind, J. E., and Brugge, J. F. (1971). “Temporal position of discharges of single auditory nerve fibers with the cycle of a sine-wave stimulus: frequency and intensity effects,” *J. Acoust. Soc. Am.* **49**, 1131–1139.
- Bowman, D. M., Brown, D. K., Eggermont, J. J., and Kimberley, B. P. (1997). “The effect of sound intensity on f_1 -sweep and f_2 -sweep distortion product otoacoustic emissions phase delay estimates in human adults,” *J. Acoust. Soc. Am.* **101**, 1550–1559.
- Bowman, D. M., Eggermont, J. J., Brown, D. K., and Kimberley, B. P. (1998). “Estimating cochlear filter response properties from distortion product otoacoustic emission (DPOAE) phase delay measurements in normal hearing adults,” *Hearing Res.* **119**, 14–26.
- Brown, A. M., Harris, F. P., and Beveridge, H. A. (1996). “Two sources of acoustic distortion products from the human cochlea,” *J. Acoust. Soc. Am.* **100**, 3260–3267.
- Brown, A. M., and Kemp, D. T. (1984). “Suppressibility of the $2f_1 - f_2$ stimulated acoustic emissions in gerbil and man,” *Hearing Res.* **13**, 29–37.
- Eggermont, J. J. (1979). “Narrow-band AP latencies in normal and recruiting human ears,” *J. Acoust. Soc. Am.* **65**, 464–470.
- Fahey, P. F., and Allen, J. B. (1997). “Measurement of distortion product phase in the ear canal of the cat,” *J. Acoust. Soc. Am.* **102**, 2880–2891.
- Goldstein, J. L., Baer, T., and Kiang, N. Y. S. (1971). “A theoretical treatment of latency, group delay and tuning characteristics for auditory nerve responses to clicks and tones,” in *Physiology of the Auditory System*, edited by M. B. Sachs (National Educational Consultants, Baltimore), pp.133–141.
- Heitmann, J., Waldmann, B., Schnitzler, H.-U., Plinkert, P. K., and Zenner, H.-P. (1998). “Suppression of distortion product otoacoustic emissions (DPOAE) near $2f_1 - f_2$ removes DP-gram fine structure - Evidence for a secondary generator,” *J. Acoust. Soc. Am.* **103**, 1527–1531.
- Kemp, D. T. (1986). “Otoacoustic emissions, travelling waves and cochlear mechanisms,” *Hearing Res.* **22**, 95–104.

- Kimberley, B. P., Brown, D. K., and Eggermont, J. J. (1993). "Measuring human cochlear traveling wave delay using distortion product otoacoustic emission phase responses," J. Acoust. Soc. Am. **94**, 1343–1350.
- Knight, R. D., and Kemp, D. T. (2000). "Indications of different distortion product otoacoustic emission mechanisms from a detailed f_1 , f_2 area study," J. Acoust. Soc. Am. **107**, 457–473.
- Kummer, P., Janssen, T., and Arnold, W. (1995). "Suppression tuning characteristics of the $2f_1 - f_2$ distortion-product otoacoustic emission in humans," J. Acoust. Soc. Am. **98**, 197–210.
- Martin, G. K., Jassir, D., Stagner, B. B., Whitehead, M. L., and Lonsbury-Martin, B. L. (1998). "Locus of generation for the $2f_1 - f_2$ vs $2f_2 - f_1$ distortion-product otoacoustic emissions in normal-hearing humans revealed by suppression tuning, onset latencies, and amplitude correlations," J. Acoust. Soc. Am. **103**, 1957–1971.
- Martin, G. K., Lonsbury-Martin, B. L., Probst, R., Scheinin, S. A., and Coats, A. C. (1987). "Acoustic distortion products in rabbit ear canal. II. Sites of origin revealed by suppression contours and pure-tone exposures," Hearing Res. **28**, 191–208.
- Moulin, A., and Kemp, D. T. (1996a). "Multicomponent acoustic distortion product otoacoustic emission phase in humans. I. General characteristics," J. Acoust. Soc. Am. **100**, 1617–1639.
- Moulin, A., and Kemp, D. T. (1996b). "Multicomponent acoustic distortion product otoacoustic emission phase in humans. II. Implications for distortion product otoacoustic emissions generation," J. Acoust. Soc. Am. **100**, 1640–1662.
- O'Mahoney, C. F., and Kemp, D. T. (1995). "Distortion product otoacoustic emission delay measurement in human ears," J. Acoust. Soc. Am. **97**, 3721–3735.
- Schneider, S., Prijs, V. F., Schoonhoven, R., and van Hengel, P. W. J. (2000). " f_1 - versus f_2 -sweep group delays of distortion product otoacoustic emissions in the guinea pig; experimental results and theoretical predictions," in *Recent Developments in Auditory Mechanics*, edited by H. Wada, T. Takasaka, K. Ikeda, K. Ohyama, and T. Koike (World Scientific, Singapore), pp. 360–366.
- Shera, C. A., and Guinan, J. J. (1999). "Evoked otoacoustic emissions arise by two fundamentally different mechanisms: A taxonomy for mammalian OAEs," J. Acoust. Soc. Am. **105**, 782–798.
- Sondhi, M. M. (1978). "Method for computing motion in a two-dimensional cochlear model," J. Acoust. Soc. Am. **63**, 1468–1477.
- Talmadge, C. L., Long, G. R., Tubis, A., and Dhar, S. (1999). "Experimental confirmation of the two-source interference model for the fine structure of distortion product otoacoustic emissions," J. Acoust. Soc. Am. **105**, 275–292.

- Talmadge, C. L., Tubis, A., Long, G. R., and Piskorski, P. (1998). “Modeling otoacoustic emission and hearing threshold fine structures,” *J. Acoust. Soc. Am.* **104**, 1517–1543.
- Talmadge, C. L., Tubis, A., Tong, C., Long, G. R., and Dhar, S. (2000). “Temporal aspects of otoacoustic emissions,” in *Recent Developments in Auditory Mechanics*, edited by H. Wada, T. Takasaka, K. Ikeda, K. Ohyama, and T. Koike (World Scientific, Singapore), pp. 353–359.
- Versnel, H., Schoonhoven, R., and Prijs, V. F. (1992). “Single-fibre and whole-nerve responses to clicks as a function of sound intensity in the guinea pig,” *Hearing Res.* **59**, 138–156.
- Viergever, M. A. (1980). “Mechanics of the ear- A mathematical approach,” Ph.D. dissertation, Delft University of Technology (Delft University Press, Delft, The Netherlands).
- Wable, J., Collet, L., and Chéry-Croze, S. (1996). “Phase delay measurements of distortion product otoacoustic emissions at $2f_1 - f_2$ and $2f_2 - f_1$ in human ears,” *J. Acoust. Soc. Am.* **100**, 2228–2235.
- Whitehead, M. L., Stagner, B. B., Martin, G. K., and Lonsbury-Martin, B. L. (1996). “Visualization of the onset of distortion-product otoacoustic emissions, and measurement of their latency,” *J. Acoust. Soc. Am.* **100**, 1663–1679.
- Zweig, G., and Shera, C. A. (1995). “The origins of periodicity in the spectrum of otoacoustic emissions,” *J. Acoust. Soc. Am.* **98**, 2018–2047.

Chapter 4

DPOAE group delays from a nonlinear transmission line model of the cochlea

Abstract

A previously developed one-dimensional transmission line model of the cochlea was used to simulate DPOAE measurements in the guinea pig. Lower sideband DPOAEs $2f_1 - f_2$, $3f_1 - 2f_2$, and $4f_1 - 3f_2$ and upper sideband DPOAE $2f_2 - f_1$ were successfully generated by the model both with an f_1 -sweep and an f_2 -sweep paradigm. From the phase-versus frequency functions, group delays were calculated. The simulated f_1 - and f_2 -sweep group delays were compared with the experimental results from chapter 2.

4.1 Introduction

Over the years, several computational cochlea models have been described in literature that attempt to reproduce the experimental results found in basilar membrane, psychophysical, auditory nerve or ear canal measurements, in order to better understand the underlying principles of cochlear mechanics (de Boer, 1996). Helmholtz (1885) proposed a model in which the cochlea is a set of uncoupled filters, performing Fourier analysis of the incoming sound. After the traveling wave experiments by von Békésy in dead cochleas more refined transmission line models, which incorporated fluid coupling of the filters (Zwislocki, 1950; Allen and Sondhi, 1979), were introduced. Later the discovery that the live cochlea is an active nonlinear system resulted in the need for more complex models, accounting for nonlinear properties like the generation of distortion products (Hall, 1974; Duifhuis *et al.*, 1985; Matthews and Molnar, 1986; Kanis and de Boer, 1993; Neely and Stover, 1993; 1997).

The research project described in this thesis was part of a collaboration with the Department of Biophysics of the University of Groningen, where in the past two decades a nonlinear cochlea model has been developed and extensively studied. This model, which uses numerical time-domain methods instead of standard frequency domain techniques (since those are less suited to solve a nonlinear system), is used here to simulate the experiments on guinea pig distortion product otoacoustic emissions described in chapter 2. In addition, the model outcome is compared with the results from the analytical wave-fixed model of DPOAE generation given in chapter 3.

4.2 Methods

4.2.1 Model description

The cochlea model used for the DPOAE simulations is based on a model developed by Duifhuis *et al.* (1985). This model has been modified and extended over the years and was used to simulate both spontaneous and distortion product otoacoustic emissions successfully (van den Raadt and Duifhuis 1990; van den Raadt *et al.*, 1993; van Hengel *et al.*, 1996; Mauermann *et al.*, 1999; van Hengel and Duifhuis, 2000; Schneider *et al.*, 2000). The basics of the model are given below (see van Hengel (1996) for a detailed description). The model is a one-dimensional non-uniform transmission line with nonlinear parameters (for justification of the one-dimensional treatment see Duifhuis (1988)). The three-channel cochlea is reduced to two channels separated by the cochlear partition, which is divided into N sections (with $N > 300$). The motion of a section of the cochlear partition at position x is given by

$$m\ddot{y}(x) + d(x, \dot{y})\dot{y}(x) + s(x)y(x) = p(x). \quad (4.1)$$

which is a second-order differential equation of motion for a harmonic oscillator driven by $p(x)$, the pressure difference between the channels on either side of the cochlear partition. The cochlear fluids are considered incompressible, resulting in instantaneous coupling of

the sections. The position x is measured from the stapes, y and \dot{y} are the displacement and velocity of the cochlear partition in vertical direction, m is the mass (per mm^2) of the cochlear partition, which is assumed to be constant over the length, $s(x)$ is the non-constant stiffness (per mm^2), thus creating a place-frequency map, and $d(x, \dot{y})$ is the damping (per mm^2) which depends on the position x and is tuned to create a constant quality factor Q for all sections. In order to obtain generation of distortion products, the damping is made a nonlinear function of the velocity \dot{y} of the section. The values for the stiffness as function of position were derived from the place-frequency relation given by Greenwood (1990) for various species

$$f(x) = A \cdot 10^{\alpha x} - B \quad (4.2)$$

where position x is in this case measured as distance from the apex. The values of the parameters A and B vary for different species. One of the most recent adaptations to the model was the use of an impedance function with negative damping and a stabilizing delayed feedback, as suggested by Zweig (1991). This “Zweig impedance” produces a high and broad excitation peak to a pure tone stimulus, which was lacking from previous versions of the model. Results with the model, including the “Zweig impedance”, obtained in Oldenburg indicated that it is well suited for simulating DPOAEs as measured in human subjects (Mauermann *et al.*, 1999). Therefore the same version of the model was chosen to perform simulations of guinea pig DPOAEs for comparison with the experimental data described in chapter 2. Several parameters in the model, normally used to simulate a human cochlea, were adjusted to fit the guinea pig cochlea (see table 4.1).

Table 4.1: Several model parameters that were adjusted to simulate the guinea pig cochlea (Hemila *et al.*, 1995; Greenwood, 1990).

	human	guinea pig
surface of tympanic membrane	60 mm^2	23.9 mm^2
resonance frequency of the middle ear	2000 Hz	4000 Hz
transformation factor of middle ear	30	39.3
cross section of cochlear channels	1 mm	0.5 mm
surface of stapes	3.0 mm^2	0.81 mm^2
Greenwood map parameter A	165.4 Hz	350 Hz
Greenwood map parameter B	145.4 Hz	297.5 Hz
Greenwood map parameter α	0.060 mm^{-1}	0.1135 mm^{-1}

4.2.2 Stimuli and data analysis

All simulations were performed at the Department of Biophysics of the University of Groningen, by dr. ir. P. W. J. van Hengel and drs. J. M. Kruseman. For the simulations with the cochlea model the same stimulus paradigms as in the experiments (chapter 2) were used and both f_1 - and f_2 -sweeps were performed. From the sound pressure at

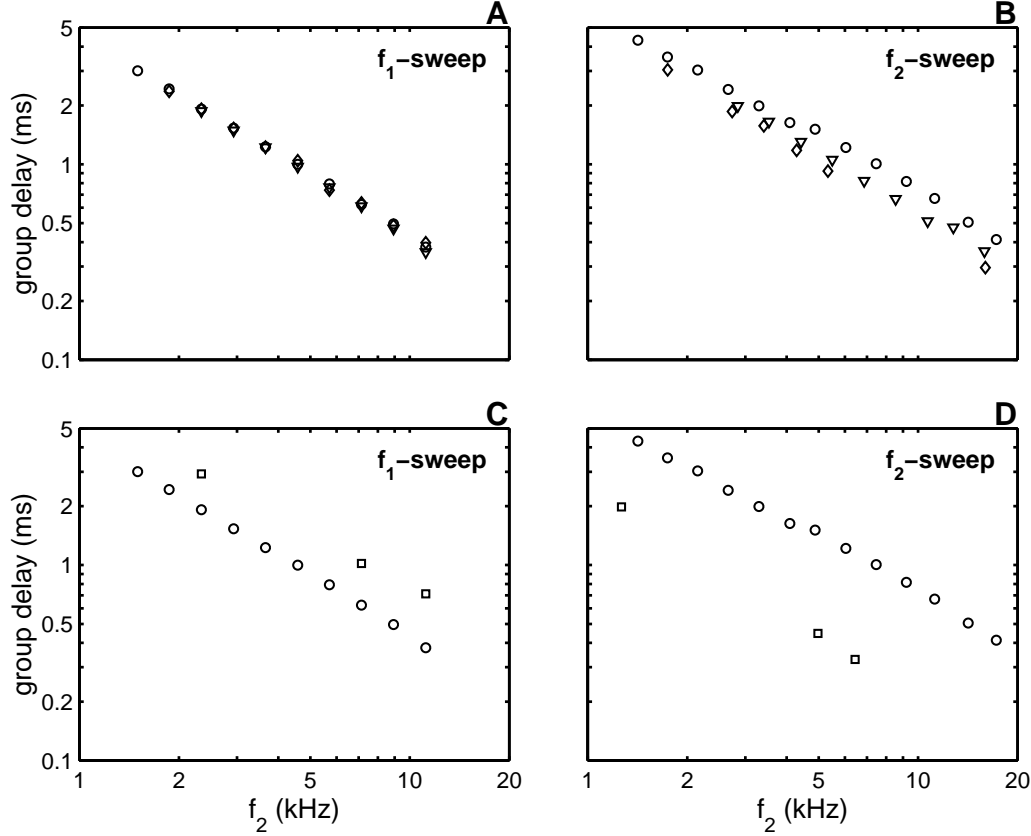


Figure 4.1: Simulated group delays from the cochlea model as a function of f_2 . (A) f_1 -sweep group delays of the three lower sideband DPOAEs $2f_1 - f_2$ (\circ), $3f_1 - 2f_2$ (∇), and $4f_1 - 3f_2$ (\diamond). (B) f_2 -sweep group delays of the three lower sideband DPOAEs. (C) f_1 -sweep group delays of $2f_1 - f_2$ (\circ) and $2f_2 - f_1$ (\square). (D) f_2 -sweep group delays of $2f_1 - f_2$ and $2f_2 - f_1$.

the eardrum thus generated, amplitude and phase versus frequency relations were derived for the different DPOAE components. The group delays D_1 (f_1 -sweep) and D_2 (f_2 -sweep) were calculated in the same way as was done with the experimental data in chapter 2, at the maximum DPOAE amplitude during the sweep. In a few sweeps the amplitude versus frequency function was rather broad or showed more than one maximum. For those cases, no group delay was determined and the data were excluded from further analysis.

4.3 Results

DPOAEs $2f_1 - f_2$, $3f_1 - 2f_2$, $4f_1 - 3f_2$, and $2f_2 - f_1$ were successfully generated by the model. The results are shown in figures 4.1 and 4.2, organized in the same way as figures 2.7 and 2.4 for the experimental data in chapter 2. In figure 4.1 the f_1 -sweep and f_2 -sweep group delays (D_1 and D_2 , respectively) from the model generated DPOAEs are shown. D_1

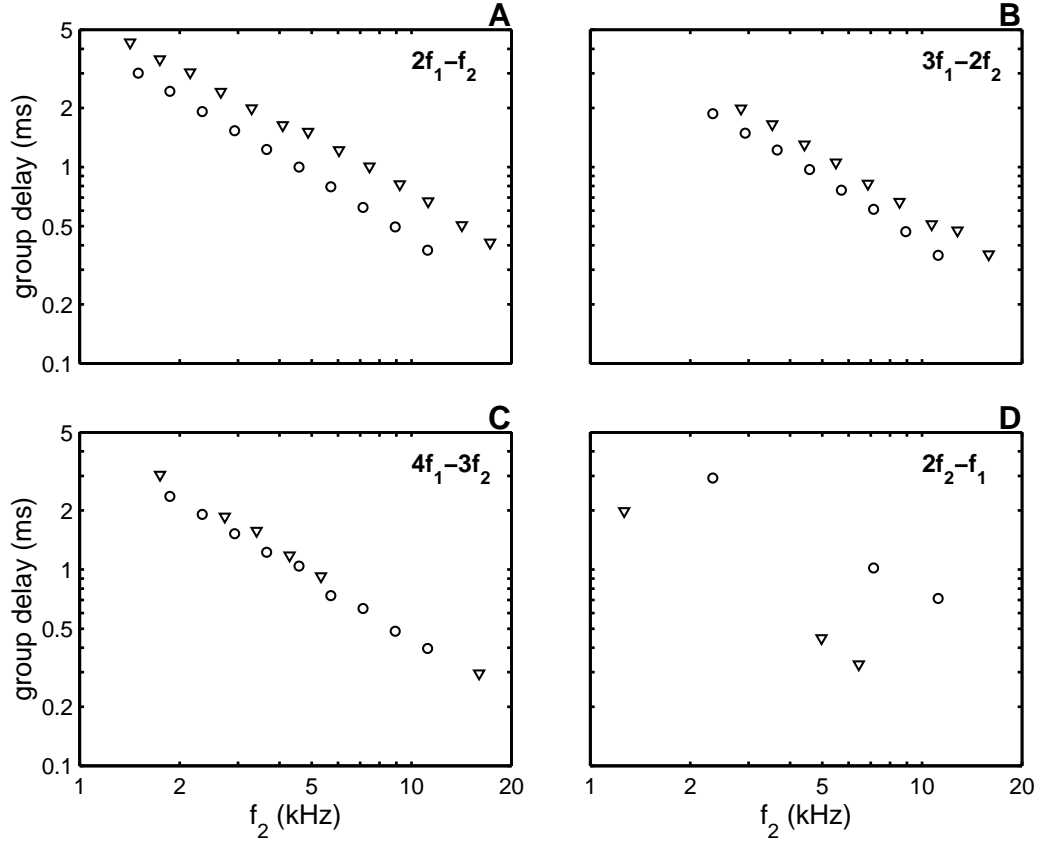


Figure 4.2: Simulated group delays from the cochlea model as a function of f_2 . Same data as in figure 4.1. Shown are the f_1 -sweep group delays (\circ) and the f_2 -sweep group delays (∇) for (A) $2f_1 - f_2$, (B) $3f_1 - 2f_2$, (C) $4f_1 - 3f_2$, and (D) $2f_2 - f_1$.

of the lower sideband DPOAEs (figure 4.1A) is independent of DPOAE order. For the f_2 -sweep paradigm, the model generated DPOAEs have a group delay that depends slightly on the DPOAE order. D_2 is larger for smaller DPOAE order (figure 4.1B). Comparing the group delays of the lower and upper sideband DPOAEs $2f_1 - f_2$ and $2f_2 - f_1$ in figure 4.1C and D, D_1 is largest for $2f_2 - f_1$ and D_2 is largest for $2f_1 - f_2$. The same group delay results are used in figure 4.2. Here, for each DPOAE component the f_1 - and f_2 -sweep group delays D_1 and D_2 can be compared. For all three lower sideband DPOAEs the group delays from the f_1 -sweep paradigm are smaller than D_2 , the group delays determined with an f_2 -sweep (figure 4.2A,B,C), although the difference is very small for $4f_1 - 3f_2$. With the upper sideband DPOAE $2f_2 - f_1$, it is the f_1 -sweep group delay that is larger.

4.4 Discussion

The cochlea model used in this chapter to simulate DPOAEs in the guinea pig, is of course a simplification of the real cochlea. The cochlear structures are simplified by one

dimensional mass, stiffness and damping terms. The model contains the basic needs to produce DPOAEs: a nonlinearity to generate the distortion products (put in the damping term), coupling of the model sections (through the fluid) to transfer the distortion product energy, and coupling to the ear canal (through a simple middle ear) to emit the distortion product energy as DPOAEs (van Hengel and Duifhuis, 2000).

The cochlea model appears to be generating DPOAEs with group delays that match the experimental results rather well, both qualitatively and quantitatively. Several trends that were seen in the experimental group delay results are reproduced by the model. All group delays (f_1 -sweep, f_2 -sweep, four DPOAE components) decrease with increasing f_2 . With f_1 -sweep, there is no difference in group delay between the three lower sideband DPOAEs (figure 4.1A). This is in accordance with the experimental data from chapter 2 (figure 2.7A) and with both the place- and the wave-fixed theory as presented in chapter 3. The simulated f_2 -sweep group delays as a function of f_2 , depend on the order of the lower sideband DPOAE component (figure 4.1B). D_2 is largest for $2f_1 - f_2$ and smallest for $4f_1 - 3f_2$. Again, this is in accordance with the experiments (figure 2.7B) and with the wave-fixed theory of distortion product generation, but it contradicts with the place-fixed theory. For the lower sideband DPOAEs, f_1 -sweep group delays are smaller than f_2 -sweep group delays, again a feature that is seen in the model data (figure 4.2A,B,C) as well as in the experimental (figure 2.4A,B,C) and wave-fixed theoretical results.

The group delays derived from the model simulations are compared with the experimental results from chapter 2 in figure 4.3. The function $\log(D) = a + b \cdot \log(f_2)$ is fitted to the model results, as was done with the experimental results in chapter 2. The model reproduces the experimental group delay values fairly well. For the lower sideband DPOAEs, however, the simulated group delays are in general slightly larger than the experimental results at low f_2 , and smaller at high f_2 . Preliminary results have shown that this can be overcome by using a non constant Q -factor in the model. Altering the Q -factor of the segments of the model affects its phase behavior. Studies on DPOAE generation by the model have shown that both generation and emission of distortion products are intimately related to the model's phase behavior (van Hengel, 1996; van Hengel and Duifhuis, 2000). When a Q that increases with \sqrt{f} is applied, the slope of the group delay as a function of f_2 can be altered to get a better match with the experimental results (see also Duifhuis *et al.*, 2003). Such a Q is also more realistic according to mechanical, physiological and psychophysical data. For the upper sideband DPOAE $2f_2 - f_1$, the model results are larger than the experimental results with f_1 -sweep. With f_2 -sweep however, the model results are smaller than the experimental data, especially at low frequencies (< 2 kHz).

The ratios of f_2 - and f_1 -sweep group delays D_2/D_1 from model, experiments (chapter 2) and wave-fixed theory (chapter 3) are shown together in figure 4.4. For the lower sideband DPOAEs the delay ratios from simulations approximate the experimental and theoretical (wave-fixed) results. In the model, the generation site of the distortion products is almost constant with f_1 -sweep, while it shifts with f_2 -sweep. So the distortion product generation in the model is approximately wave-fixed. Note that there is no roughness incorporated in the cochlea model, which means that there is no reflection component from the DPOAE frequency region. The behavior of the cochlea model therefore differs from the two-source

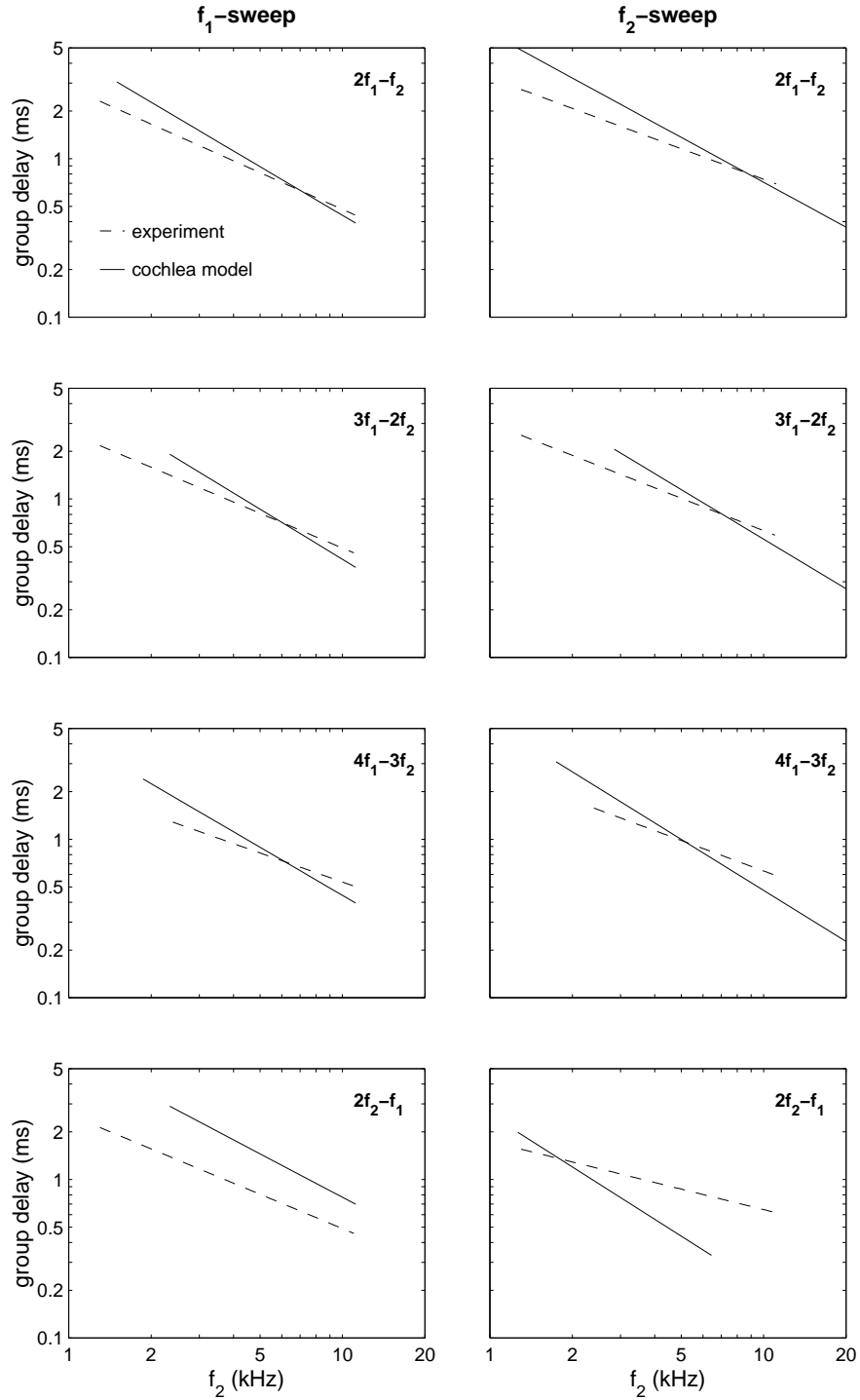


Figure 4.3: Fitted f_1 - and f_2 -sweep group delays (left and right column, respectively) from cochlea model (solid) and experiments (dashed) for DPOAEs $2f_1 - f_2$, $3f_1 - 2f_2$, $4f_1 - 3f_2$, and $2f_2 - f_1$ from top to bottom.

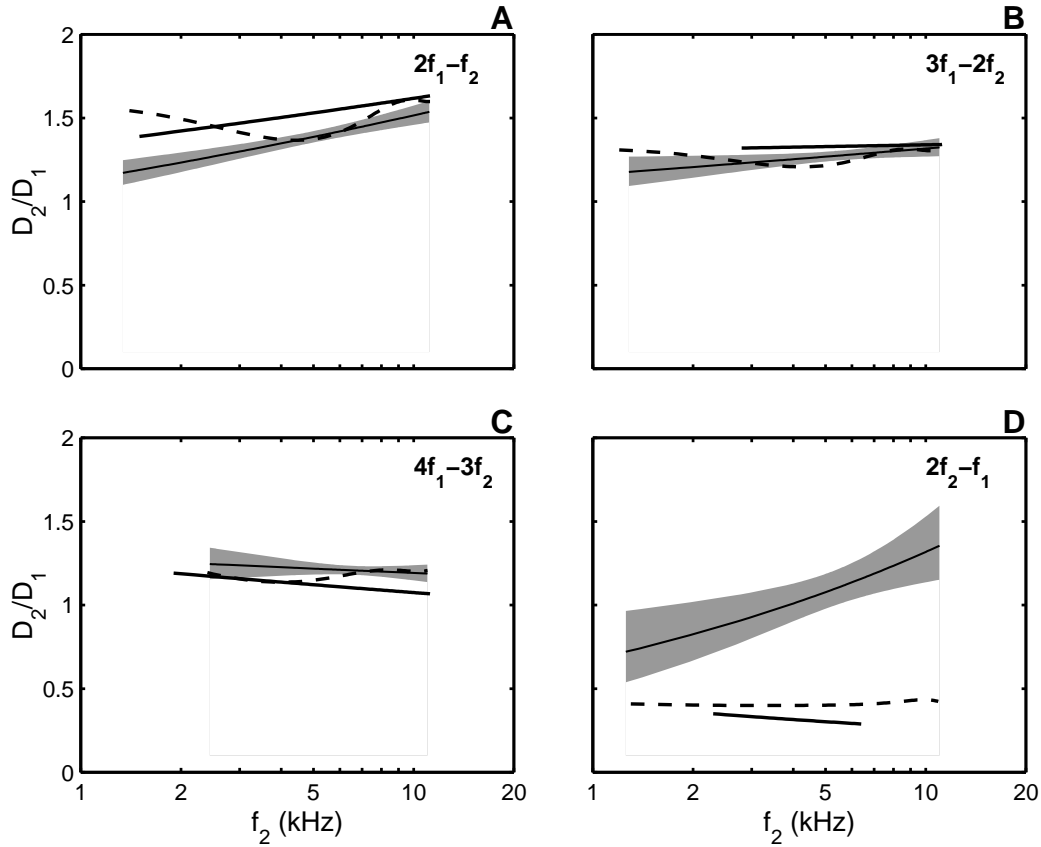


Figure 4.4: Ratio of the f_1 - and f_2 -sweep group delays D_2/D_1 plotted as a function of f_2 . Model results (thick solid line), experimental results (thin solid line and shaded area, representing mean and 95% confidence interval), and prediction from the wave-fixed theory (dashed line). Results for the three lower sideband DPOAEs $2f_1 - f_2$ (A), $3f_1 - 2f_2$ (B), $4f_1 - 3f_2$ (C), and the upper sideband DPOAE $2f_2 - f_1$ (D).

model of DPOAE generation. The modelled DPOAEs in this study are mainly the result of nonlinear interaction in the overlap region of the primaries. In a different DPOAE study with the same cochlea model Mauermann *et al.* (1999) have shown that applying roughness, especially at the DPOAE resonance place, causes DPOAE fine structure.

The cochlea model is unable to reproduce the experimental delay ratios for the upper sideband DPOAE (figure 4.4D). This can also be concluded from figure 4.3 (bottom row), where modelled f_1 -sweep delays were larger and f_2 -sweep delays were smaller than the experimental delays. The model results, however, show a reasonably close match with the wave-fixed prediction. This could indicate that the phase behavior of the upper sideband distortion product in the cochlea model is according to the wave-fixed theory, even though, as we concluded in chapter 3, this is not appropriate for upper sideband DPOAE generation.

It is concluded that the model in its present stage is properly reproducing several properties of the data like the dependence on the order of the LSB DPOAEs and on

the sweep paradigm. The group delays of the upper sideband DPOAE $2f_2 - f_1$ are not reproduced correctly by the model. The quantitative values of the LSB group delays and the dependence on f_2 are closely matched. Current considerations on model parameters that need to be revised, like the quality factor Q (Duifhuis *et al.*, 2003) suggest that further improvements on these points are possible without affecting the conceptual nature of the model. Implications and interpretations of such changes in model parameters for its cochlear mechanical behavior in a broader context will have to be further analysed.

References

- Allen, J. B. and Sondhi, M. M. (1979). “Cochlear Macromechanics – Time domain solutions,” *J. Acoust. Soc. Am.* **66**, 123–132.
- Boer, E. de (1996). “Mechanics of the cochlea: modeling efforts,” in *The Cochlea*, edited by P. Dallos, A. N. Popper, and R. R. Fay (Springer, New York), pp. 258–317.
- Duifhuis, H. (1988). “Cochlear Macromechanics,” in *Neurobiological Basis of Hearing*, edited by G. M. Edelman, W. E. Gall, and W. M. Cowan (Wiley), pp. 189–211.
- Duifhuis, H., Hoogstraten, H. W., Netten, S. M. van, Diependaal, R. J., and Bialek, W. (1985). “Modelling the cochlear partition with coupled Van der Pol oscillators,” in *Peripheral Auditory Mechanisms*, edited by J. B. Allen, J. L. Hall, A. E. Hubbard, S. T. Neely, and A. Tubis (Springer, New York), pp. 290–297.
- Duifhuis, H., Kruseman, J. M., and van Hengel, P. W. J. (2003). “An improved cochlea model with a general user interface,” in *Biophysics of the Cochlea: from Molecules to Models*, edited by A. W. Gummer (World Scientific, Singapore), pp. 376–382.
- Greenwood, D. D. (1990). “A cochlear frequency-position function for several species: 29 years later,” *J. Acoust. Soc. Am.* **87**, 2592–2605.
- Hall, J. L. (1974). “Two-tone distortion products in a nonlinear model of the basilar membrane,” *J. Acoust. Soc. Am.* **56**, 1818–1828.
- Helmholtz, H. L. F. (1885). *On the sensations of tone* (Dover, New York).
- Hemila, Nummela, and Reuter (1995). “What middle ear parameters tell about impedance matching and high frequency hearing,” *Hearing Res.* **85**, 31–44.
- Hengel, P. W. J. van (1996). *Emissions from cochlear modelling*. PhD thesis, University of Groningen, The Netherlands.
- Hengel, P. W. J. van, and Duifhuis, H. (2000). “The generation of distortion products in a nonlinear transmission line model of the cochlea,” in *Recent Developments in Auditory Mechanics*, edited by H. Wada, T. Takasaka, K. Ikeda, K. Ohyama, and T. Koike (World Scientific, Singapore), pp. 409–415.

- Hengel, P. W. J. van, Duifhuis, H., and Raadt, M. P. M. G. van den (1996). "Spatial periodicity in the cochlea: The result of interaction of spontaneous emissions?" J. Acoust. Soc. Am. **99**, 3566–3571.
- Kanis, L. J. and de Boer, E. (1993). "The emperor's new clothes: DP emissions in a locally-active nonlinear model of the cochlea," in *Biophysics of hair cell sensory systems*, edited by H. Duifhuis, J. W. Horst, P. van Dijk, and S. M. van Netten (World Scientific, Singapore), pp. 304–311.
- Matthews, J. W. and Molnar, C. E. (1986). "Modeling intracochlear and ear canal distortion product ($2f_1 - f_2$)," in *Peripheral Auditory Mechanisms*, edited by J. B. Allen, J. L. Hall, A. Hubbard, S. T. Neely, and A. Tubis, pp. 258–265.
- Mauermann, M., Uppenkamp, S., Hengel, P. W. J. van, Kollmeier, B. (1999). "Evidence for the distortion product frequency place as a source of distortion product otoacoustic emission (DPOAE) fine structure in humans. I. Fine structure and higher-order DPOAE as a function of the frequency ratio f_2/f_1 ," J. Acoust. Soc. Am. **106**, 3473–3483.
- Neely, S. T. and Stover, L. J. (1993). "Otoacoustic emissions from a nonlinear active model of cochlear mechanics," in *Biophysics of hair cell sensory systems*, edited by H. Duifhuis, J. W. Horst, P. van Dijk, and S. M. van Netten (World Scientific, Singapore), pp. 64–71.
- Neely, S. T. and Stover, L. J. (1997). "A generation of distortion products in a model of cochlear mechanics," in *Diversity in Auditory Mechanics*, edited by E. R. Lewis, G. R. Long, R. F. Lyon, P. M. Narins, C. R. Steele, and E. L. Hecht-Poinar (World Scientific, Singapore), pp. 434–440.
- Raadt, M. P. M. G. van den, and Duifhuis, H. (1990). "A generalized van der Pol oscillator model," in *The Mechanics and Biophysics of Hearing*, edited by P. Dallos, C. D. Geisler, J. W. Matthews, M. A. Ruggero, and C. R. Steele (Springer-Verlag, Berlin), pp. 227–234.
- Raadt, M. P. M. G. van den, Hengel, P. W. J. van, and Duifhuis, H. (1993). "Quantitative evaluation of spontaneous otoacoustic emissions in a one-dimensional macromechanical nonlinear cochlea model," in *Advances in Otoacoustic Emissions - Volume I*, edited by F. Grandori.
- Schneider, S., Prijs, V. F., Schoonhoven, R., and van Hengel, P. W. J. (2000). " f_1 - versus f_2 -sweep group delays of distortion product otoacoustic emissions in the guinea pig; experimental results and theoretical predictions," in *Recent Developments in Auditory Mechanics*, edited by H. Wada, T. Takasaka, K. Ikeda, K. Ohyama, and T. Koike (World Scientific, Singapore), pp. 360–366.
- Zweig, G. (1991). "Finding the impedance of the organ of Corti," J. Acoust. Soc. Am. **89**, 1229–1254.

Zwislocki, J. J. (1950). "Theory of the acoustical action of the cochlea," J. Acoust. Soc. Am. **22**, 778–784.

Chapter 5

Amplitude versus frequency functions of distortion product otoacoustic emissions in the guinea pig

Abstract

The amplitude versus frequency relations of distortion product otoacoustic emissions were studied in the guinea pig, using both the f_1 - and the f_2 -sweep paradigms to vary the primary frequency separation. The amplitude of the DPOAEs $2f_1 - f_2$, $3f_1 - 2f_2$, $4f_1 - 3f_2$, and $2f_2 - f_1$, plotted as a function of DP frequency, exhibited a bandpass structure. The separation of the primaries for which the DPOAE level is maximum is referred to as the optimum ratio f_2/f_1 . For the lower sideband DPOAEs ($f_{dp} < f_1, f_2$), the optimum ratio varies nonmonotonically with the primary frequency region. At an f_2 around 4.4 kHz, the optimum ratio for $2f_1 - f_2$ reaches a maximum of about 1.46 while elsewhere it is in the more commonly found 1.2–1.3 range. The width of the amplitude profiles was studied by determining their Q_{10dB} . The f_2 -sweep yielded significantly larger Q_{10dB} than f_1 -sweep, for the lower sideband DPOAEs. The amplitude versus frequency functions of the lower sideband DPOAEs approximately line up. Upon closer inspection, however, with f_1 -sweep the $2f_1 - f_2$ DPOAE has its maximum at a slightly smaller DP frequency than the higher order DPOAEs. With f_2 -sweep, on the contrary, the $2f_1 - f_2$ tends to peak at a higher DP frequency than the other lower sideband distortion products. When the amplitude is considered as a function of the ratio between f_{dp} and f_2 , the difference between f_1 - and f_2 -sweep with respect to the width and the alignment of the amplitude functions disappears. The amplitude profiles of the lower sideband DPOAEs are a function of the DPOAE frequency f_{dp} relative to f_2 .

5.1 Introduction

When the cochlea is stimulated with frequencies f_1 and f_2 ($f_1 < f_2$), distortion products with frequencies $f_{dp} = mf_1 + nf_2$ are generated which can be detected in the ear canal as distortion product otoacoustic emissions (DPOAEs). Besides on cochlear status, the amplitude of the DPOAEs also depends on the level and frequency of the primaries, and on the frequency ratio f_2/f_1 (for review see Probst *et al.*, 1991).

The amplitude as a function of frequency ratio reveals a bandpass structure (Wilson, 1980; Fahey and Allen, 1986; Harris *et al.*, 1989; Brown and Gaskill, 1990a; Gaskill and Brown, 1990). A maximum amplitude is reached at a certain separation of the primary frequencies, while for smaller and larger separations the amplitude rapidly declines. In human subjects the maximum amplitude of the $2f_1 - f_2$ distortion product is elicited by a frequency ratio of approximately 1.22 (Harris *et al.*, 1989; Gaskill and Brown, 1990). The optimum ratio increases slightly towards smaller frequencies (Harris *et al.*, 1989; Bowman *et al.*, 2000; Moulin, 2000). In other species (rat, gerbil, guinea pig, rabbit, cat, rhesus monkey) the optimum ratios found for $2f_1 - f_2$ are usually between 1.2 and 1.4 (Fahey and Allen, 1986; Lonsbury-Martin *et al.*, 1987; Brown and Gaskill, 1990a; Whitehead *et al.*, 1992; Allen and Fahey, 1993; Lasky *et al.*, 1995).

When several orders of distortion products with frequencies smaller than the primaries (the so-called ‘lower sideband’ or ‘apical’ distortion products), like $2f_1 - f_2$ and $3f_1 - 2f_2$, are measured with f_2 fixed, the amplitude functions appear to peak at approximately the same DPOAE frequency, independent of DPOAE order (Fahey and Allen, 1986; Brown and Gaskill, 1990a). Consequently, the optimum ratio is smaller for higher DPOAE orders.

In psychophysical and neural distortion product measurements, the bandpass structure is not found (Goldstein, 1967; Wilson, 1980; Zwicker, 1980; Smoorenburg *et al.*, 1976). As in the ear canal recordings, the distortion product levels decrease with increasing primary separation. However, no level decrease is found when the primaries are brought closer together.

Several hypotheses have been proposed in literature to explain the form of the amplitude versus frequency functions of the DPOAEs. The decrease of DPOAE amplitude with increasing ratio f_2/f_1 can be explained by the decreasing overlap of the f_1 and f_2 excitation patterns in the generation region around the f_2 tonotopic place. However, the amplitude decrease when f_1 and f_2 are brought closer together, is less easy to explain. One option that has been discussed in literature is filtering of the DPOAE. The difference between psychophysical and ear canal distortion products, and the fact that the DPOAEs peak at the same frequency independent of order, has led Brown and Gaskill (1990a) and Allen and Fahey (1993) to assume that there is a second filter mechanism involved. According to their theory, the distortion products are filtered in the cochlea, subsequent to their generation, by a filter tuned at the frequency corresponding to the peak of the amplitude function. Others have argued against the second filter mechanism. In models of cochlear mechanics, a bandpass structure is produced without the presence of a second filter mechanism (Matthews and Molnar, 1986; Neely and Stover, 1997; Kanis and de Boer, 1997; Talmadge *et al.*, 1998). An interference effect, resulting from the presence of an extended generation

region, was shown to produce the bandpass characteristic in the model of Talmadge *et al.* (1998).

The places and mechanisms of DPOAE generation obviously play an important role in the origin of the bandpass character of the amplitude versus frequency functions. Two models, describing the DPOAE generation mechanism and especially the influence of the changing primaries on the generation site, were proposed by Kemp (1986) and further developed by Moulin and Kemp (1996) and ourselves (chapter 3): the place-fixed and the wave-fixed model. An assumption in both models is that the generation is concentrated close to the f_2 tonotopic place. In the place-fixed model the generation site is fixed with respect to the cochlear partition when one or both primaries are slightly changed. Wave-fixed refers to a generation site which is fixed to the excitation pattern of the f_2 wave, and therefore moves along the cochlear partition during an f_2 -sweep.

The most recent view on DPOAE generation is that the lower sideband distortion products are generated in the region around the f_2 tonotopic place, where the overlap of the f_1 and f_2 excitation patterns is maximum, then propagated both basally and apically, and reflected at the f_{dp} tonotopic place (Shera and Guinan, 1999; Talmadge *et al.*, 1998; 1999). The generation region at the f_2 place is wave-fixed, while the reflection around the f_{dp} tonotopic place is supposed to be a place-fixed phenomenon. The relative contributions of the two regions differ with stimulus parameters, in a way that the wave-fixed component from the f_2 generation region is dominant at the optimum primary frequency ratio (Knight and Kemp, 2000; Tubis *et al.*, 2000). For the upper sideband DPOAEs, the situation is quite different. They are generated basally from the f_2 tonotopic place, probably close to the f_{dp} site (Martin *et al.*, 1998). Their behavior differs from that of the lower sideband DPOAEs in several ways.

In this chapter we present a comprehensive set of amplitude versus frequency data, measured in the guinea pig. The study concentrates on the three lower sideband DPOAEs $2f_1 - f_2$, $3f_1 - 2f_2$, and $4f_1 - 3f_2$, and the upper sideband $2f_2 - f_1$. The optimum f_2/f_1 ratio for eliciting maximum DPOAE amplitude is determined with both f_1 - and f_2 -sweeps in the f_2 frequency region 1–11 kHz. The alignment of the maxima of different lower sideband DPOAE orders is studied, as well as the tuning quality (Q_{10dB}) of the amplitude profiles. Comparing the different DPOAE orders, and especially the different sweep paradigms, reveals information about the influence of the frequency parameters on the origin of the amplitude bandpass profiles.

5.2 Methods

The experimental protocol of this study was described in detail in chapter 2. In that chapter the group delay data were presented, while in this chapter the amplitude data of the same experiments will be discussed. A short description of the methods will be given here. The data have been obtained from 5 female pigmented guinea pigs with a weight of 500–700 g. They were anesthetized with an intramuscular injection of ketamine hydrochloride (Ketalar, 20 mg/kg) and xylazine (Rompun, 15 mg/kg). The amplitude and phase of the distortion products $2f_1 - f_2$, $3f_1 - 2f_2$, $4f_1 - 3f_2$, and $2f_2 - f_1$ were

recorded as a function of frequency, with a modified version of CUBDIS[©] software and an ER10B probe (Etymotic) connected to an Ariel DSP board. Both the f_1 - and the f_2 -sweep paradigm were used to modify the DPOAE frequency, with an f_2/f_1 range of 1.01–1.70. With f_1 -sweep, fixed f_2 values were between 1 and 11 kHz. The fixed f_1 values were a factor 1.25 lower. Stimulus levels were fixed at $L_1 = 65$ and $L_2 = 55$ dB SPL. Of all f_1 - and f_2 -sweep recordings, the maximum of the amplitude function was determined, as well as the corresponding primary frequency ratio f_2/f_1 (the optimum ratio). In some cases the maximum could not be reliably determined, due to low signal to noise ratio (< 10 dB) or the existence of more than one maximum of equal height. In these cases, the data were excluded from further analysis. The $Q_{10\text{dB}}$ values of the DPOAE level versus frequency functions were determined by dividing the DPOAE frequency at maximum DPOAE level by the frequency bandwidth 10 dB below maximum level. The experimental protocol and use of the animals reported on in this study were approved by the Animal Care Committee of the University of Leiden (nr. 9609).

5.3 Results

5.3.1 Amplitude versus frequency

Figure 5.1 shows amplitude versus frequency functions, measured with the f_1 - or the f_2 -sweep paradigm. For a few representative measurements, all in the same animal, the amplitudes L_{dp} of the DPOAEs $2f_1 - f_2$, $3f_1 - 2f_2$, $4f_1 - 3f_2$ and $2f_2 - f_1$ are plotted as a function of DPOAE frequency f_{dp} . The left column shows f_1 -sweeps, and in the right column results for f_2 -sweeps are plotted. Clearly, the amplitude profile has a bandpass character. The maxima of the three lower sideband distortion product orders approximately line up as a function of f_{dp} . The upper sideband DPOAE $2f_2 - f_1$ peaks at a much higher DP frequency and has a less pronounced bandpass structure.

5.3.2 Maximum amplitude

The maximum amplitude reached during a sweep depends on the frequency region and on DPOAE order. For all f_1 - and f_2 -sweeps pooled, the maximum L_{dp} is plotted as a function of f_2 in figure 5.2, with the four different distortion products in separate panels. Note that for both sweeps, the maximum amplitude is plotted versus the f_2 value at which the maximum occurred. This is the fixed primary for f_1 -sweep and the varying primary for f_2 -sweep. The DPOAE $2f_1 - f_2$ reaches levels up to 30 dB SPL at the highest stimulus frequencies f_2 that were used in this study, with $L_1, L_2 = 65, 55$ dB SPL (figure 5.2A). The maximum DPOAE level increases with stimulus frequency f_2 for the lower sideband DPOAEs (figure 5.2A, B, C). For the upper sideband DPOAE $2f_2 - f_1$, the maximum L_{dp} does not vary systematically with f_2 (figure 5.2D).

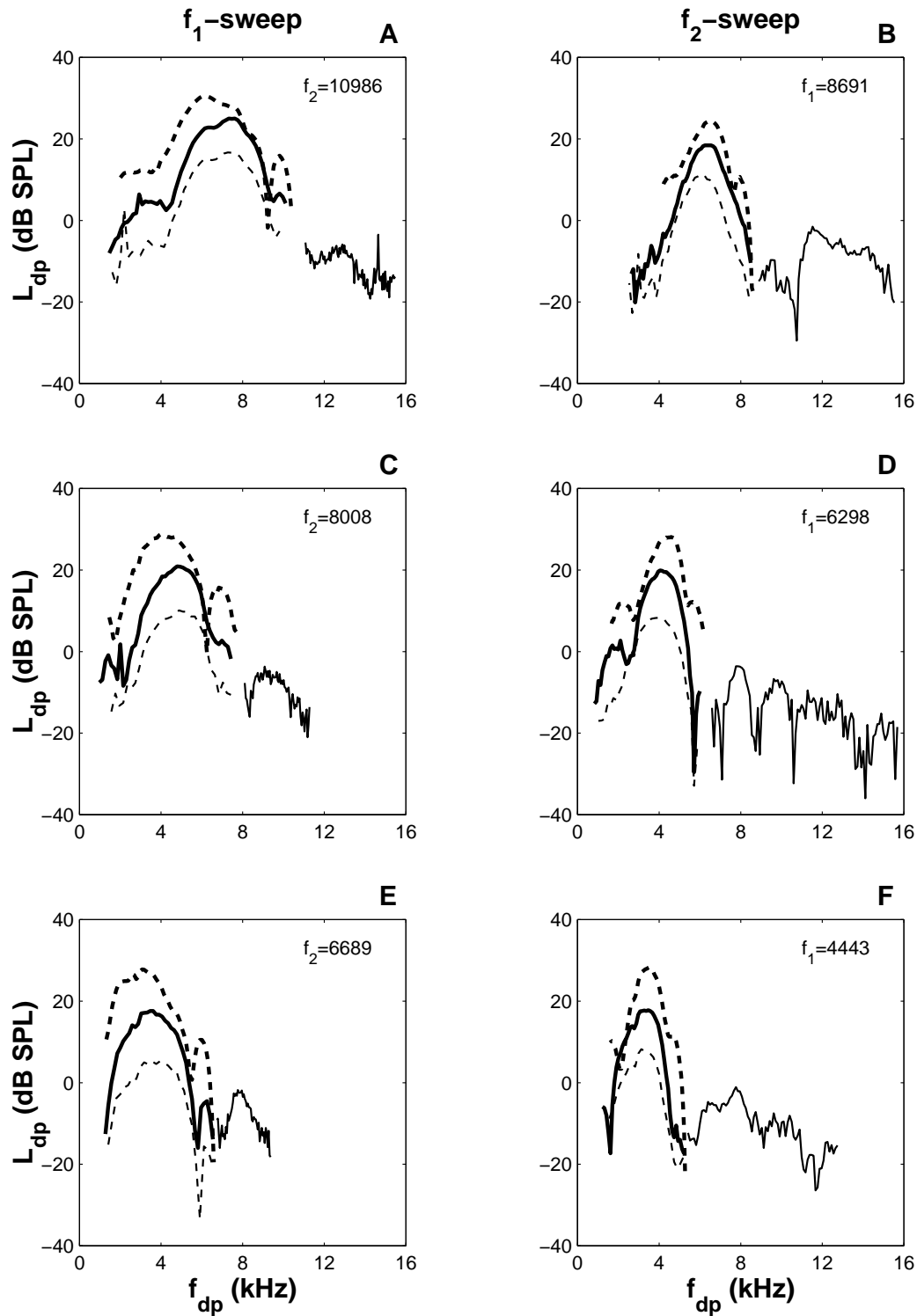


Figure 5.1: Representative examples of DPOAE amplitude L_{dp} as a function of f_{dp} for $2f_1 - f_2$ (dashed, thick), $3f_1 - 2f_2$ (solid, thick), $4f_1 - 3f_2$ (dashed, thin) and $2f_2 - f_1$ (solid, thin). Left panels: f_1 -sweep. Right panels: f_2 -sweep.

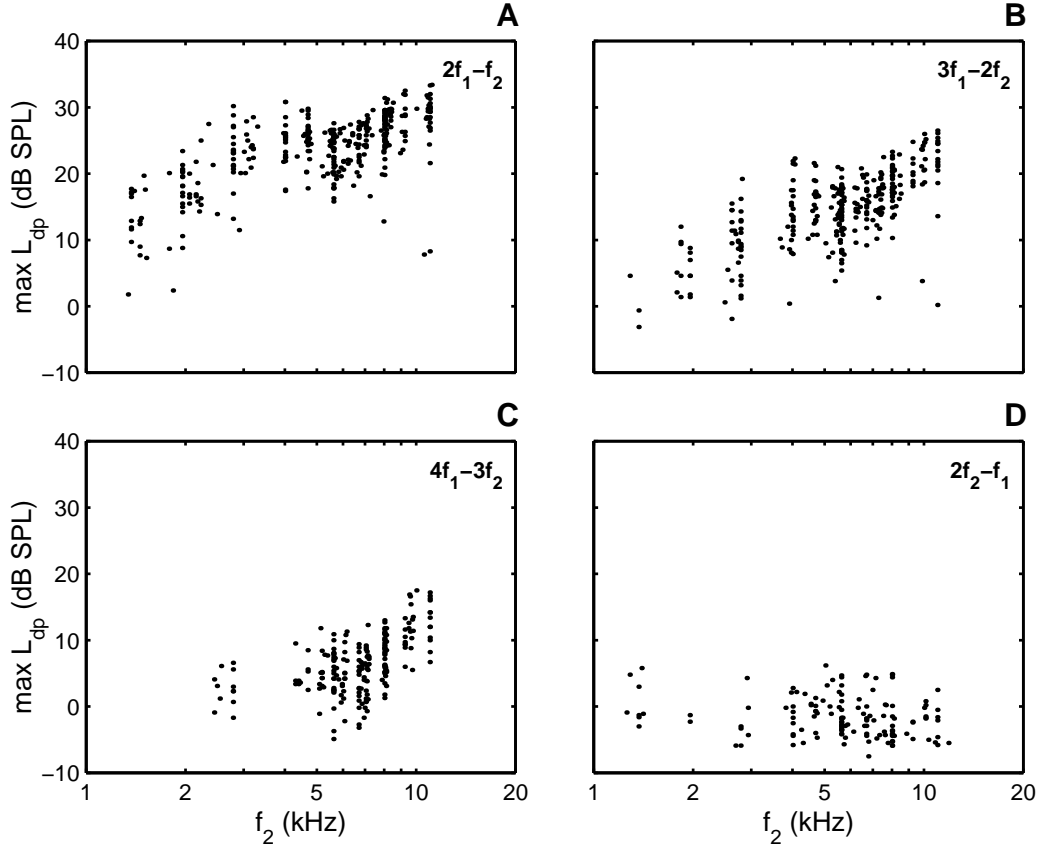


Figure 5.2: Maximum DPOAE amplitude reached during each f_1 - and f_2 -sweep, as a function of the corresponding f_2 .

5.3.3 Optimum ratio

From each sweep measurement, the primary frequency ratio that elicits the maximum DPOAE amplitude was determined. In figure 5.3 these optimum ratios are presented in scatterplots, as a function of f_2 frequency (again, fixed with f_1 -sweep and varying with f_2 -sweep). Data from all experiments are pooled. Polynomial fits (solid lines, fifth order for lower sideband DPOAEs, first order for $2f_2 - f_1$) with 95% confidence intervals (dashed lines) are indicated. It is clear that the lower sideband DPOAEs all show a nonmonotonic dependence of optimum ratio on f_2 (figure 5.3A, B, C). In the frequency area around 4.4 kHz, the maximum DPOAE amplitude is reached at a wider separation of the primaries than at the surrounding frequencies. The optimum ratio for $2f_1 - f_2$ increases from 1.28 ± 0.06 at 1 kHz to 1.46 ± 0.06 at 4.4 kHz, and decreases again to 1.25 ± 0.06 at 11 kHz. The nonmonotonic effect is not seen in the upper sideband data (figure 5.3D). Comparing the different lower sideband DPOAEs, the optimum ratios decrease with increasing order. This is directly related to the fact that the amplitude functions of the several orders are approximately aligned as was seen in figure 5.1.

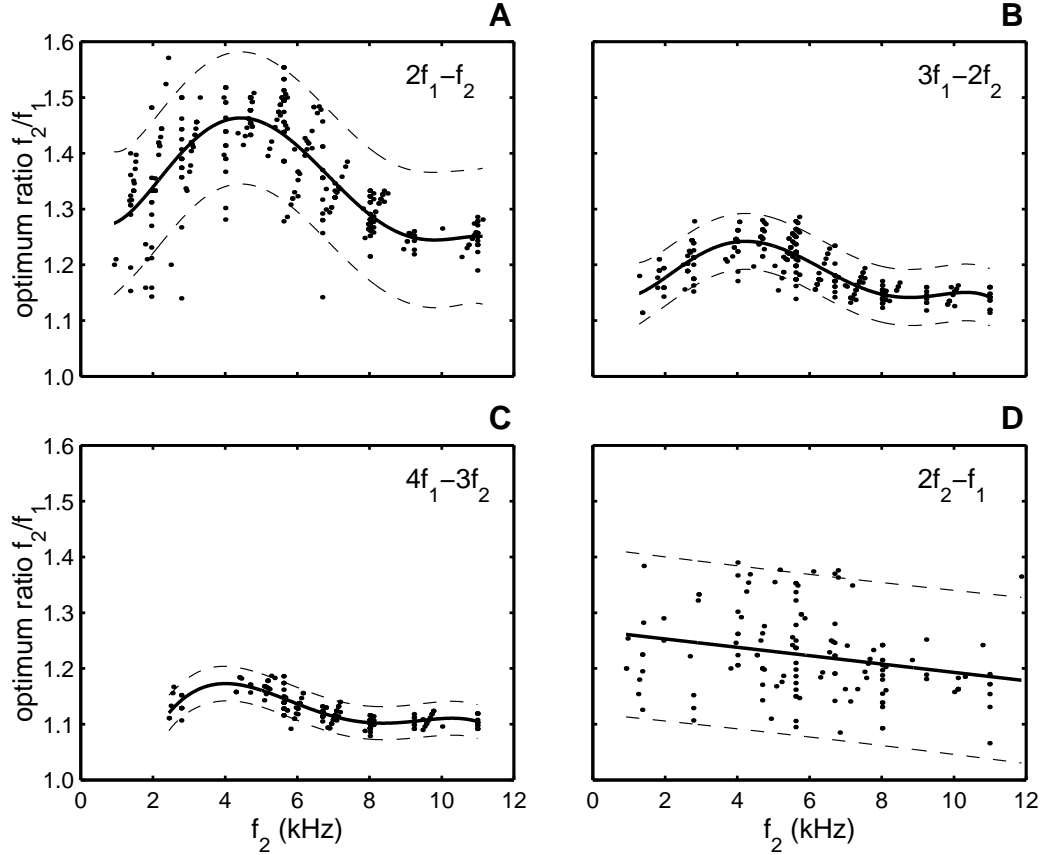


Figure 5.3: Frequency ratio f_2/f_1 at maximum DPOAE level, as a function of the corresponding f_2 . Polynomial fits (solid) with 95% confidence intervals (dashed).

5.3.4 Alignment

As reported in the literature, amplitude functions line up approximately when plotted as a function of f_{dp} , as shown in figure 5.1. However, closer inspection of the data in this figure reveals that the DPOAE with the lowest order ($2f_1 - f_2$) peaks at a slightly different frequency than the $3f_1 - 2f_2$ and $4f_1 - 3f_2$. With f_1 -sweep the maximum amplitude of $2f_1 - f_2$ occurs at a frequency f_{dp} lower than that where the higher order DPOAEs peak, and with f_2 -sweep at a higher f_{dp} . So there is an apparent difference here between f_1 - and f_2 -sweep data. A complicating factor in the interpretation of the f_2 -sweep data is that the different DPOAE orders peak at different optimum ratios f_2/f_1 , and f_2 varies with f_2 -sweep; therefore we are comparing (in figure 5.1B) maximum levels that occurred at a different value for f_2 (so at a different generation region). This problem does not arise with f_1 -sweep, since f_2 is fixed then, so the maxima in figure 5.1A all occurred at the same f_2 .

This ambiguity can be eliminated by plotting the amplitude versus the ratio of f_{dp} and f_2 , thus treating f_1 - and f_2 -sweep equally. In figure 5.4 the data of the lower panels of figure 5.1 are therefore replotted as a function of f_{dp}/f_2 . For f_1 -sweep, in the left panel

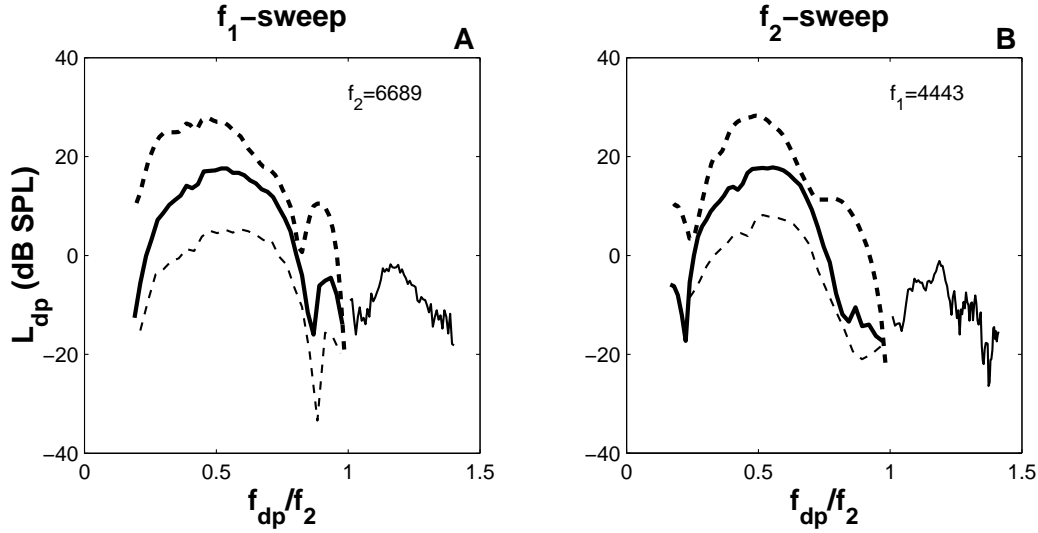


Figure 5.4: DPOAE amplitude L_{dp} of the lower panels of figure 5.1 replotted as a function of f_{dp}/f_2 , for the four distortion products $2f_1 - f_2$ (dashed, thick), $3f_1 - 2f_2$ (solid, thick), $4f_1 - 3f_2$ (dashed, thin), and $2f_2 - f_1$ (solid, thin). A: f_1 -sweep. B: f_2 -sweep.

of figure 5.4, the plot has not changed apart from the scaling on the x -axis, since f_2 is fixed. For f_2 -sweep, however, the curves shift with respect to one another. The apparent difference between f_1 - and f_2 -sweep data with respect to the alignment of the amplitude functions has disappeared qualitatively; both the f_1 - and f_2 -sweep measurement now show a shift of the $2f_1 - f_2$ maximum amplitude towards a lower f_{dp}/f_2 .

The presence of this effect in a survey of all data is shown in figure 5.5. Scatterplots are presented of the f_{dp}/f_2 at maximum level for one DPOAE order, versus another order. When the maximum amplitudes would line up exactly across order, the data would be on the $y = x$ line (f_{dp}/f_2 at maximum level would be the same for all orders). However, figure 5.5A and B show that with f_1 - as well as f_2 -sweep, the f_{dp}/f_2 at maximum level is lower for $2f_1 - f_2$ than for $3f_1 - 2f_2$ (data above the $y = x$ line). The same applies for the comparison between $2f_1 - f_2$ and $4f_1 - 3f_2$ (figure 5.5C and D). Paired t-tests showed significant deviations from equality ($p < 0.001$) for all comparisons made in figure 5.5, except for $3f_1 - 2f_2$ versus $4f_1 - 3f_2$ with f_2 -sweep (figure 5.5F).

5.3.5 Width of the amplitude functions

For all lower sideband DPOAE amplitude versus frequency functions yielding a maximum at least 10 dB above the noise level, Q_{10dB} was calculated. In some cases the amplitude 10 dB below maximum was not reached on one or two sides of the amplitude function, so those had to be excluded from the Q_{10dB} analysis. Since the upper sideband DPOAE $2f_2 - f_1$ has a less pronounced bandpass structure, and in several cases no bandpass at all,

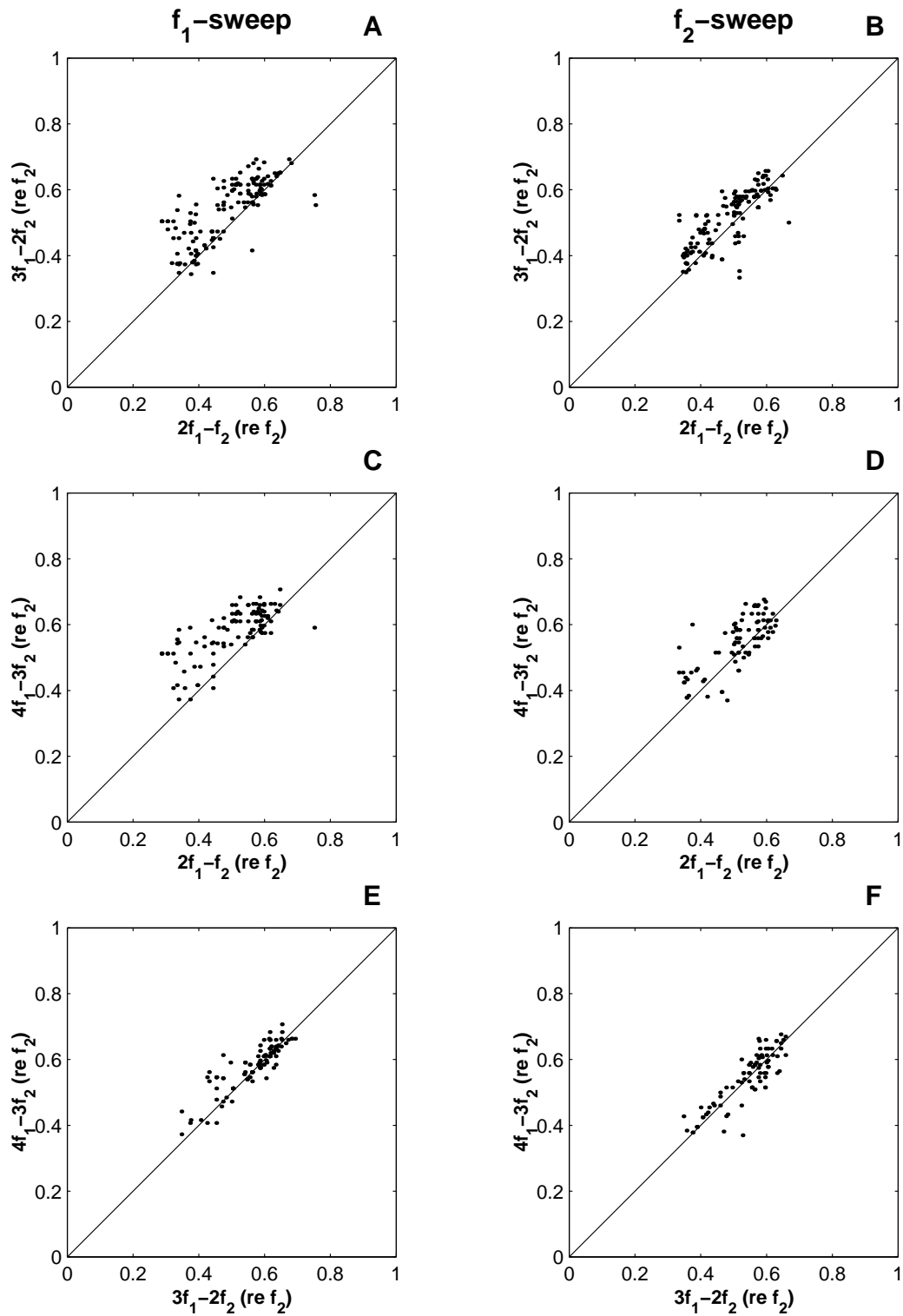


Figure 5.5: DPOAE frequency f_{dp} relative to f_2 in octaves, at the DPOAE amplitude peak, for one lower sideband DPOAE order versus another.

this analysis was not made for the $2f_2 - f_1$.

Figure 5.6 shows the $Q_{10\text{dB}}$ values of the DPOAE amplitude versus frequency curves. $Q_{10\text{dB}}$ increases with DP frequency. With f_1 -sweep, $Q_{10\text{dB}}$ is lower than with f_2 -sweep. With f_1 -sweep, there is no significant difference between the $Q_{10\text{dB}}$ values of the different orders. With f_2 -sweep, however, $Q_{10\text{dB}}$ increases with decreasing order (narrowest bandpass structures for $2f_1 - f_2$). To eliminate the effect of the changing DP generation site with f_2 -sweep, and compare f_1 - and f_2 -sweep more fairly, as was done in figure 5.4, an alternative $Q_{10\text{dB}}^*$ is calculated from amplitude versus f_{dp}/f_2 functions (as in figure 5.4), and plotted versus f_{dp}/f_2 instead of f_2 , in figure 5.7. In these alternative $Q_{10\text{dB}}^*$ distributions the differences between sweep paradigms and lower sideband DPOAE orders have disappeared.

In conclusion, the width of the amplitude function is independent of sweep paradigm and DPOAE order when the amplitude is considered as a function of f_{dp}/f_2 .

5.4 Discussion

In this study a comprehensive set of DPOAE amplitude data was presented for the guinea pig. Amplitude versus frequency functions of lower sideband DPOAEs $2f_1 - f_2$, $3f_1 - 2f_2$, and $4f_1 - 3f_2$ showed a bandpass character, for which the maximum amplitude, optimum frequency ratio f_2/f_1 and filter quality $Q_{10\text{dB}}$ were determined. Also the alignment of the maxima of the different lower sideband DPOAE orders was studied. For the upper sideband DPOAE $2f_2 - f_1$, much more variability was found in the amplitude functions, most of which did not show a strong bandpass character. The maximum amplitude and corresponding optimum frequency ratio were calculated whenever possible, but an analysis of the width of the amplitude functions was omitted since $Q_{10\text{dB}}$ could not be reliably determined in most cases. This is consistent with the finding of Talmadge *et al.* (1998), that the $2f_2 - f_1$ DPOAE does not show a bandpass shape in their model. As can be seen in figure 5.1, sharp minima occur in some of the amplitude functions of the lower sideband DPOAEs. These minima are closely related to irregularities in the phase versus frequency relations, and are most likely caused by an interference effect. They are thought to be part of the fine structure, which is the result of the interaction between the DPOAE component generated at the f_2 region and the component reflected at the f_{dp} site (Heitmann *et al.*, 1998; Talmadge *et al.*, 1998, 1999; Shera and Guinan, 1999). Further analysis of these features is beyond the scope of this study.

5.4.1 Optimum ratio

It was shown that in the guinea pig the maximum level of the lower sideband DPOAEs occurred at unexpectedly high primary frequency ratios in the frequency area around 4.4 kHz. In that region f_1 and f_2 were further apart at maximum DPOAE level than at lower or higher frequencies. The optimum ratio for eliciting maximum DPOAE amplitudes was studied before in the guinea pig and in several other species. Harris *et al.* (1989) measured $2f_1 - f_2$ DPOAEs in human subjects, in the f_2 frequency range 1–4 kHz, using several stimulus levels. The optimum ratio, averaged over all stimulus conditions, was 1.22. Allen

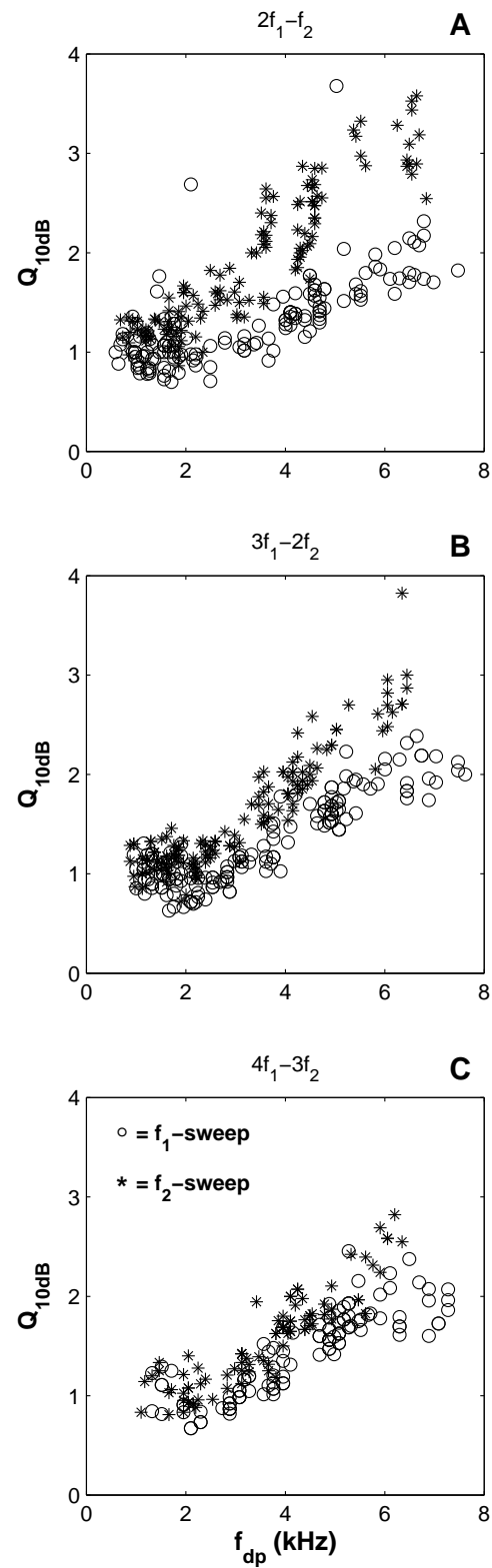


Figure 5.6: Filter quality of the amplitude profiles (Q_{10dB}) versus f_{dp} (at maximum level) for f_1 -sweep (\circ) and f_2 -sweep (*).

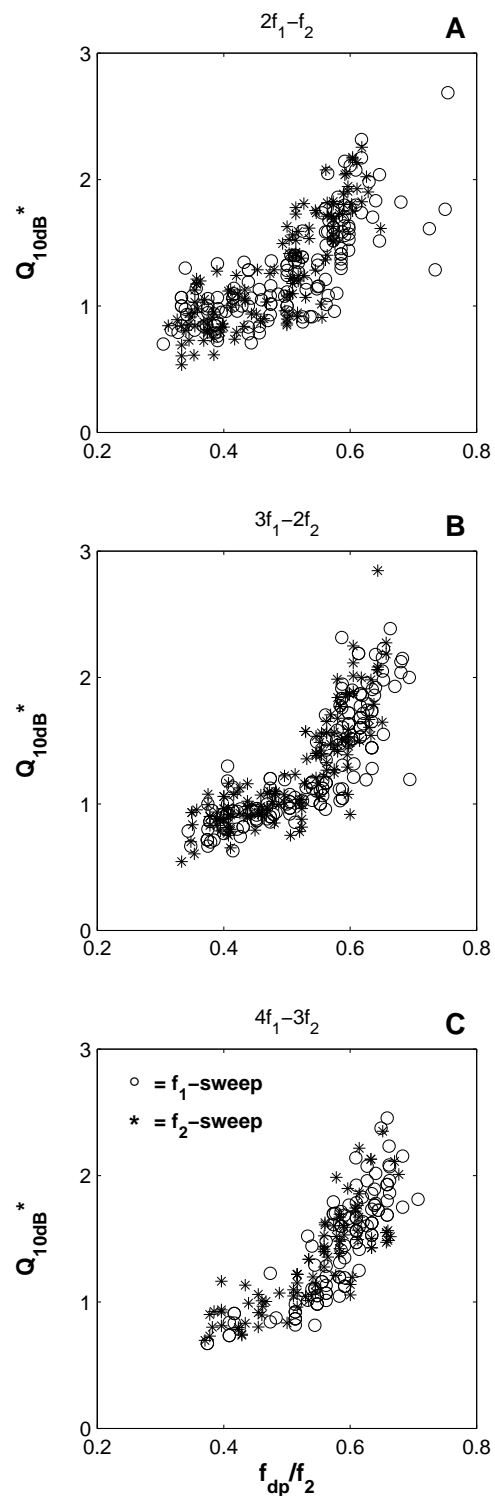


Figure 5.7: Alternative Q_{10dB} calculated from amplitude versus f_{dp}/f_2 functions, plotted as a function of f_{dp}/f_2 , for f_1 -sweep (○) and f_2 -sweep (*).

and Fahey (1993) found a relationship between f_{dp} at the amplitude peak and f_2 for cats and for humans, which can be translated in optimum ratios that decrease with increasing f_2 . For $2f_1 - f_2$, with f_2 ranging from 2 to 8 kHz, the optimum ratio ranges from 1.40 to 1.27 in cats, and from 1.19 to 1.17 in humans. Lasky *et al.* (1995) reported an optimum ratio of 1.225 for human and rhesus monkey, with f_2 between 2 and 12 kHz. Brown and Gaskill (1990a) found the same optimum ratio of 1.225 for human (f_2 in the range 1.5–6.3 kHz) and also for guinea pig (f_2 from 6.3 to 10 kHz; i.e., largely in the high frequency range of the present study). In another publication by the same authors (Brown and Gaskill, 1990b), the DPOAE level is shown as a function of frequency for one individual guinea pig. For an f_1 of 4 kHz, the optimum ratio has increased to approximately 1.34, so this is at an f_2 of 5.4 kHz. At $f_1 = 2$ kHz, the ratio at maximum level is even higher: approximately 1.38 ($f_2 = 2.8$ kHz). These values are well within the 95% confidence interval of our measurements in the guinea pig (figure 5.3). In the rabbit, the maximum for $2f_1 - f_2$ occurred at a ratio of 1.3 (for $f_2 = 3.7$ kHz), and 1.25 ($f_2 = 6.7$ and 13.3 kHz), measured with f_1 -sweep at $L_1 = L_2 = 70$ dB SPL (Lonsbury-Martin *et al.*, 1987). Taschenberger *et al.* (1995) reported optimum ratios for $2f_1 - f_2$ measured in barn owls and lizards. In the barn owl, the optimum ratio depended nonmonotonically on f_2 frequency. The highest values (1.3) were found for $f_2 = 5.8$ kHz, while the optimum ratio at the outermost sides of the frequency range, 1.6 and 9.2 kHz, were close to 1. In lizards, the optimum ratios ranged from 1.03 to 1.50.

Summarizing, there is a large range of optimum ratios found for the $2f_1 - f_2$ DPOAE both across frequency and in different species. The ratios we found in the guinea pig around 2 and 8 kHz are in the same range as most other values. The data found by Brown and Gaskill (1990b) at frequencies in between, are well within the 95% confidence interval of our observations. However, an increase in optimum frequency ratio, like we observed in the region around 4.4 kHz, is not commonly seen in other species, except in the barn owl. The high values we found in the guinea pig (maximum 1.46 for $2f_1 - f_2$) were only reported in the lizard.

The nonmonotonicity in optimum ratio could be related to a nonmonotonicity in other cochlear mechanical properties in the guinea pig, like cochlear tuning. However, such a nonmonotonicity in, e.g., Q_{10dB} of single fibre tuning curves has not been reported.

As opposed to the lower sidebands, the upper sideband DPOAE $2f_2 - f_1$ did not show nonmonotonic behavior of the optimum ratio. Several other DPOAE properties are known to be different in upper sidebands and the explanation for these phenomena is sought in a different location of the generation site, more basally than the lower sideband generation region at X_2 (Martin *et al.*, 1998). The absence of nonmonotonicity in the $2f_2 - f_1$ is another argument that the observed nonmonotonicity in optimum ratio for the lower sidebands can not simply be explained by an anomaly in some cochlear mechanical property like tuning since we would have expected to see the same effect for the upper sidebands, albeit in a different frequency region.

5.4.2 Alignment

In a number of publications the alignment of the amplitude versus frequency functions of the different lower sideband DPOAE orders was reported. Generally, the peak of the DPOAE amplitude is stated to occur at the DPOAE frequency approximately half an octave below f_2 (Brown and Gaskill, 1990a; Allen and Fahey, 1993). This would correspond to optimum ratios of 1.17 ($2f_1 - f_2$), 1.11 ($3f_1 - 2f_2$), and 1.08 ($4f_1 - 3f_2$). However, as was already indicated by Taschenberger *et al.* (1995) and Stover *et al.* (1999) and is shown by the reported optimum ratios (section 5.1), the half octave relationship is not generally valid. In fact, the alignment of amplitude versus frequency profiles is found at DPOAE frequencies varying from less than half an octave to more than a full octave relative to f_2 . In our data, we have seen the approximate alignment of the lower sideband distortion products in the entire frequency region. The distance in octaves however between f_{dp} and f_2 at the amplitude peak varied with f_2 , reflected by the nonmonotonicity in the optimum ratio functions.

A closer look at the alignment of the lower sideband DPOAE amplitude profiles revealed that the maximum amplitude of the $2f_1 - f_2$ DPOAE is shifted towards a lower f_{dp} than the higher order DPOAEs, measured with f_1 -sweep, and towards a higher f_{dp} with f_2 -sweep. The same results for f_1 -sweep measurements were reported before by Brown and Gaskill (1990a) and Brown and Williams (1993) in human subjects, guinea pigs and gerbils. It occurred with stimulus levels L_2 at or above 40 dB SPL. Talmadge *et al.* (1998) observed the same effect in their model simulations; $2f_1 - f_2$ tended to peak at a slightly smaller DPOAE frequency than the higher order DPOAEs (with the same f_2). In the present study, a shift in the opposite direction was observed with f_2 -sweep. However, when the variation in generation site is eliminated by plotting L_{dp} as a function of f_{dp}/f_2 , the effect is independent of the sweep paradigm; $2f_1 - f_2$ peaks at a smaller f_{dp} relative to f_2 than the higher orders.

Stover *et al.* (1999) reported a shift of the $2f_1 - f_2$ amplitude peak towards a smaller f_{dp} relative to f_2 with increasing stimulus levels. This and the fact that the loss of alignment of $2f_1 - f_2$ with respect to the higher order DPOAEs was found at stimulus levels higher than 40 dB SPL (Brown and Gaskill, 1990; Brown and Williams, 1993) suggests that the shift is related to the changing of the excitation patterns of f_1 , f_2 and possibly f_{dp} at high stimulus levels. The amplitude of the $2f_1 - f_2$ DPOAE peaks at a larger distance between f_1 and f_2 than the higher order DPOAEs, which could be a reason for the fact that the changing of the excitation patterns has a stronger influence on $2f_1 - f_2$ than on the higher order DPOAEs.

5.4.3 Width of the amplitude functions

The width of the DP amplitude versus DP frequency curves was quantified by the Q_{10dB} value. For the lower sideband DPOAEs Q_{10dB} increased with DP frequency. With the idea that the DPOAE tuning is somehow related to the cochlear filter process, these data are in agreement with the common view that the filter quality increases towards the base of the cochlea. Here, the Q_{10dB} values for DPOAEs (mean 1–3 in frequency range 2–8

kHz) are smaller than the $Q_{10\text{dB}}$ from cochlear nerve fibre tuning curves measured in the guinea pig (Versnel *et al.*, 1990). We have seen that f_2 -sweep produces narrower bandpass structures than f_1 -sweep, and that with f_2 -sweep $Q_{10\text{dB}}$ increases with decreasing DPOAE order. These effects disappear when we correct for the variation in generation site with f_2 -sweep by plotting the amplitude functions versus f_{dp}/f_2 instead of f_{dp} . Then, the bandpass structures have the same width with both sweep paradigms, and with all lower sideband orders. The DPOAE group delays from the same experiments showed a similar dependence on sweep paradigm and DPOAE order: group delays measured with f_2 -sweep are larger than f_1 -sweep delays, and only the f_2 -sweep delays depend on DPOAE order (chapter 2). These differences can also be explained by the variation in the generation site with f_2 -sweep (chapter 3).

5.4.4 Second filter

Brown and Gaskill (1990a) and Allen and Fahey (1993) proposed a second filter mechanism as an explanation for the bandpass character and the fact that LSB DPOAEs peak at (almost) the same frequency independent of order, while psychophysical distortion products do not show a bandpass character at all. They suggested the tectorial membrane as the structure responsible for the filtering of the distortion products on their way back to the ear canal. This hypothesis was tested by Taschenberger *et al.* (1995), who measured DPOAE amplitude versus frequency functions in species with a different tectorial membrane (barn owl) and with no tectorial membrane at all (lizard). They found the same kind of ‘tuning’ as was found in mammals. This argues against the tectorial membrane as the structure responsible for the second filtering. An argument against the second filter as such came from the field of cochlear mechanical modeling. Several authors suggested that a second filter is not needed to obtain a bandpass structure in the amplitude versus frequency functions. Models which do not incorporate a second filter produce a bandpass structure as well (Matthews and Molnar, 1986; Neely and Stover, 1997; Kanis and de Boer, 1997; Talmadge *et al.*, 1998). In those models, the bandpass structure arises from interference between DPOAE traveling waves generated over a range of different positions near the f_2 tonotopic place along the basilar membrane. It was also shown in those models that two-tone suppression, the mutual suppression of the primaries when they are close together, is not an explanation for the decrease of DPOAE amplitude at small ratios f_2/f_1 .

5.5 Conclusions

In the guinea pig, DPOAE amplitude versus DPOAE frequency (or primary frequency separation) shows a bandpass character. For $2f_1 - f_2$, the optimum f_2/f_1 ratio behaves nonmonotonically with a peak of about 1.46 in the 4–5 kHz region and values close to 1.25 in the lower (1 kHz) and higher (11 kHz) f_2 frequency regions. Other lower sideband DPOAEs also show an increase in optimum ratio in the 4–5 kHz region. The upper sideband DPOAE $2f_2 - f_1$ does not show nonmonotonic behavior of optimum ratio. Lower sideband DPOAE amplitude functions (L_{dp} vs f_{dp}) approximately line up at the same f_{dp} ; however,

the peak for $2f_1 - f_2$ is shifted towards a slightly smaller f_{dp} in the f_1 -sweep paradigm and a slightly larger f_{dp} in the f_2 -sweep paradigm. The difference between the sweep paradigms disappears when L_{dp} is considered as a function of f_{dp}/f_2 . The sharpness of the bandpass character of the amplitude profiles, determined by Q_{10dB} , is larger with f_2 -sweep than with f_1 -sweep, and only with f_2 -sweep it depends on DPOAE order. These differences disappear when an alternative Q_{10dB} is considered, derived from L_{dp} versus f_{dp}/f_2 functions. This indicates that the DPOAE amplitude profiles are determined by the distance between f_{dp} and f_2 .

References

- Allen, J. B., and Fahey, P. F. (1993). "A second cochlear-frequency map that correlates distortion product and neural tuning measurements," *J. Acoust. Soc. Am.* **94**, 809–816.
- Bowman, D. M., Brown, D. K., and Kimberley, B. P. (2000). "An examination of gender differences in DPOAE phase delay measurements in normal-hearing human adults," *Hear. Res.* **142**, 1–11.
- Brown, A. M., and Gaskill, S. A. (1990a). "Can basilar membrane tuning be inferred from distortion product measurement?" in *The mechanics and biophysics of hearing*, edited by P. Dallos, C. D. Geisler, J. W. Matthews, M. A. Ruggero, and C. R. Steele (Springer-Verlag, New York), pp. 164–169.
- Brown, A. M., and Gaskill, S. A. (1990b). "Measurement of acoustic distortion reveals underlying similarities between human and rodent mechanical responses," *J. Acoust. Soc. Am.* **88**, 840–849.
- Brown, A. M., and Williams, D. M. (1993). "A second filter in the cochlea," in *Biophysics of hair cell sensory systems*, edited by H. Duifhuis, J. W. Horst, P. van Dijk, and S. M. van Netten (World Scientific, Singapore), pp. 72–77.
- Fahey, P. F. and Allen, J. B. (1986). "Characterization of cubic intermodulation distortion products in the cat external auditory meatus," in *Peripheral Auditory Mechanisms*, edited by J. B. Allen, J. L. Hall, A. E. Hubbard, S. T. Neely, and A. Tubis (Springer-Verlag, Berlin) pp. 314–321.
- Gaskill, S. A. and Brown, A. M. (1990). "The behavior of the acoustic distortion product, $2f_1 - f_2$, from the human ear and its relation to auditory sensitivity," *J. Acoust. Soc. Am.* **88**, 821–839.
- Goldstein, J. L. (1967). "Auditory nonlinearity," *J. Acoust. Soc. Am.* **41**, 676–689.
- Harris, F. P., Lonsbury-Martin, B. L., Stagner, B. B., Coats, A. C., and Martin, G. K. (1989). "Acoustic distortion products in humans: Systematic changes in amplitude as a function of f_2/f_1 ratio," *J. Acoust. Soc. Am.* **85**, 220–229.
- Heitmann, J., Waldmann, B., Schnitzler, H-U., Plinkert, P. K., and Zenner, H-P. (1998). "Suppression of distortion product otoacoustic emissions (DPOAE) near $2f_1 - f_2$ removes DP-gram fine structure—Evidence for a secondary generator," *J. Acoust. Soc. Am.* **103**, 1527–1531.

- Kanis, L. J., and de Boer, E. (1997). "Frequency dependence of acoustic distortion products in a locally active model of the cochlea," *J. Acoust. Soc. Am.* **101**, 1527–1531.
- Kemp, D. T. (1986). "Otoacoustic emissions, travelling waves and cochlear mechanisms," *Hear. Res.* **22**, 95–104.
- Knight, R. D., and Kemp, D. T. (2000). "Indications of different distortion product otoacoustic emission mechanisms from a detailed f_1 , f_2 area study," *J. Acoust. Soc. Am.* **107**, 457–473.
- Lasky, R. E., Snodgrass, E. B., Laughlin, N. K., and Hecox, K. E. (1995). "Distortion product otoacoustic emissions in *Macaca mulatta* and humans," *Hear. Res.* **89**, 35–51.
- Lonsbury-Martin, B. L., Martin, G. K., Probst, R., and Coats, A. C. (1987). "Acoustic distortion products in rabbit ear canal. I. Basic features and physiological vulnerability," *Hear. Res.* **28**, 173–189.
- Martin, G. K., Jassir, D., Stagner, B. B., Whitehead, M. L., and Lonsbury-Martin, B. L. (1998). "Locus of generation for the $2f_1 - f_2$ vs $2f_2 - f_1$ distortion-product otoacoustic emissions in normal-hearing humans revealed by suppression tuning, onset latencies, and amplitude correlations," *J. Acoust. Soc. Am.* **103**, 1957–1971.
- Matthews, J. W., and Molnar, C. E. (1986). "Modeling intracochlear and ear canal distortion product ($2f_1 - f_2$)," in *Peripheral auditory mechanisms*, edited by J. B. Allen, J. L. Hall, A. E. Hubbard, S. T. Neely, and A. Tubis (Springer-Verlag, Berlin), pp. 258–265.
- Moulin, A. (2000). "Influence of primary frequencies ratio on distortion product otoacoustic emissions amplitude. II. Interrelations between multicomponent DPOAEs, tone-burst-evoked OAEs, and spontaneous OAEs," *J. Acoust. Soc. Am.* **107**, 1471–1486.
- Moulin, A., and Kemp, D. T. (1996). "Multicomponent acoustic distortion product otoacoustic emission phase in humans. II. Implications for distortion product otoacoustic emission generation," *J. Acoust. Soc. Am.* **100**, 1640–1662.
- Neely, S. T., and Stover, L. J. (1997). "A generation of distortion products in a model of cochlear mechanics," in *Diversity in auditory mechanics*, edited by E. Lewis, G. Long, R. Lyon, P. Narins, and C. Steele (World Scientific, Singapore), pp. 434–440.
- Probst, R., Lonsbury-Martin, B. L., and Martin, G. K. (1991). "A review of otoacoustic emissions," *J. Acoust. Soc. Am.* **89**, 2027–2067.
- Shera, C. A., and Guinan, J. J. (1999). "Evoked otoacoustic emissions arise by two fundamentally different mechanisms: A taxonomy for mammalian OAEs," *J. Acoust. Soc. Am.* **105**, 782–798.
- Smootenburg, G. F., Gibson, M. M., Kitzes, L. M., Rose, J. E., and Hind, J. E. (1976). "Correlates of combination tones observed in the response of neurons in the anteroventral cochlear nucleus of the cat," *J. Acoust. Soc. Am.* **59**, 945–962.

- Stover, L. J., Neely, S. T., and Gorga, M. P. (1999). "Cochlear generation of intermodulation distortion revealed by DPOAE frequency functions in normal and impaired ears," J. Acoust. Soc. Am. **106**, 2669–2678.
- Talmadge, C. L., Tubis, A., Long, G. R., and Piskorski, P. (1998). "Modeling otoacoustic emission and hearing threshold fine structures," J. Acoust. Soc. Am. **104**, 1517–1543.
- Talmadge, C. L., Long, G. R., Tubis, A., and Dhar, S. (1999). "Experimental confirmation of the two-source interference model for the fine structure of distortion product otoacoustic emissions," J. Acoust. Soc. Am. **105**, 275–292.
- Taschenberger, G., Gallo, L., and Manley, G. A. (1995). "Filtering of distortion-product otoacoustic emissions in the inner ear of birds and lizards," Hear. Res. **91**, 87–92.
- Tubis, A., Talmadge, C. L., Long, G. R., Dhar, S., and Tong, C. (2000). "Amplitude and group-delay finestructures of distortion product otoacoustic emissions as functions of primary levels and frequency ratios," Abstr. Assoc. Res. Otolaryngol. **23**, 139.
- Versnel, H., Prijs, V. F., and Schoonhoven, R. (1990). "Single-fibre responses to clicks in relationship to the compound action potential in the guinea pig," Hear. Res. **46**, 147–160.
- Whitehead, M. L., Lonsbury-Martin, B. L., and Martin, G. K. (1992). "Evidence for two discrete sources of $2f_1 - f_2$ distortion-product otoacoustic emission in rabbit: I. Differential dependence on stimulus parameters," J. Acoust. Soc. Am. **91**, 1587–1607.
- Wilson, J. P. (1980). "The combination tone, $2f_1 - f_2$, in psychophysics and ear-canal recording," in *Psychophysical, physiological, and behavioral studies in hearing*, edited by G. van den Brink, and F. A. Bilsen (Delft U.P., Delft, The Netherlands), pp. 43–50.
- Zwicker, E. (1980). "Cubic difference tone level and phase dependence on frequency difference and level of primaries," in *Psychophysical, physiological, and behavioral studies in hearing*, edited by G. van den Brink, and F. A. Bilsen (Delft U.P., Delft, The Netherlands), pp. 268–273.

Chapter 6

Amplitude and phase of distortion product otoacoustic emissions in the guinea pig in an (f_1, f_2) area study

Abstract

Lower sideband distortion product otoacoustic emissions (DPOAEs), measured in the ear canal upon stimulation with two continuous pure tones, are the result of interfering contributions from two different mechanisms, the nonlinear distortion component and the linear reflection component. The two contributors have been shown to have a different amplitude and, in particular, a different phase behavior as a function of the stimulus frequencies. The dominance of either component was investigated in an extensive (f_1, f_2) area study of DPOAE amplitude and phase in the guinea pig, which allows for both qualitative and quantitative analysis of isophase contours. Making a minimum of additional assumptions, simple relations between the direction of constant phase in the (f_1, f_2) plane and the group delays in f_1 -sweep, f_2 -sweep and fixed f_2/f_1 paradigms can be derived, both for distortion (wave-fixed) and reflection (place-fixed) components. The experimental data indicate the presence of both components in the lower sideband DPOAEs, with the reflection component as the dominant contributor for low f_2/f_1 ratios and the distortion component for intermediate ratios. At high ratios the behavior can not be explained by dominance of either component.

6.1 Introduction

Distortion product otoacoustic emissions have, since their first appearance in literature in 1979 (Kemp), been of great interest to researchers in the field of cochlear mechanics. In the past several years, the main focus has been on the generation mechanisms of the DPOAE and the places in the cochlea involved in the generation. Evidence for the two-source model of DPOAE generation, first proposed by Kim (1980), was collected and there is now a solid basis for Kim's theory that the lower sideband DPOAEs (with $f_{dp} < f_1, f_2$) consist of at least two components, one coming from the overlap region of the primaries near X_2 and one coming from the DP characteristic place X_{dp} (Kummer *et al.*, 1995; Brown *et al.*, 1996; Heitmann *et al.*, 1998; Mauermann *et al.*, 1999; Talmadge *et al.*, 1999; Shera and Guinan, 1999). However, Shera and Guinan (1999) and Kalluri and Shera (2001) have argued that the fundamental difference between the two components that contribute to the DPOAE in the ear canal is in the mechanism, not just in the location of the source. Instead of 'two-source model', they use the term 'two-mechanism model'. In this model, nonlinear distortion at the overlap region near X_2 generates the initial component that travels both basally and apically, while linear coherent reflection at the apical DP place results in the second backward traveling component (Talmadge *et al.*, 1998; Shera and Guinan, 1999; Kalluri and Shera, 2001). Together with multiple internal reflections they add up to the DPOAE in the ear canal. Note that the dichotomy between distortion component and reflection component breaks down in the limit of f_2/f_1 approaching 1. In this limit, the lower sideband DPOAEs are not reflected, but actually generated near their resonance place.

The less studied upper sideband DPOAEs (with $f_{dp} > f_1, f_2$) can not be described by the two-mechanism model, at least not with a distortion source at X_2 and a reflection at X_{dp} , since the distortion product can not propagate as a wave on the basilar membrane from X_2 to the basal X_{dp} . If the upper sideband DPOAEs are generated by nonlinear distortion at X_2 , the basilar membrane might be driven at X_{dp} by a different mechanism (e.g. fluid coupling or evanescent waves), so the distortion product is re-emitted at X_{dp} . Data suggesting that these DPOAEs arise directly from around the DP frequency place was presented by Martin *et al.* (1987; 1998).

The nonlinear distortion mechanism has proven to be a wave-fixed mechanism, meaning that the source location is fixed to the traveling wave pattern, in this case of f_2 (Kemp, 1986; Shera and Guinan, 1999). On the other hand, linear reflection is a place-fixed phenomenon, occurring at irregularities in the mechanics of the cochlea around the DP characteristic place (Shera and Guinan, 1999). Originally, the terms place-fixed and wave-fixed were not coupled to the two distinct locations in the cochlea but were seen as two possible mechanisms for DPOAE generation at X_2 (Kemp, 1986; O'Mahoney and Kemp, 1995; Moulin and Kemp, 1996).

The distortion component and the reflection component show a different phase behavior as a function of frequency, which is the main reason they were recognised as being the result of two such different mechanisms (Talmadge *et al.*, 1998; Knight and Kemp, 2000; Kalluri and Shera, 2001). Phase versus frequency measurements can be used to determine

the presence of the different components. Several experimental paradigms are in use for measuring DPOAE phase behavior. Phase versus frequency curves have been measured with f_1 -sweep or f_2 -sweep (respectively fixing f_2 , varying f_1 and fixing f_1 , varying f_2) but also with constant f_2/f_1 (Kimberley *et al.*, 1993; O'Mahoney and Kemp, 1995; Knight and Kemp, 1999; Shera *et al.*, 2000). Comparing the results of these paradigms is difficult due to the fact that the place of generation, tightly linked to the envelope of the f_2 -wave, remains fixed in an f_1 -sweep, but moves in different ways along the basilar membrane in the other sweep paradigms (chapter 3; Tubis *et al.*, 2000). Phase slope delays of lower sideband DPOAEs measured with f_2 -sweep, at intermediate frequency ratios, are larger than delays measured with f_1 -sweep (chapter 2; O'Mahoney and Kemp, 1995; Moulin and Kemp, 1996). This observation can be understood by considering the shift of generation site in the f_2 -sweep paradigm in the wave-fixed model, combined with the assumption of scaling invariance of the cochlea (chapter 3; Schneider *et al.*, 2000; Shera *et al.*, 2000; Talmadge *et al.*, 2000; Tubis *et al.*, 2000). When measuring the DPOAEs by varying both f_1 and f_2 in small frequency steps and so mapping part of the (f_1, f_2) plane in detail, phase slope delays in all directions like constant f_1 , constant f_2 , and constant f_2/f_1 can be deduced (Knight and Kemp, 2000). This gives a more detailed view of the DPOAE phase behavior than single sweeps.

The phase of the nonlinear distortion component is roughly constant when measured with constant frequency ratio f_2/f_1 , which can be understood by assuming cochlear scale invariance, since in that case the relative phases of the three components f_1 , f_2 , and f_{dp} remain unchanged (Talmadge *et al.*, 1998; Shera and Guinan, 1999; Knight and Kemp, 2000; Shera *et al.*, 2000). Using their unmixing strategy, Kalluri and Shera (2001) showed that the phase of the reflection component, analogous to the SFOAE, changes fast with frequency in a constant f_2/f_1 paradigm. Interference of the two components with different phase behavior, the distortion component with the shallow phase gradient and the reflection component with the steep phase gradient, results in fine structure in the DPOAE amplitude (Talmadge *et al.*, 1998; 1999; Heitmann *et al.*, 1998). Suppression of the reflection component by using a third tone close to f_{dp} yields a shallow phase gradient and a smooth DPOAE amplitude (Heitmann *et al.*, 1998; Talmadge *et al.*, 1999; Kalluri and Shera, 2001). The relative contribution of each component to the total DPOAE varies with stimulus parameters, especially frequency ratio f_2/f_1 (Knight and Kemp, 2000) and stimulus level (Fahey and Allen, 1997). Knight and Kemp (2000) found shallow phase gradients for intermediate ratios ($f_2/f_1=1.1-1.3$) and steep phase gradients for a small ratio (1.05). Which of the two components dominates the total DPOAE as a function of stimulus parameters is an important question, for instance for the interpretation of clinical DPOAE data, and obviously DPOAE phase behavior is an important clue in answering this question.

In this chapter we report extensive measurements of guinea pig DPOAE amplitude and phase in an (f_1, f_2) area. The measurements are an extension of some of our previous work (chapter 2; chapter 5), in which we presented DPOAE phase-frequency and amplitude-frequency data measured with f_1 - and f_2 -sweeps, and group delays determined at optimum ratio only. In several respects, the data and their analysis are also an extension and further

elaboration of the work of Knight and Kemp (2000; 2001). Because of the higher signal-to-noise ratio in the guinea pig (chapter 2) more detailed information could be obtained on higher order DPOAEs. Besides the presentation of amplitude and phase maps, several more quantitative ways of analyzing the data are elaborated, concentrating on group delays and their mutual relations as a function of f_2/f_1 ratio. To investigate the influence of stimulus level ratio on the relative contribution of the distortion and reflection components, we used two sets of stimulus levels. Finally, some interesting results on fine structure in guinea pig DPOAEs are considered.

6.2 Theory

The (f_1, f_2) area representation that we use in this chapter is schematically shown in figure 6.1, as an empty (f_1, f_2) matrix on which amplitude and phase can be plotted. Both upper and lower sideband DPOAEs ($f_{dp} > f_1, f_2$ and $f_{dp} < f_1, f_2$ respectively) will be shown in the same representation, with f_2 on the horizontal axis. Lines of constant DP frequency are parallel in this representation, and shown for the cubic distortion product $2f_1 - f_2$ (solid). Their slope depends on DPOAE order. Lines of constant frequency ratio f_2/f_1 (dashed) radiate from the origin (0,0). When DPOAE phase is known in all points neighbouring (f_1, f_2) in this representation, phase slope delays in all desired directions can be obtained. Phase slope delay (often called group delay) is defined as

$$D = -\frac{1}{2\pi} \frac{d\varphi_{dp}}{df_{dp}} \quad (6.1)$$

with φ_{dp} the phase of the distortion product and $f_{dp} = (n+1)f_1 - nf_2$ (n integer, and $f_1 < f_2$). A group delay is usually measured by changing the DPOAE frequency f_{dp} in one of three controlled manners; by changing f_1 while keeping f_2 fixed (f_1 -sweep), by changing f_2 while keeping f_1 fixed (f_2 -sweep), and by changing both f_1 and f_2 at a fixed frequency ratio. We term the resulting delays respectively D_1 , D_2 , and $D_{12|R}$. In the (f_1, f_2) area representation, trigonometrical relations hold between the phase gradients in the two perpendicular directions and the phase gradient in an oblique direction at angle α (see figure 6.1). However, these phase gradients are not derivatives to the DPOAE frequency f_{dp} . The f_1 - and f_2 -sweep group delays can be calculated from the phase gradients as follows:

$$D_1 = -\frac{1}{2\pi} \frac{d\varphi}{df_{dp}}|_{f_2} = -\frac{1}{2\pi} \frac{1}{n+1} \frac{\partial\varphi}{\partial f_1}, \quad (6.2)$$

$$D_2 = -\frac{1}{2\pi} \frac{d\varphi}{df_{dp}}|_{f_1} = \frac{1}{2\pi} \frac{1}{n} \frac{\partial\varphi}{\partial f_2}. \quad (6.3)$$

The group delay in any direction α can be calculated by expressing the DPOAE phase change and frequency change as a function of α and the change in f_2 . At constant α the DPOAE phase change is given by

$$d\varphi|_\alpha = \left(\frac{\partial\varphi}{\partial f_1} \cdot \tan \alpha + \frac{\partial\varphi}{\partial f_2} \right) df_2 = -2\pi ((n+1) \cdot \tan \alpha \cdot D_1 - n \cdot D_2) df_2 \quad (6.4)$$

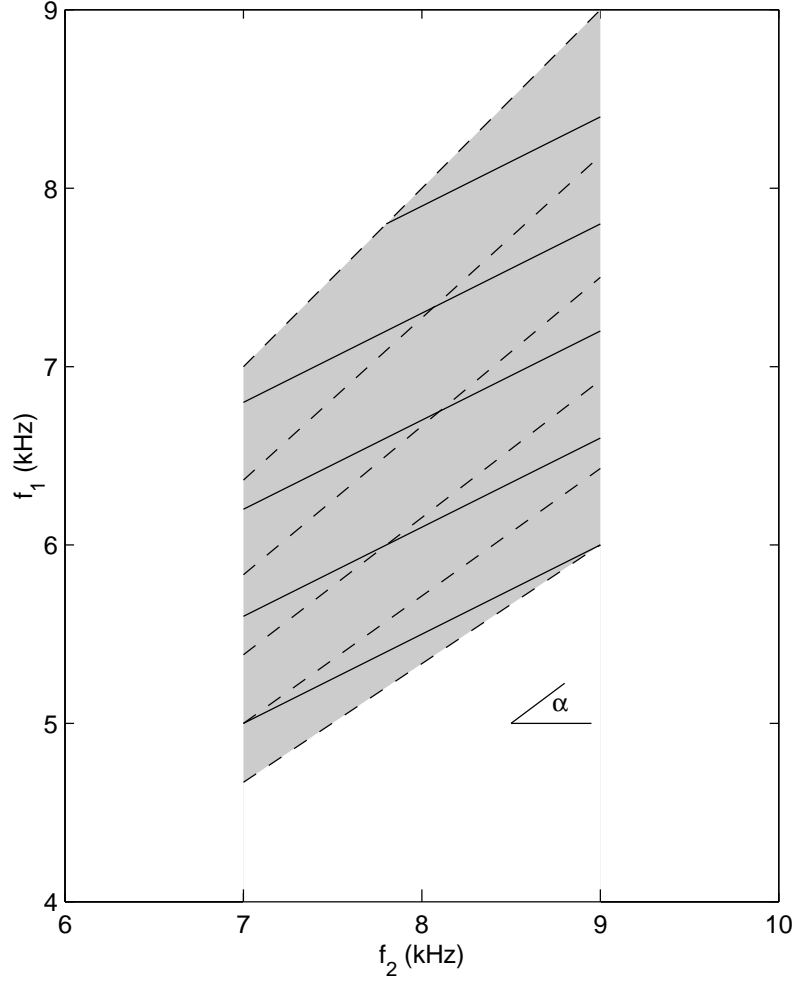


Figure 6.1: The (f_1, f_2) area representation. Amplitude and phase will be plotted on this empty (f_1, f_2) matrix. Lines of constant f_{dp} are parallel in this representation, and are shown for the $2f_1 - f_2$ distortion product (solid). Their slope depends on DPOAE order. Lines of constant f_2/f_1 (dashed) radiate from the origin $(0,0)$.

while the associated DPOAE frequency change is given by

$$df_{dp}|_{\alpha} = ((n+1) \cdot \tan \alpha - n) df_2. \quad (6.5)$$

Combining equations 6.1, 6.4, and 6.5 results in the group delay for constant α in a point (f_1, f_2) , which depends on the f_1 - and f_2 -sweep group delays D_1 and D_2 according to:

$$D(\alpha) = -\frac{1}{2\pi} \frac{d\varphi}{df_{dp}}|_{\alpha} = \frac{(n+1) \cdot \sin \alpha \cdot D_1 - n \cdot \cos \alpha \cdot D_2}{(n+1) \cdot \sin \alpha - n \cdot \cos \alpha}. \quad (6.6)$$

This reduces to the f_1 -sweep group delay D_1 for $\alpha = 90^\circ$ and the f_2 -sweep group delay D_2 for $\alpha = 0^\circ$. For a sweep with constant frequency ratio f_2/f_1 , the group delay $D_{12|R}$ can be

derived from D_1 and D_2 by applying equation 6.6 using $\alpha = \arctan(f_1/f_2)$ and

$$\rho_n = \frac{n+1}{nR} \quad (6.7)$$

with $R = f_2/f_1$. This results in

$$D_{12|R} = \frac{\rho_n \cdot D_1 - D_2}{\rho_n - 1}. \quad (6.8)$$

This expression, which is independent of any model or generation mechanism, relates the three phase-gradient delays, and is in fact the same relation Shera *et al.* (2000, equation 22) have derived.

6.2.1 Distortion component

For the distortion component (or wave-fixed DPOAE component), under the assumptions of a logarithmic place-frequency map and frequency-shift invariance, the phase profiles of the components involved in DPOAE generation are fixed when the frequency ratio f_2/f_1 is kept constant (chapter 3; Talmadge *et al.*, 1998). This implies that changing the DPOAE frequency in a fixed-ratio-sweep yields a flat phase versus frequency curve for the distortion component, resulting in

$$D_{12|R} = 0. \quad (6.9)$$

Combining equations 6.8 and 6.9 gives the previously derived relation between D_1 and D_2 for the wave-fixed model (chapter 3; Schneider *et al.*, 2000; Talmadge *et al.*, 2000)

$$\frac{D_2}{D_1} = \frac{n+1}{n} \frac{f_1}{f_2} = \rho_n. \quad (6.10)$$

So, the group delays of a DPOAE consisting only of the distortion component (a wave-fixed emission), are expected to obey equations 6.9 and 6.10, which express exactly the same feature as isophase contours in the direction of constant f_2/f_1 in the area representation. This holds for both lower sideband and upper sideband DPOAEs, with a distortion component generated at any place along the basilar membrane.

6.2.2 Reflection component

When the reflection component (a place-fixed emission) dominates the total lower sideband DPOAE, the phase is expected to be constant in a direction of constant f_{dp} (Knight and Kemp, 2000), implying

$$D(\alpha) = 0 \quad (6.11)$$

with $\tan(\alpha) = \frac{n}{n+1}$. Substituting this in equation 6.6 results in

$$\frac{D_2}{D_1} = 1. \quad (6.12)$$

Subsequently, with equation 6.8 this results in

$$D_{12|R} = D_1 = D_2. \quad (6.13)$$

This relation, for the case of a dominant reflection component, has also been predicted by Tubis *et al.* (2000).

A similar analytical treatment of the upper sideband DPOAEs based on their re-emission at the more basal X_{dp} has not been derived so far, albeit that for the USB re-emission component $D_{12|R}$ will be different from zero. In addition, equations 6.12 and 6.13 will hold for $f_2/f_1 = 1$ and large f_2/f_1 . Possible small deviations may occur for midrange ratios (Knight and Kemp, 2000).

6.3 Methods

6.3.1 Animal care and preparation

The results presented in this study have been obtained from acute experiments in 6 female albino guinea pigs with a body weight of 440–545 g ($n=5$) or 900 g ($n=1$). They all showed healthy middle ears upon otoscopic inspection and positive Preyer's reflexes. The guinea pigs were premedicated with atropine-sulphate (75 $\mu\text{g/kg}$, intramuscular) and anaesthetized with an intramuscular injection of thalamonal (1.6 ml/kg), which is a combination of fentanyl (0.05 mg/ml) and droperidol (2.5 mg/ml), followed 15 minutes later by nembutal (23 mg/kg, intraperitoneal). Supplementary doses were administered approximately every 60 min (fentanyl, 0.08 mg/kg) and every 80 minutes (nembutal, 2.7 mg/kg). Body temperature was maintained at $38 \pm 0.5^\circ\text{C}$ using a thermostatically controlled heating pad. The guinea pigs were tracheotomised and the trachea was cleared at least every hour. The ear with the highest $2f_1 - f_2$ amplitude at $f_2 = 8$ kHz (with $f_2/f_1 = 1.3$, $L_1 = 65$ dB SPL, $L_2 = 55$ dB SPL) was used in the experiments. The pinna of this ear was removed leaving a small part of the external auditory meatus. The head was stabilized with a bite-ring, an earbar in the contralateral external auditory meatus, and a probeholder in the ipsilateral external auditory meatus (with removed pinna). The microphone probe assembly was sealed into the external auditory meatus through the probeholder. This experimental approach was chosen because of the desired stable recording conditions over a long duration of data collection. Procedures were approved by the animal care committee of the Leiden University.

6.3.2 Material

DPOAEs were measured using a Tucker Davis Technologies (TDT) system, consisting of a signal processing board, AD- and DA-converters, a trigger device, a clock-generator, headphone buffers, and programmable attenuators. Customized software, developed in Delphi (Borland) was used. The clock-generator provided a clock rate of 100 kHz, which synchronized the trigger device, AD-, and DA-converters and served as the sample rate for both AD and DA conversion. Stimulus tones f_1 and f_2 were played from two separate

DA channels, attenuated separately and delivered to separate ER2 transducers (Etymotics Research). A low-noise microphone ER10-B (Etymotics Research), housed in a customized probe, recorded the frequency response in the ear canal. The microphone signal was preamplified 40 dB.

6.3.3 DPOAE recording paradigms

DPOAEs were measured at 2233 stimulus frequency combinations arranged in the (f_1, f_2) plane as indicated in figure 6.2. Frequency f_2 varied between 7 and 9 kHz, and the frequency ratio f_2/f_1 was kept between 1.01 and 1.50. In both directions, frequency steps were 48.8 Hz. These stimulus frequency combinations were played as f_1 -sweeps from low to high frequency ratio, starting with a fixed f_2 of 7 kHz and ending with f_2 at 9 kHz. First, DPOAEs were measured for all 2233 combinations at stimulus levels $L_1 = 65$ dB SPL, $L_2 = 55$ dB SPL. Including intermittent calibrations and DPgrams, this took about 4.5 hours for 1 guinea pig ear. Second, the procedure was repeated in the same ear for stimulus levels $L_1 = 55$ dB SPL, $L_2 = 65$ dB SPL. At each (f_1, f_2) stimulus tones were played

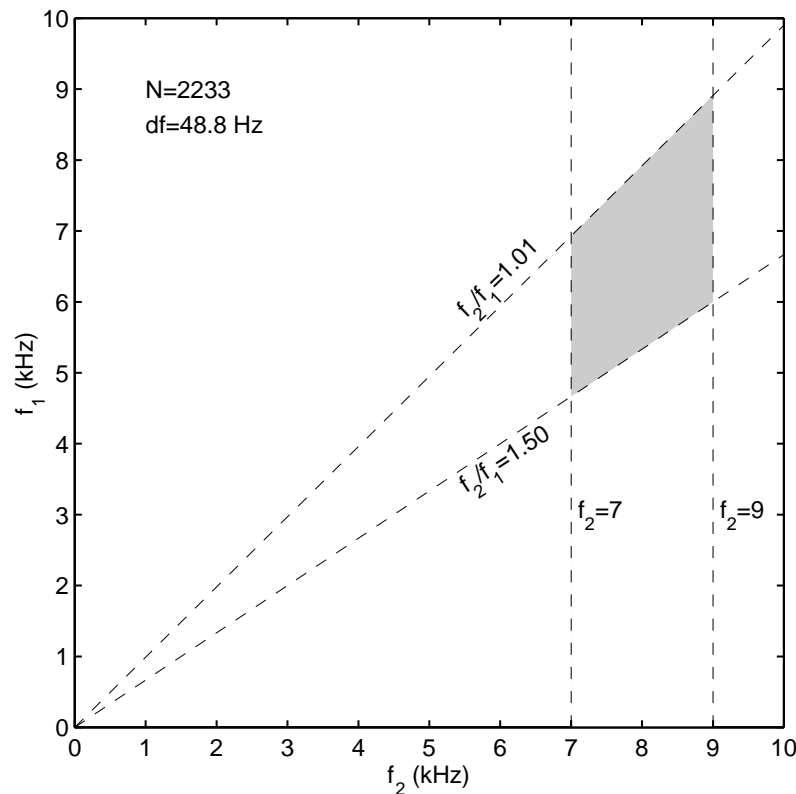


Figure 6.2: Area (shaded) of frequency combinations in the (f_1, f_2) plane at which the DPOAE measurements were done. Frequency f_2 varied from 7 to 9 kHz, ratio f_2/f_1 from 1.01 to 1.50. With a frequency spacing of 48.8 Hz in both directions, the area contains 2233 stimulus frequency pairs.

continuously during 204 windows of 20.48 ms. After an onset of 4 windows, 200 windows were averaged adding up to a total recording time of 4.096 seconds per stimulus frequency combination. Phase changes in the probe were corrected by subtracting $2\varphi_1 - \varphi_2$ from the measured DPOAE phase (for $f_{dp} = 2f_1 - f_2$) where φ_1 and φ_2 are the phases of f_1 and f_2 at the location of the microphone. During the entire experiment, at regular intervals a calibration procedure was performed to set the levels of the stimulus tones. Also $2f_1 - f_2$ DPgrams were measured at $f_2 = 4, 5.6$, and 8 kHz, with $f_2/f_1 = 1.3$ and $L_1, L_2 = 65, 55$ dB SPL. When the DPOAE amplitude at 8 kHz differed more than 3 dB from the previously measured DPgram, the ear canal was checked and the probe replaced. Stable recordings over the entire measurement time could be obtained in most ears, although in rare occasions an apparent change in the response over time could not be explained. The six animals for which data are elaborated here represent the more stable recordings in a larger group of animals.

6.3.4 Data analysis

Apart from online processing in Delphi (Borland) to monitor the course of the experiment, data analysis was done offline with custom-designed MATLAB routines. From the averaged acoustic response for each (f_1, f_2) the amplitude and phase spectra were calculated using an FFT algorithm. For five distortion products ($2f_1 - f_2$, $3f_1 - 2f_2$, $4f_1 - 3f_2$, $2f_2 - f_1$, and $3f_2 - 2f_1$) the amplitudes, noise levels, and phases were taken from those spectra. Noise level was defined as the average amplitude of the six frequency bins closest to the DPOAE frequency. For each distortion product, amplitude and phase were represented in an (f_1, f_2) area plot. The phase was unwrapped in two dimensions (f_1 and f_2), to eliminate 2π phase jumps. Due to phase jumps of approximately π , and missing points that did not meet the signal-to-noise criterion, unwrapping in two dimensions is sometimes ambiguous and then the outcome depends on the order in which the (f_1, f_2) plane is crossed. Care was taken to unwrap the phase plane as neatly as possible, especially at the small ratio side. In each (f_1, f_2) point, the slope of the phase plane was determined in two directions (constant f_1 and constant f_2), by fitting a linear regression line over 3 points ((f_1, f_2) and the two neighbouring points). This was only done if the amplitudes in all three points met the signal-to-noise criterion of 6 dB. To prevent phase irregularities due to unwrapping or other problems to contaminate the results, the phase slope was excluded from further analysis if the correlation coefficient was smaller than 0.988 (corresponding to $p = 0.10$). From the phase slopes in the two perpendicular directions in the (f_1, f_2) plane, group delays D_1 and D_2 were calculated. Note that the difference with the slopes is that the group delays are phase derivatives to f_{dp} instead of f_1 or f_2 . Equation 6.8 was used to determine $D_{12|R}$, the group delay for fixed frequency ratio. The criterion for the correlation coefficient was estimated to lead to maximum errors in $D_{12|R}$ in the order of 0.2 ms.

6.4 Results

6.4.1 Incidence of the different DPOAE orders

For all five DPOAEs and the two sets of stimulus levels the percentage of (f_1, f_2) combinations at which the signal-to-noise ratio was larger than 6 dB was calculated, as a measure for the relative incidence of the DPOAE orders. Table 6.1 shows the averages of six experiments with standard deviations. All percentages are referenced to 2233, the maximum number of (f_1, f_2) points in the chosen area. Note that the DPOAE frequency $4f_1 - 3f_2$ is negative for frequency ratios above 1.33, so the maximum number of (f_1, f_2) combinations for that DPOAE is 1638 which corresponds to 73%. Table 6.1 shows that at stimulus levels $L_1 = 65, L_2 = 55$ dB SPL the lower sideband DPOAE $2f_1 - f_2$ performs best. When stimulus levels $L_1 = 55, L_2 = 65$ dB SPL are used, which are not considered optimal for the $2f_1 - f_2$ DPOAE, a decrease is seen in the incidence of all lower sideband DPOAEs but a dramatic increase occurs in the incidence of the upper sideband DPOAEs, especially for $3f_2 - 2f_1$. With $L_1 = 55, L_2 = 65$ dB SPL $2f_1 - f_2$ and $2f_2 - f_1$ are equally well represented.

Table 6.1: Percentage of (f_1, f_2) combinations at which the signal-to-noise ratio > 6 dB. Averaged results of 6 experiments, with standard deviations.

DPOAE	$L_1, L_2 = 65, 55$	$L_1, L_2 = 55, 65$
$2f_1 - f_2$	$96 \pm 2\%$	$90 \pm 4\%$
$3f_1 - 2f_2$	$85 \pm 2\%$	$53 \pm 10\%$
$4f_1 - 3f_2$	$55 \pm 3\%$	$23 \pm 4\%$
$2f_2 - f_1$	$76 \pm 10\%$	$89 \pm 5\%$
$3f_2 - 2f_1$	$29 \pm 2\%$	$79 \pm 5\%$

6.4.2 Amplitude and phase characteristics in the (f_1, f_2) plane

Stimulus levels $L_1, L_2 = 65, 55$ dB SPL

In figure 6.3 amplitude and unwrapped phase of the lower sideband DPOAEs $2f_1 - f_2$, $3f_1 - 2f_2$, and $4f_1 - 3f_2$, measured in one guinea pig (GP55), are shown in the (f_1, f_2) area representation. These results are obtained with stimulus levels $L_1 = 65, L_2 = 55$ dB SPL. Only data with a signal-to-noise ratio better than 6 dB are shown. The area where the amplitude is maximum runs approximately in the direction of a constant frequency ratio (figure 6.3A, C, E; cf figure 6.1). There are also some valleys, e.g. in figure 6.3A for small frequency ratios, that run in a different direction, approximately constant f_{dp} . Note that these amplitude valleys seem to have corresponding isophase profiles (figure 6.3A vs 6.3B). Generally however, isophase contours run in the directions of constant frequency ratio, as do the amplitude maxima.

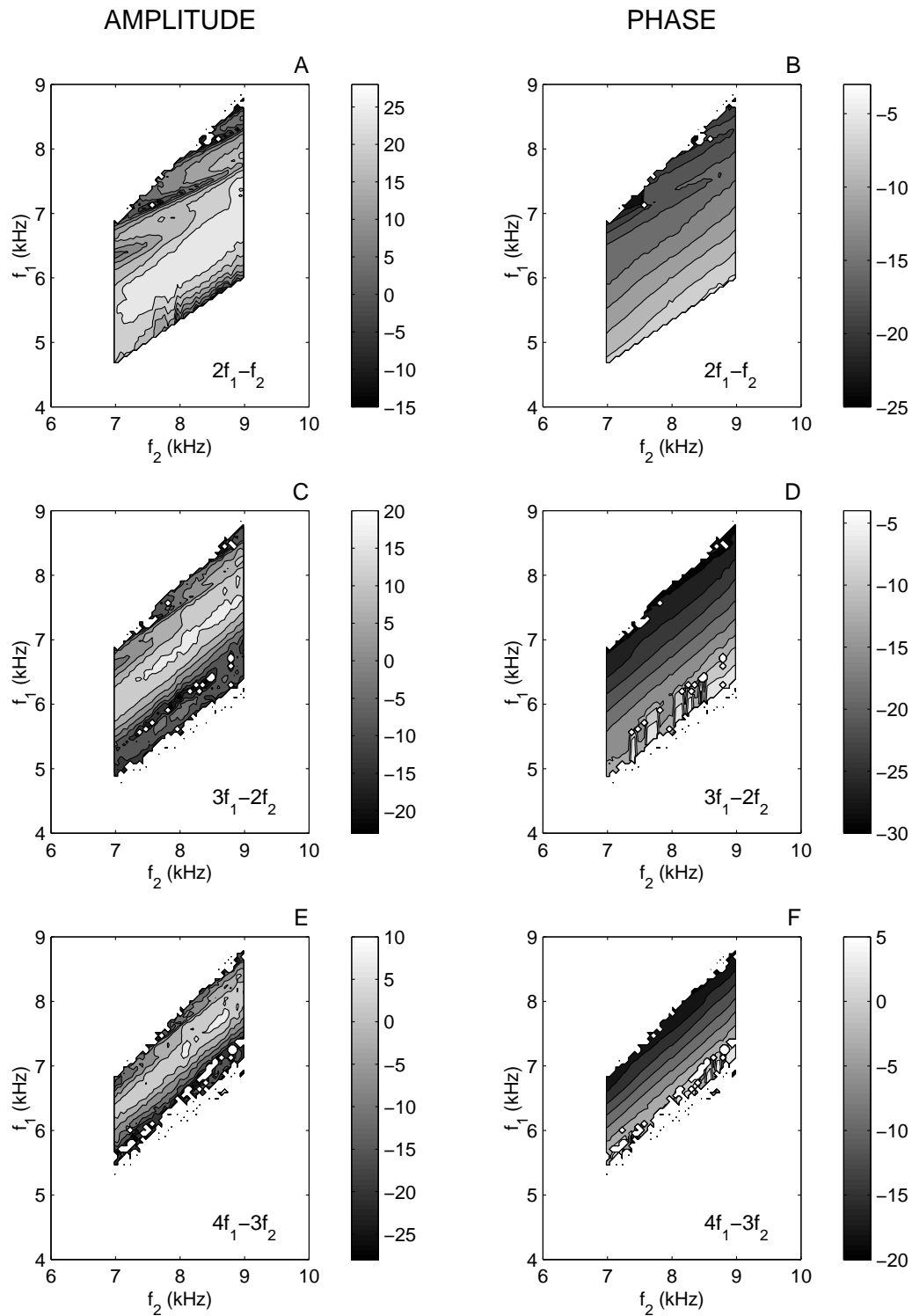


Figure 6.3: Amplitude (left) and unwrapped phase (right) of the three lower sideband DPOAEs in the (f_1, f_2) area representation. Measured at $L_1, L_2 = 65, 55$ dB SPL, in GP55. Grayscales indicate amplitude in dB SPL and phase in radians.

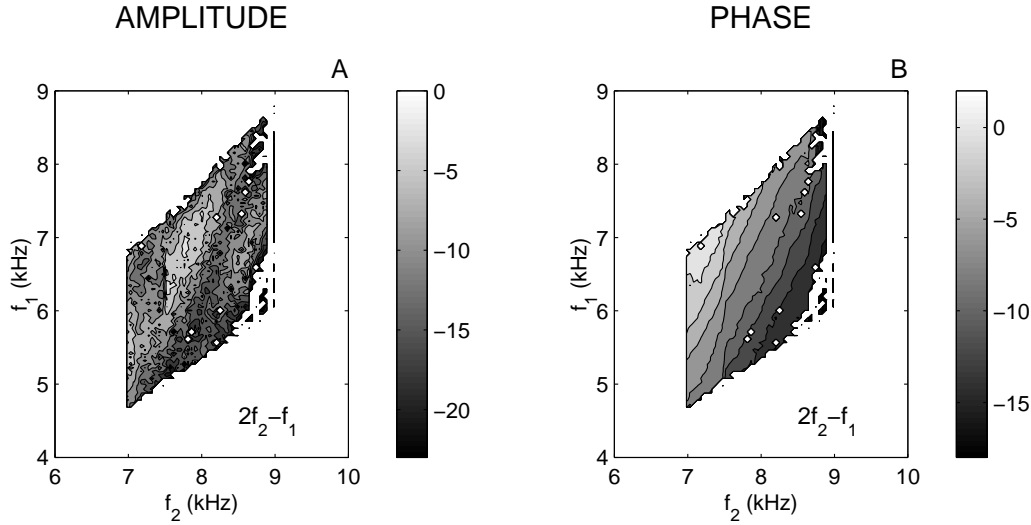


Figure 6.4: Amplitude (left) and unwrapped phase (right) of the upper sideband DPOAE $2f_2 - f_1$, measured in GP70 at $L_1, L_2 = 65, 55$ dB SPL.

The amplitude and phase data of the upper sideband DPOAE $2f_2 - f_1$ measured in GP70 are plotted in figure 6.4. Stimulus levels were again $L_1 = 65, L_2 = 55$ dB SPL. Constant phase now appears to be in a completely different direction than in figure 6.3 for the lower sideband DPOAEs. Isophase contours approximately follow the direction of constant DPOAE frequency. Again there is a correspondence between amplitude and phase patterns. The results shown in figures 6.3 and 6.4 for GP55 and GP70 were representative for all other animals.

Stimulus levels $L_1, L_2 = 55, 65$ dB SPL

Figure 6.5 shows the amplitude and phase patterns of the lower sideband DPOAEs measured with the second set of stimulus levels, $L_1 = 55, L_2 = 65$ dB SPL, in GP55. With this set of stimulus levels there is only a small portion of the (f_1, f_2) area in which $4f_1 - 3f_2$ has a good signal-to-noise ratio (see also table 6.1). When the amplitude pattern of the $2f_1 - f_2$ DPOAE with these stimulus levels is compared with the $2f_1 - f_2$ amplitude at $L_1, L_2 = 65, 55$ dB SPL (figure 6.3A) it is evident that the overall DPOAE amplitude is smaller but also that the maximum amplitude occurs in a different region and, notably, follows the direction of constant f_{dp} instead of constant f_2/f_1 as in figure 6.3. Now the maximum amplitude and isophase contours are generally not in the same direction; isophase contours still follow the direction of constant frequency ratio, as in figures 6.3B, D, and F with stimulus levels $L_1, L_2 = 65, 55$ dB SPL.

In figure 6.6 the amplitude and phase of the upper sideband DPOAE $2f_2 - f_1$ are shown, measured in GP70 with stimulus levels $L_1 = 55, L_2 = 65$ dB SPL. Maximum amplitude and constant phase follow lines in the direction of constant DPOAE frequency, as with the first set of stimulus levels in figure 6.4.

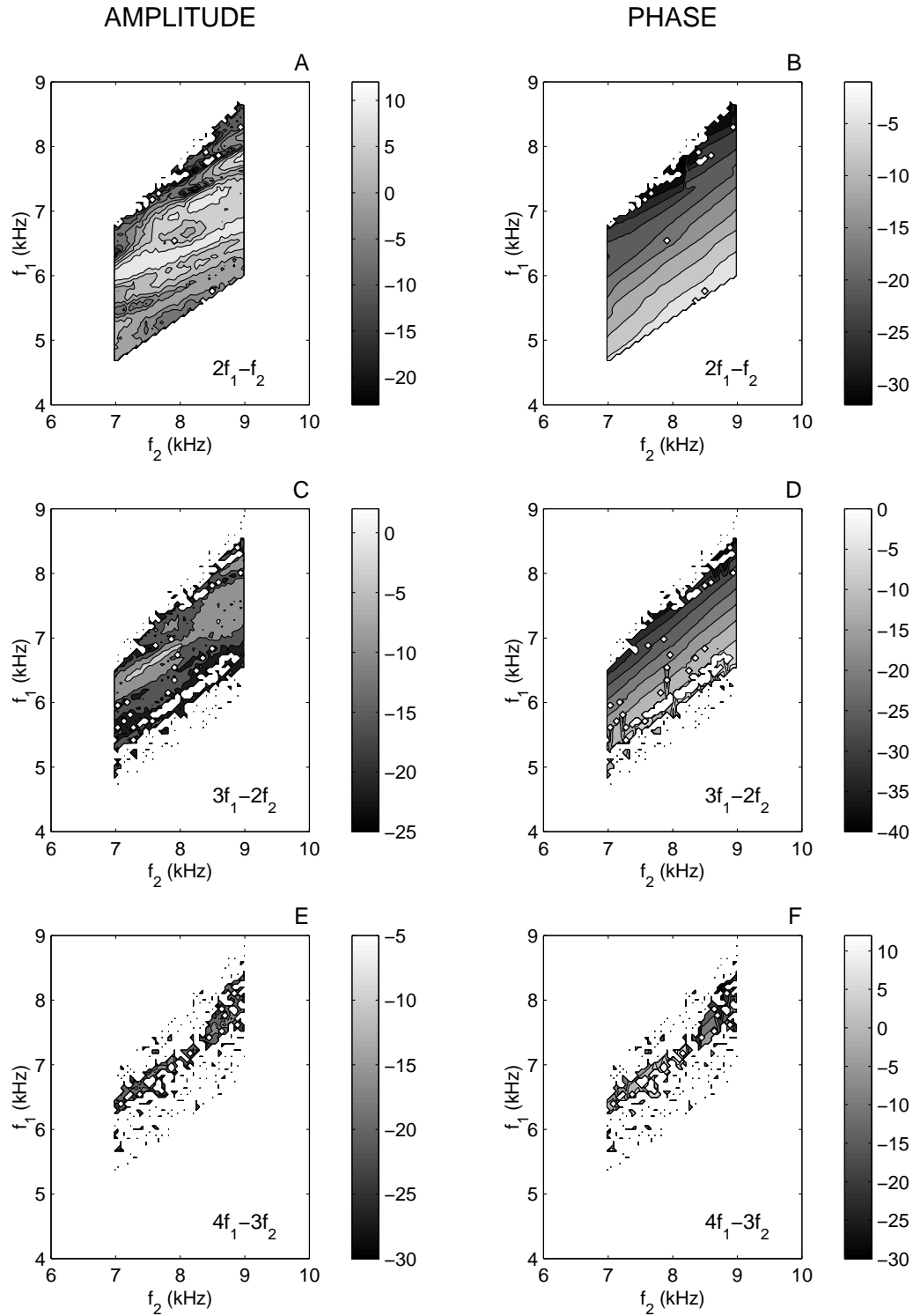


Figure 6.5: Amplitude (left) and unwrapped phase (right) of the three lower sideband DPOAEs measured in GP55, with $L_1, L_2 = 55, 65$ dB SPL.

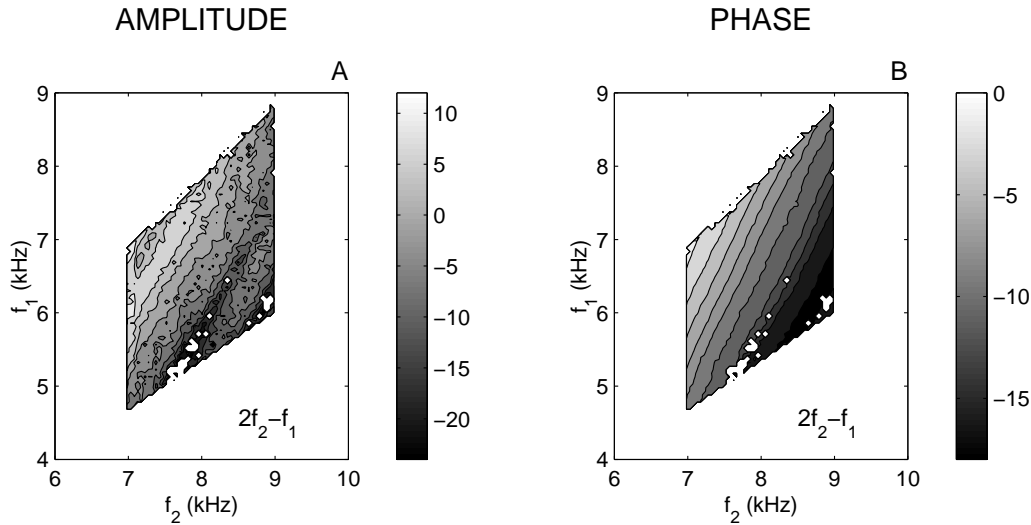


Figure 6.6: Amplitude (left) and unwrapped phase (right) of the upper sideband DPOAE $2f_2 - f_1$, measured in GP70 with stimulus levels $L_1, L_2 = 55, 65$ dB SPL.

6.4.3 Group delays

From all phase planes, group delays D_1 and D_2 were determined at every combination (f_1, f_2) , and $D_{12|R}$ derived using equation 6.8. In figure 6.7A, pooled $D_{12|R}$ data is plotted as a function of f_2/f_1 for the lower sideband DPOAE $2f_1 - f_2$, with $L_1 = 65, L_2 = 55$ dB SPL. Only group delays from fits with a correlation coefficient $r > 0.988$ (corresponding to $p < 0.10$) are shown. The solid line at $D_{12|R} = 0$ is the prediction from the wave-fixed model, describing the nonlinear distortion component (equation 6.9). The wave-fixed hypothesis is met for the intermediate frequency ratios, but not for f_2/f_1 below approximately 1.20 and not towards the higher ratios that were explored (> 1.35). As was shown in section 6.2, the relation between $D_{12|R}$, D_1 and D_2 implies that if $D_{12|R} = 0$, equation 6.10 holds for D_2/D_1 . In figure 6.7B, D_2/D_1 versus f_2/f_1 is shown for the same DPOAE together with the prediction from equation 6.10, and again it is clear that the wave-fixed hypothesis is met in a limited intermediate range of f_2/f_1 . For small frequency ratios D_2/D_1 approaches 1, in accordance with equation 6.12, indicating that for f_2/f_1 close to 1 the reflection component is dominant. Note that the same data was used for figures 6.7A and 6.7B, and that the results are equivalent as expected from section 6.2.

For figure 6.8, the f_2/f_1 axis was divided into segments of width 0.02. In all segments the mean D_2/D_1 over all tested ears was calculated as well as the standard error of the mean (s.e.m). The error bars indicate plus and minus twice the s.e.m. In the left column, the results for four DPOAEs are given, measured with $L_1 = 65, L_2 = 55$ dB SPL, and in the right column the same is done for stimulus levels $L_1 = 55, L_2 = 65$ dB SPL. In each subplot, the prediction from the wave-fixed hypothesis (equation 6.10) is given with a solid line. For the higher order DPOAEs with stimulus levels $L_1 = 65, L_2 = 55$ dB SPL (figures 6.8C,E), the error bars are quite large at high frequency ratios. This is due to the fact that

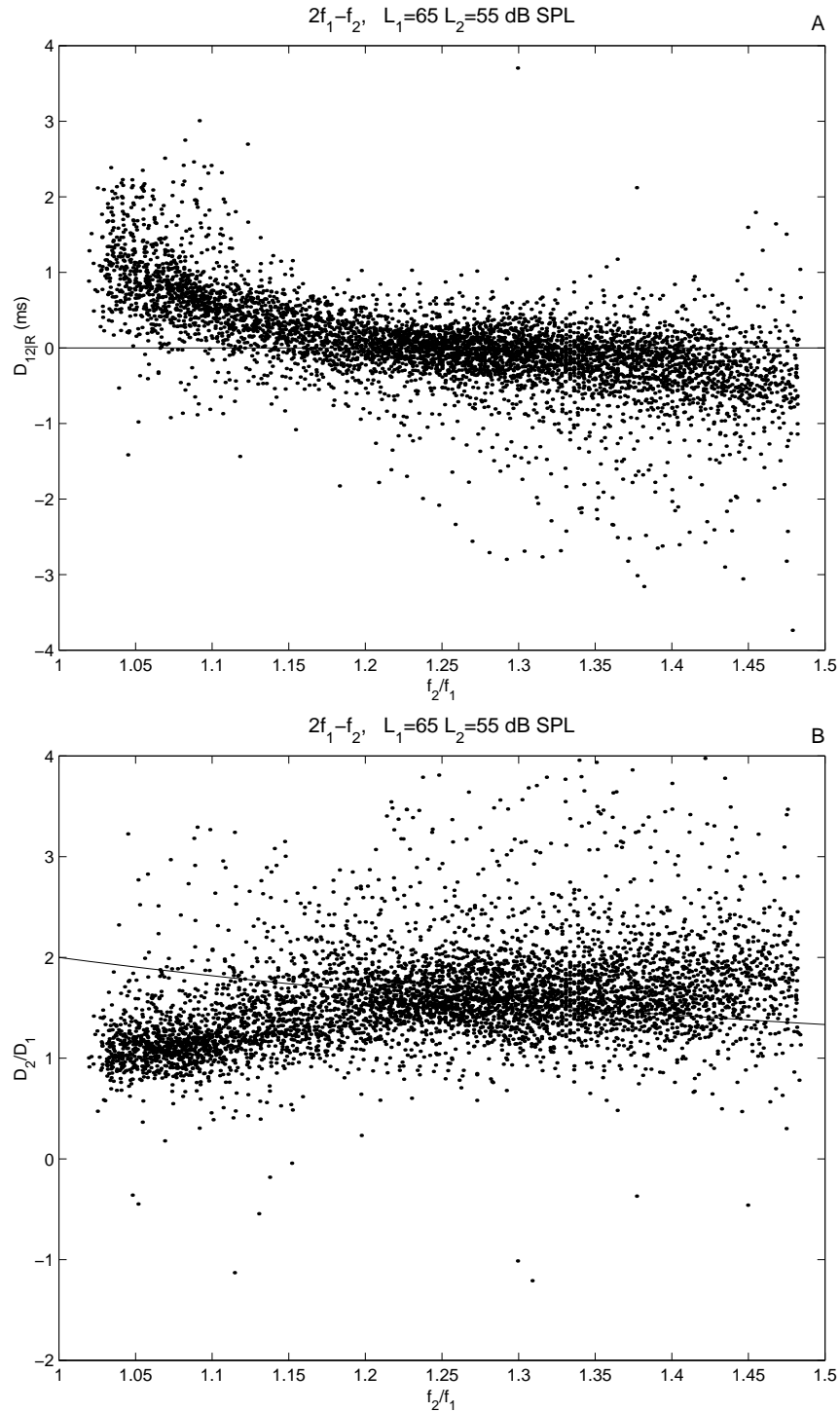


Figure 6.7: A.) Group delay $D_{12|R}$ (constant frequency ratio) as a function of f_2/f_1 . Pooled data from 6 experiments, $L_1, L_2 = 65, 55$ dB SPL. B.) Ratio of f_2 - and f_1 -sweep group delays D_2/D_1 plotted as a function of frequency ratio f_2/f_1 . Again for the DPOAE $2f_1 - f_2$, pooled data, with $L_1, L_2 = 65, 55$ dB SPL. Solid lines in A). and B). represent predictions of the wave-fixed model.

the DPOAE frequency approaches zero (for $3f_1 - 2f_2$ at $f_2/f_1=1.50$ and for $4f_1 - 3f_2$ at $f_2/f_1=1.33$) which gives a poor signal to noise ratio. In figure 6.8F it is clear that no conclusions can be drawn for the $4f_1 - 3f_2$ component measured with $L_1 = 55, L_2 = 65$ dB SPL, also due to a bad signal to noise ratio (see also table 6.1). Based on a strict reasoning with the 95% confidence interval, the wave-fixed model is obeyed only for $f_2/f_1=1.19-1.27$ ($2f_1 - f_2$, with $L_1, L_2 = 65, 55$ dB SPL, figure 6.8A). The frequency ratio range where the data fits the wave-fixed prediction is centered at lower ratios for higher order DPOAEs (figures 6.8C,E). With the second set of stimulus levels, the range of the agreement with the wave-fixed prediction is wider, from 1.15 to 1.35 for the $2f_1 - f_2$ (figure 6.8B). The higher order DPOAE $3f_1 - 2f_2$ obeys the wave-fixed prediction for a wider range of f_2/f_1 , starting at a lower value. In figures 6.8G and H the results for the upper sideband DPOAE $2f_2 - f_1$ are shown. For both stimulus level combinations the delay ratio D_2/D_1 is close to one, independent of frequency ratio.

6.4.4 Fine structure

In figure 6.9 data from GP55 are presented as a series of f_1 -sweeps. In the upper panels the DPOAE amplitude ($2f_1 - f_2$) is plotted; for each successive f_1 -sweep ($f_2 = 7$ kHz at the bottom and 9 kHz at the top of the chart) the amplitude is shifted by an amount of 2 dB for presentation purposes. In the lower panels the corresponding phase versus frequency curves are shown, with each curve shifted by 2 radians. The notches in the DPOAE amplitude are approximately aligned at the same f_{dp} (figures 6.9A,B). These amplitude notches are accompanied by irregularities in the DPOAE phase as can be seen by comparing the upper and lower panels. Sometimes these phase irregularities equal π , resulting in ambiguities with phase unwrapping. In figure 6.9B there are also amplitude irregularities aligned in an oblique direction, not comprehensibly related to f_{dp} or one of the stimulus frequencies. Figure 6.10 shows another example of a series of f_1 -sweeps (as in figure 6.9), now measured in GP70. Again, the irregularities in amplitude are accompanied by phase irregularities, aligned at f_{dp} for stimulus levels $L_1, L_2 = 65, 55$ dB SPL (figure 6.10A,C). At the second set of stimulus levels however (figure 6.10B,D), the pattern of fine structure is approximately aligned at a fixed frequency ratio ($f_2/f_1 \approx 1.10$).

6.5 Discussion

6.5.1 Incidence of the different DPOAE orders

Optimal detectability of DPOAEs is commonly assumed to occur when the amplitudes of the basilar membrane vibrations for the two primaries at the site of generation is similar, because then nonlinear interaction is largest. Indeed, many studies indicate that taking L_1 larger than L_2 is optimal for the detection of the most commonly studied $2f_1 - f_2$, both at the generally used primary levels in the order of 60 dB SPL and at lower levels (Kummer *et al.*, 2000). Higher order lower sideband (LSB) DPOAEs have lower amplitudes and are therefore less detectable against the background noise. Our findings summarized in table

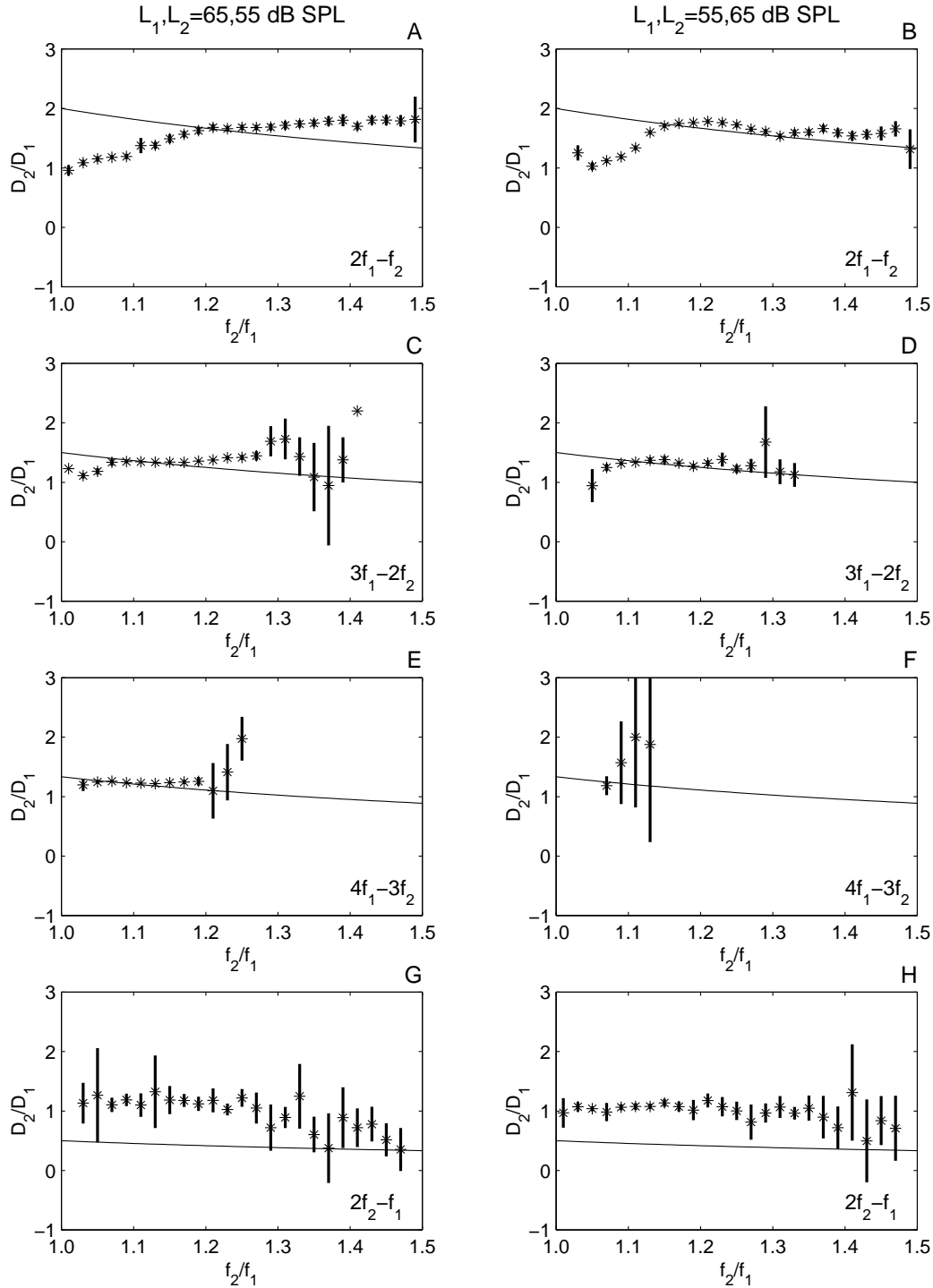


Figure 6.8: Averaged D_2/D_1 with \pm twice the s.e.m., for the DPOAEs $2f_1 - f_2$, $3f_1 - 2f_2$, $4f_1 - 3f_2$, and $2f_2 - f_1$. Left column: Stimulus levels $L_1, L_2 = 65, 55$ dB SPL. Right column: $L_1, L_2 = 55, 65$ dB SPL. Solid lines indicate the prediction from the wave-fixed model. For many data the s.e.m. is small and therefore the error bar seemingly absent.

6.1 agree with these literature data for the LSB components, in that detectability decreases for higher order components, and is better for the $L_1, L_2 = 65, 55$ than for the $L_1, L_2 = 55, 65$ condition. For the upper sideband (USB) components detectability also decreases with increasing order of the component but, contrary to the LSB DPOAEs, is significantly better for the $L_1, L_2 = 55, 65$ than for the $L_1, L_2 = 65, 55$ condition (table 6.1). The cause of this difference could possibly be found in the difference in components (distortion, reflection, re-emission or other) that contribute to the LSB and USB DPOAEs.

6.5.2 Amplitude and phase characteristics in the (f_1, f_2) plane

The presentation of our data was given in a different format from the main other area study published, that by Knight and Kemp (2000). In our area representation, the stimulus parameters f_1 and f_2 are fixed on the y- and x-axis respectively, so all DPOAEs are shown in separate plots. One of the formats used by Knight and Kemp (2000), with the DP frequency on the x-axis and f_2/f_1 on the y-axis, is convenient for showing features that align either with f_{dp} or with f_2/f_1 because such patterns are exactly horizontal or vertical. However, this requires a different set of stimulus frequencies, with a quite large range of f_1 and f_2 . Since we were interested in the full range of frequency ratios from 1.01 to 1.50, but needed to take care not to use too large a range of f_2 (especially around $f_2 = 4$ kHz some unexplained anomalies were found to occur in guinea pig DPOAEs, chapter 5), we could not use the same $(f_{dp}, f_2/f_1)$ representation that Knight and Kemp (2000) did.

In this DPOAE area study in the guinea pig, features of the DPOAE amplitude and phase generally correspond to characteristics found by Knight and Kemp (2000) in their human area study. In both studies, amplitude valleys were found for $2f_1 - f_2$ that follow lines of approximately constant DP frequency. In addition, notches in phase were found to coincide with amplitude valleys, which is a characteristic of two wave mixing. Except at low ratios, isophase contours for LSB DPOAEs run in the direction of constant frequency ratio, while for USB DPOAEs those contours follow lines of constant DP frequency at all frequency ratios. The transition for $2f_1 - f_2$ occurs at a ratio of 1.1 to 1.15 in the study by Knight and Kemp (2000), in the present study that ratio is slightly larger (1.15 to 1.20) and depends on the stimulus levels. Both studies showed that the transition occurs at smaller ratios for higher order LSB DPOAEs.

A disadvantage of the (f_1, f_2) representation we chose seems to be that it is difficult to see the alignment of constant phase or amplitude with f_{dp} or f_2/f_1 . Isophase lines in these directions are oblique in our representation. Therefore, instead of only qualitatively studying the phase maps, one could quantitatively analyse the direction of constant phase by calculating the angle in the (f_1, f_2) area at which the phase gradient equals zero. This angle β can be shown to be directly related to the DPOAE order and the f_1 - and f_2 -sweep group delays D_1 and D_2 as follows:

$$\beta = \arctan \left(\frac{n}{(n+1)} \frac{D_2}{D_1} \right) \quad (6.14)$$

Therefore, instead of analyzing the angle β of the isophase lines, it is equivalent to consider D_2/D_1 and this is exactly what we did in figures 6.7B and 6.8. The prediction of Knight

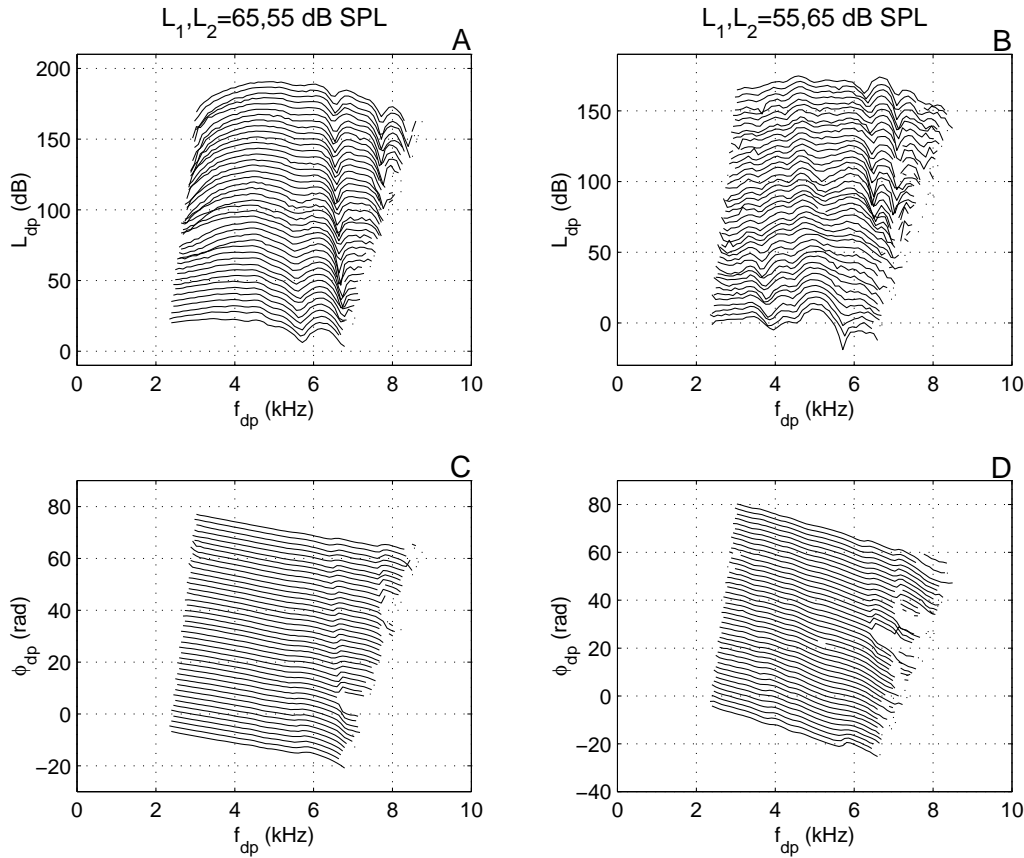


Figure 6.9: DPOAE amplitude and phase as a function of f_{dp} from successive f_1 -sweeps, for the lower sideband DPOAE $2f_1 - f_2$, measured in GP55. The amplitude curves of successive sweeps (with increasing f_2) were shifted 2 dB, phase curves 2 rad. Stimulus levels were $L_1, L_2 = 65, 55$ dB SPL (left) and $L_1, L_2 = 55, 65$ dB SPL (right).

and Kemp (2000) that the phase change of the reflection component is zero for constant f_{dp} can be translated to $\beta = \arctan\left(\frac{n}{n+1}\right)$, which, by equation 6.14, results in $D_2/D_1 = 1$.

6.5.3 Group delays

In this and many other studies the term group delay is used for DPOAE phase slope delays. These delays are not true time delays, since the DPOAE phase also depends on the behavior of the generation place during the sweep paradigm and on interference of several components in the cochlea. As a result, DPOAE phase slope delays can even be zero or negative under certain experimental conditions.

In line with earlier reports (chapter 2; chapter 3; Schoonhoven *et al.*, 2001) we concentrated our analysis not on D_1 and D_2 as such, but rather on their ratio D_2/D_1 (figures 6.7B and 6.8) and on $D_{12|R}$ (figure 6.7A) as quantities that potentially distinguish between different DPOAE generation mechanisms. It should be noticed that, for each (f_1, f_2) com-

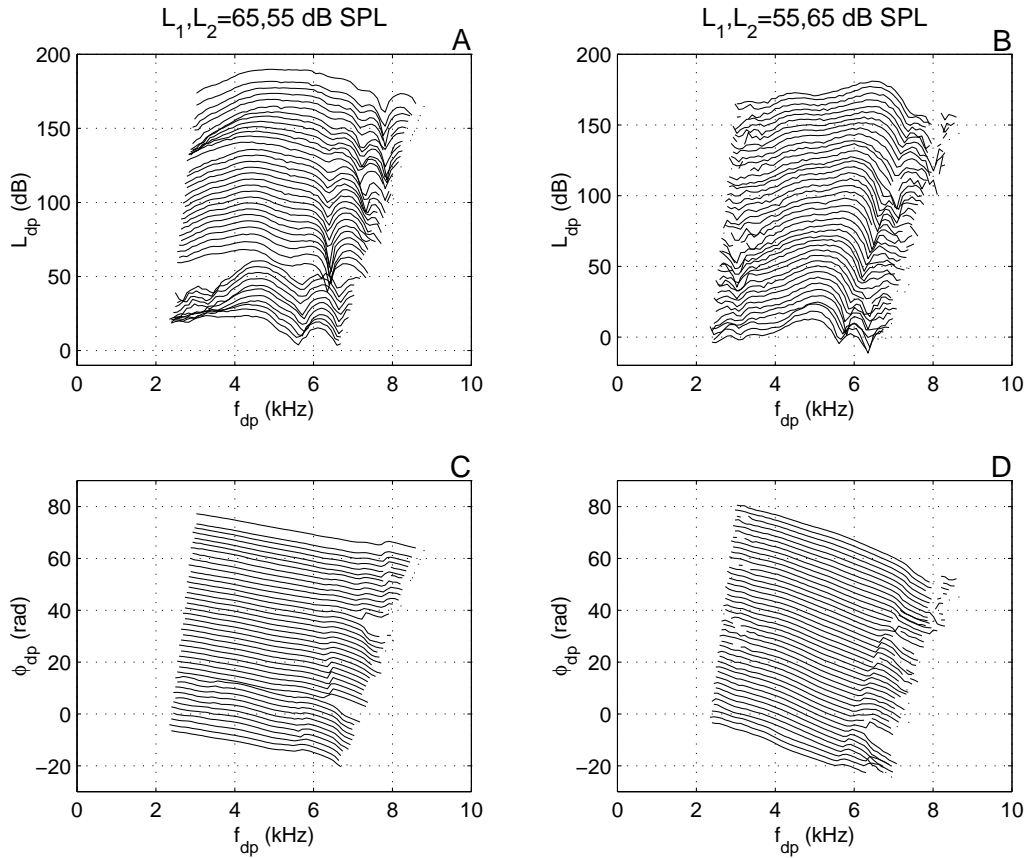


Figure 6.10: Similar to figure 6.9, but now for GP70.

bination, only conclusions about the dominant DPOAE component are obtained, unlike the analysis of Knight and Kemp (2001) in which the two components were separated through a frequency domain analysis and inverse Fourier transforms. From the theoretical analysis, $D_{12|R} = 0$ for the distortion component with the wave-fixed character. In figure 6.7A this property is observed for the $2f_1 - f_2$ DPOAE for f_2/f_1 ratios from about 1.20 to 1.35, from a rough visual estimation. This range is slightly narrower than the 1.1–1.35 range reported for humans by Knight and Kemp (2001), though the statistical significance of the data in figure 6.7A may not be unequivocal. Similar conclusions can be drawn in a different way from figure 6.7B, which shows that the D_2/D_1 ratio follows the theoretical wave-fixed relation for f_2/f_1 from 1.20 to 1.35. For the smaller f_2/f_1 ratios D_2/D_1 approaches a value of one, the prediction for the reflection component, and towards higher f_2/f_1 ratios D_2/D_1 becomes larger than the prediction for the wave-fixed model, corresponding to $D_{12|R} < 0$ in figure 6.7A. The uncertainties in $D_{12|R}$ and D_2/D_1 , based on the uncertainties in the phase slopes with the criterion of a correlation coefficient > 0.988 , are in the order of 0.2 ms and 14% respectively, which is much smaller than the variability in the data of figures 6.7A and 6.7B. From this we conclude that the scatter in figures 6.7A and 6.7B is of biological origin.

To allow for more statistically solid conclusions, mean D_2/D_1 is plotted in figure 6.8

together with twice the standard errors, not only for $2f_1 - f_2$ but also for the other LSB and USB components, and for both combinations of primary levels. From figure 6.8A follows that the range over which the $2f_1 - f_2$ data at $L_1, L_2 = 65, 55$ dB SPL follow the wave-fixed model in the strict sense of a 95% confidence interval is actually quite small, with f_2/f_1 from 1.19 to 1.27. For the higher order DPOAEs similar conclusions can be drawn, i.e. D_2/D_1 following the wave-fixed prediction for an intermediate range of primary frequency ratios, with D_2/D_1 smaller for lower, and larger for higher f_2/f_1 (figure 6.8C,E); note that the associated range of f_2/f_1 ratios shifts to lower values which is directly related to the observation that DPOAE characteristics at different orders line up with f_{dp} i.e. at increasingly smaller f_2/f_1 ratios for the higher order component (chapter 5; Talmadge *et al.*, 1998). When considering the $L_1, L_2 = 55, 65$ condition (figure 6.8B,D,F) similar observations are made, the most notable difference being that the wave-fixed prediction is followed to f_2/f_1 ratios as high as about 1.35 for the $2f_1 - f_2$ component, and associated high ratios for the $3f_1 - 2f_2$ component. So the range of frequency ratios where the distortion component dominates the DPOAE is different with these stimulus levels. A possible explanation could be that the frequency ratio where the dominance of the distortion component changes into dominance of the reflection component depends on the overlap of the excitation patterns of f_1 and f_2 on the basilar membrane. That overlap is quite different with stimulus levels $L_1, L_2 = 55, 65$ dB SPL, which could explain that the change from wave-fixed (distortion component dominant) to place-fixed (reflection component dominant) occurs at a different f_2/f_1 . Once again, the behavior of the $2f_2 - f_1$ USB component in its D_2/D_1 ratio is different from the LSB components (figure 6.8G,H): D_2/D_1 takes a value of about one, independent of f_2/f_1 , and never follows the wave-fixed prediction (see section 6.2.2). These findings suggest that the USB DPOAE is not ruled by the distortion component, corresponding to the results of Knight and Kemp (2000) in humans.

6.5.4 Fine structure

Unlike prior statements (Brown and Gaskill, 1990) guinea pigs do exhibit fine structure. Note that in the guinea pig the modulations in amplitude are rather coarse, compared with the fine structure in human subjects. Fine structure is considered to be the result of interference of at least two DPOAE components, a nonlinear distortion component from the X_2 place and a linear reflection component from the X_{dp} place (Talmadge *et al.*, 1998;1999). As reported in earlier human studies, the patterns in phase and amplitude are correlated; abrupt changes in amplitude often coincide with jumps in the phase spectrum, which is considered an indicator of interference between the two different contributing sources (Talmadge *et al.*, 1998;1999; Mauermann *et al.*, 1999). In the present study, such covarying patterns were found to have several alignment modes: with f_{dp} (figure 6.9A,B and figure 6.10A), with f_2/f_1 (figure 6.10B) and other directions (figure 6.9B). Alignment with f_{dp} has been predicted and measured before (Talmadge *et al.* 1998;1999; Mauermann *et al.*, 1999). The relative phase difference between the two components contributing to the DPOAE in the ear canal mainly depends on f_{dp} through the fast rotating phase of the reflection component, which gives rise to a fine structure that is aligned with f_{dp} . We can

not yet give such a simple interpretation for the other observed alignment modes.

References

- Brown, A. M., and Gaskill, S. A. (1990). "Measurement of acoustic distortion reveals underlying similarities between human and rodent mechanical responses," J. Acoust. Soc. Am. **88**, 840–849.
- Brown, A. M., Harris, F. P., and Beveridge, H. A. (1996). "Two sources of acoustic distortion products from the human cochlea," J. Acoust. Soc. Am. **100**, 3260–3267.
- Fahey, P. F., and Allen, J. B. (1997). "Measurement of distortion product phase in the ear canal of the cat," J. Acoust. Soc. Am. **102**, 2880–2891.
- Heitmann, J., Waldmann, B., Schnitzler, H.-U., Plinkert, P. K., and Zenner, H.-P. (1998). "Suppression of distortion product otoacoustic emissions (DPOAE) near $2f_1 - f_2$ removes DP-gram fine structure—Evidence for a secondary generator," J. Acoust. Soc. Am. **103**, 1527–1531.
- Kalluri, R., and Shera, C. A. (2001). "Distortion-product source unmixing: A test of the two-mechanism model for DPOAE generation," J. Acoust. Soc. Am. **109**, 622–637.
- Kemp, D. T. (1979). "Evidence of mechanical nonlinearity and frequency selective wave amplification in the cochlea," Arch. Otorhinolaryngol. **224**, 37–45.
- Kemp, D. T. (1986). "Otoacoustic emissions, travelling waves and cochlear mechanisms," Hear. Res. **22**, 95–104.
- Kim, D. O. (1980). "Cochlear mechanics: implications of electrophysiological and acoustical observations," Hear. Res. **2**, 297–317.
- Kimberley, B. P., Brown, D. K., and Eggermont, J. J. (1993). "Measuring human cochlear traveling wave delay using distortion product otoacoustic emission phase responses," J. Acoust. Soc. Am. **94**, 1343–1350.
- Knight, R. D., and Kemp, D. T. (1999). "Relationships between DPOAE and TEOAE amplitude and phase characteristics," J. Acoust. Soc. Am. **106**, 1420–1435.
- Knight, R. D., and Kemp, D. T. (2000). "Indications of different distortion product otoacoustic emission mechanisms from a detailed f_1 , f_2 area study," J. Acoust. Soc. Am. **107**, 457–473.

- Knight, R. D., and Kemp, D. T. (2001). “Wave and place fixed DPOAE maps of the human ear,” *J. Acoust. Soc. Am.* **109**, 1513–1525.
- Kummer, P., Janssen, T., and Arnold, W. (1995). “Suppression tuning characteristics of the $2f_1 - f_2$ distortion product otoacoustic emission in humans,” *J. Acoust. Soc. Am.* **98**, 197–210.
- Kummer, P., Janssen, T., Hulin, P., and Arnold, W. (2000). “Optimal $L_1 - L_2$ primary tone level separation remains independent of test frequency in humans,” *Hear. Res.* **146**, 47–56.
- Martin, G. K., Jassir, D., Stagner, B. B., Whitehead, M. L., and Lonsbury-Martin, B. L. (1998). “Locus of generation for the $2f_1 - f_2$ vs $2f_2 - f_1$ distortion-product otoacoustic emissions in normal-hearing humans revealed by suppression tuning, onset latencies, and amplitude correlations,” *J. Acoust. Soc. Am.* **103**, 1957–1971.
- Martin, G. K., Lonsbury-Martin, B. L., Probst, R., Scheinin, S. A., and Coats, A. C. (1987). “Acoustic distortion products in rabbit ear canal. II. Sites of origin revealed by suppression contours and pure-tone exposures,” *Hear. Res.* **28**, 191–208.
- Mauermann, M., Uppenkamp, S., van Hengel, P. W. J., and Kollmeier, B. (1999). “Evidence for the distortion product frequency place as a source of distortion product otoacoustic emission (DPOAE) fine structure in humans. I. Fine structure and higher-order DPOAE as a function of the frequency ratio f_2/f_1 ,” *J. Acoust. Soc. Am.* **106**, 3473–3483.
- Moulin, A., and Kemp, D. T. (1996). “Multicomponent acoustic distortion product otoacoustic emission phase in humans. II. Implications for distortion product otoacoustic emissions generation,” *J. Acoust. Soc. Am.* **100**, 1640–1662.
- O’Mahoney, C. F., and Kemp, D. T. (1995). “Distortion product otoacoustic emission delay measurement in human ears,” *J. Acoust. Soc. Am.* **97**, 3721–3735.
- Schneider, S., Prijs, V. F., Schoonhoven, R., and van Hengel, P. W. J. (2000). “ f_1 - versus f_2 -sweep group delays of distortion product otoacoustic emissions in the guinea pig; experimental results and theoretical predictions,” in *Recent Developments in Auditory Mechanics*, edited by H. Wada, T. Takasaka, K. Ikeda, K. Ohyama, and T. Koike (World Scientific, Singapore), pp. 360–366.
- Schoonhoven, R., Prijs, V. F., and Schneider, S. (2001). “DPOAE group delays versus electrophysiological measures of cochlear delay in normal human ears,” *J. Acoust. Soc. Am.* **109**, 1503–1512.
- Shera, C. A., and Guinan, J. J. (1999). “Evoked otoacoustic emissions arise by two fundamentally different mechanisms: A taxonomy for mammalian OAEs,” *J. Acoust. Soc. Am.* **105**, 782–798.

- Shera, C. A., Talmadge, C. L., and Tubis, A. (2000). “Interrelations among distortion-product phase-gradient delays: Their connection to scaling symmetry and its breaking,” *J. Acoust. Soc. Am.* **108**, 2933-2948.
- Talmadge, C. L., Long, G. R., Tubis, A., and Dhar, S. (1999). “Experimental confirmation of the two-source interference model for the fine structure of distortion product otoacoustic emissions,” *J. Acoust. Soc. Am.* **105**, 275–292.
- Talmadge, C. L., Tubis, A., Long, G. R., and Piskorski, P. (1998). “Modeling otoacoustic emission and hearing threshold fine structure,” *J. Acoust. Soc. Am.* **104**, 1517–1543.
- Talmadge, C. L., Tubis, A., Tong, C., Long, G. R., and Dhar, S. (2000). “Temporal aspects of otoacoustic emissions,” in *Recent Developments in Auditory Mechanics*, edited by H. Wada, T. Takasaka, K. Ikeda, K. Ohyama, and T. Koike (World Scientific, Singapore), pp. 353–359.
- Tubis, A., Talmadge, C. L., Tong, C., and Dhar, S. (2000). “On the relationships between the fixed- f_1 , fixed- f_2 , and fixed-ratio phase derivatives of the $2f_1 - f_2$ distortion product otoacoustic emission,” *J. Acoust. Soc. Am.* **108**, 1772–1785.

Summary

Amplitude and phase characteristics of distortion product otoacoustic emissions

In the late seventies the first experimental proof was given that the ear not only receives and processes, but also produces sounds. With a sensitive microphone in the ear canal, tones which were termed otoacoustic emissions (OAEs), after the Greek word *οτο* which means ear, could be detected both spontaneously and after stimulation. One type of OAE is the distortion product otoacoustic emission (DPOAE) which is generated in the healthy inner ear (cochlea) upon stimulation with two tones of different frequencies f_1 and f_2 ($f_1 < f_2$). Other than in the ear canal, distortion products can also be detected psychophysically and in neural recordings.

The cochlea, a coiled fluid filled tube with many specialized structures, is the sensory part of the peripheral auditory system where the conversion of mechanical energy to electrical energy takes place. It is divided in compartments, separated by the basilar membrane. Upon sinusoidal stimulation the pressure differences above and below the basilar membrane result in a movement of the basilar membrane, which can be described as a traveling wave propagating from the base of the cochlea towards the apex. The place where the maximum basilar membrane excitation is, called the characteristic place, depends on the frequency of the tone. High frequencies have their characteristic place near the base of the cochlea while the characteristic place of a lower frequency is located more apically. The excitation patterns of the basilar membrane can be influenced by outer hair cells which are located in the organ of Corti on the basilar membrane. These OHCs act as tiny motors, which can add energy to the movement of the basilar membrane. This active mechanism is nonlinear and therefore causes the generation of cochlear mechanical distortion products which can be detected in the ear canal as DPOAEs. When the ear is stimulated with two sinusoidal tones of frequencies f_1 and f_2 , the distortion products have frequencies $f_{dp} = (n+1)f_1 - nf_2$. The emission with frequency $2f_1 - f_2$ usually is the strongest. The same mechanism that is responsible for the DPOAEs is indispensable for the proper functioning of the inner ear.

DPOAE amplitudes of people with a cochlear hearing deficit are generally lower than those of normal hearing subjects or even absent, and therefore DPOAEs can be useful to gather information about inner ear damage through objective measurement.

The aim of the research project, the results of which are presented in this thesis, was to increase the knowledge of the peripheral auditory mechanisms involved in the generation of DPOAEs. This goal was pursued by studying the amplitude and phase behavior of DPOAEs both experimentally and theoretically.

For a better understanding of cochlear mechanics and for the interpretation of clinical DPOAE results it is important to know which frequency regions in the cochlea are involved in the generation process of DPOAEs. The distortion products with frequencies lower than those of the stimulus tones (the so-called lower sideband DPOAEs, e.g. $2f_1 - f_2$) are generated in the region where the excitation profiles of the stimuli have the largest overlap, near the characteristic place of the frequency f_2 . These distortion products, however, give a response at their own characteristic place, apical from the generation region, which also contributes to the DPOAE in the ear canal. There are indications that the distortion products with frequencies higher than those of the stimuli (the basal or upper sideband DPOAEs, e.g. $2f_2 - f_1$) are mostly generated in a region basal from the characteristic places of the stimulus frequencies.

Studying cochlear delays is a way to gather more information about generation places of the DPOAEs. A commonly used method is the phase-gradient method, in which the DPOAE frequency is slightly changed in successive measurements, either with varying f_1 and fixed f_2 or with varying f_2 and fixed f_1 frequency (the f_1 -sweep and the f_2 -sweep paradigm, respectively). This results in a phase-frequency curve that is approximately linear for small frequency changes. The slope of this curve, generally called the group delay, is an estimate of the traveling wave delay of the stimulus tones to the generation place plus the traveling wave delay of the distortion product from the generation place back to the ear canal. There appears to be a difference between group delays measured with the f_1 -sweep paradigm and group delays measured with the f_2 -sweep paradigm. At the beginning of this research project, there was no proper explanation for this observation.

Chapter 1 of this thesis provides background information on the anatomy of the ear and the mechanics of the inner ear, as well as an introduction on distortion product otoacoustic emissions and an explanation of the principle of group delay.

In chapter 2 an extensive experimental study on DPOAE group delays in the guinea pig is described. The differences between group delays measured with the f_1 -sweep and the f_2 -sweep paradigm are examined, as well as the differences in group delays between the DPOAEs $2f_1 - f_2$, $3f_1 - 2f_2$, $4f_1 - 3f_2$, and $2f_2 - f_1$. It appears that the f_2 -sweep group delays are larger than the f_1 -sweep group delays, but only for the lower sideband DPOAEs (with $f_{dp} < f_1, f_2$). For the upper sideband DPOAE $2f_2 - f_1$ no significant difference was found between the two paradigms, except for the highest and lowest f_2 -frequencies. Comparing the group delays of the different DPOAEs shows that all four examined distortion products have the same group delays when measured with f_1 -sweep. With the f_2 -sweep paradigm, however, the delays of the lower sideband DPOAEs are larger and in addition dependent on the order of the distortion product.

In chapter 3 a theoretical analysis of DPOAE group delays is presented, designed to explain the experimentally found differences between f_1 - and f_2 -sweep and the dependence on the DPOAE order. Two models for DPOAE generation are elaborated, the place-fixed and the wave-fixed model. In the first model the assumption is made that the generation place is fixed for small frequency changes. In the second model the shifting of the presumed generation place X_2 in the f_2 -sweep paradigm is accounted for. The use of a local approximation of the scaling symmetry of the cochlea enables a mathematical conversion of phase-place to phase-frequency gradients in the wave-fixed model. Under the assumption that the DPOAE (determined at the optimal frequency ratio f_2/f_1) is dominated by the contribution of the generation place and not by e.g. reflection components, the analysis results in a simple analytical expression for the relation between f_1 - and f_2 -sweep group delays which can be compared directly with the experimental results. Validation of the models against experimental data from chapter 2 indicates that the results of the lower sideband DPOAEs ($2f_1 - f_2$, $3f_1 - 2f_2$, and $4f_1 - 3f_2$) are most consistent with the wave-fixed model of DPOAE generation. The difference between the group delays obtained with f_1 - and f_2 -sweeps could be fully explained by the shift of the X_2 generation site in the f_2 -sweep paradigm. The results of the upper sideband DPOAE $2f_2 - f_1$ fit neither the place-fixed nor the wave-fixed model.

The research project described in this thesis was part of a collaboration with the Department of Biophysics of the University of Groningen, where a nonlinear mathematical cochlea model was developed in the past. This model was used to simulate the DPOAE experiments in the guinea pig as described in chapter 2. The results of these simulations are given in chapter 4, where they are compared with the experimental data and with the results of the wave-fixed model for DPOAE generation of chapter 3. The lower sideband DPOAEs generated by the cochlea model have group delays that match the experimental data reasonably close, both qualitatively and quantitatively. Features seen in the experimental results are reproduced by the model. Group delay values decrease with increasing f_2 ; f_1 -sweep group delays are equal for all four DPOAE orders; f_2 -sweep group delays are larger than f_1 -sweep group delays; and f_2 -sweep group delays are larger with smaller DPOAE order. The ratio of simulated f_2 - and f_1 -sweep group delays is in accordance with the experimental results and the theoretical wave-fixed prediction. The cochlea model is unable to reproduce the experimental results for the upper sideband DPOAE $2f_2 - f_1$.

Besides on cochlear status, DPOAE amplitude depends on stimulus parameters like the frequency ratio f_2/f_1 . In chapter 5 several properties concerning the amplitude of DPOAEs measured in the guinea pig are described. The amplitude versus frequency functions of the lower sideband DPOAEs show a bandpass shape. The frequency ratio yielding the maximum DPOAE amplitude is measured, which shows a pattern as a function of f_2 different from that known in humans and several other species. Especially at an f_2 of approximately 4 kHz the optimum frequency ratio is very large in the guinea pig. The width of the amplitude versus frequency functions is studied as well as the alignment of the maxima of the three different lower sideband DPOAEs $2f_1 - f_2$, $3f_1 - 2f_2$ and $4f_1 - 3f_2$. Differences in these features between DPOAE order and between the two sweep paradigms show that the DPOAE amplitude is best described as a function of f_{dp}/f_2 .

Chapter 6 reports on a detailed two-dimensional DPOAE study exploring the (f_1, f_2) plane. At many combinations of f_1 and f_2 the amplitude and phase of several distortion products were measured in the guinea pig, creating amplitude and phase maps. Phase-frequency slopes in the directions of fixed f_1 , fixed f_2 , and fixed f_2/f_1 were calculated for all (f_1, f_2) combinations, representing the f_2 -sweep group delay, f_1 -sweep group delay, and constant f_2/f_1 -sweep group delay. Comparing these experimental delay values with the predictions from the place- and wave-fixed theories, both directly and by considering the ratio of f_1 - and f_2 -sweep group delays, we are able to determine at which frequency ratios (or distance between the stimulus tone characteristic places) the phase behavior of the DPOAE is wave-fixed. For the lower sideband DPOAEs this appears to be the case at intermediate frequency ratios (around 1.2–1.3 for the $2f_1 - f_2$ DPOAE). In those cases the DPOAE component arising directly from the generation region near X_2 is dominant. This is important for the interpretation of clinical DPOAE data, which are generally measured at these intermediate frequency ratios. At frequency ratios close to one the place-fixed reflection component from the DP resonance region is dominant. At high ratios the behavior cannot be explained by dominance of either component.

Summarizing, this research project has resulted in the almost full understanding of lower sideband DPOAE generation. The combination of experimental and theoretical investigation of DPOAE phase has led to insight in the frequency ratios at which the DPOAE is dominated by the wave-fixed component, generated around place X_2 , and the frequency ratios at which the place-fixed component (coming from place X_{dp}) is dominant. We know the relations between the different group delays and can fully explain the difference between f_1 -sweep and f_2 -sweep group delay, measured at the optimum ratio. Furthermore, from studying the amplitude characteristics of the lower sideband DPOAEs we could conclude that DPOAE amplitude is best described as a function of f_{dp}/f_2 , or the distance between the generation site X_2 and the reflection site X_{dp} in the cochlea.

At the end of this project, several questions are left unanswered. The puzzling fact we discovered during the experiments described in chapter 5, the increased optimum frequency ratio in the 4 kHz region of the guinea pig cochlea, remains unexplained. Also, the behavior of the upper sideband DPOAE $2f_2 - f_1$, which is different from the lower sideband DPOAEs in many respects, still cannot be explained satisfactorily. Hopefully the amplitude and phase characteristics of $2f_2 - f_1$ given in this thesis will contribute in the future to the final understanding of the generation and propagation of upper sideband distortion products.

Samenvatting

Amplitude en fase kenmerken van distorsie product otoakoestische emissies

Eind jaren 70 werd voor het eerst in experimenten aangetoond dat het oor niet alleen geluiden ontvangt en verwerkt, maar ook produceert. Met een gevoelig microfoontje in de gehoorgang konden zowel spontaan als na stimulatie tonen worden gedetecteerd die men otoakoestische emissies (OAEs) noemde, naar het Griekse woord *οτο* dat oor betekent. Eén type OAE is de distorsie product otoakoestische emissie (DPOAE), die in een gezond binnenoor (cochlea) gegenereerd wordt wanneer men dit stimuleert met twee tonen met verschillende frequenties f_1 en f_2 ($f_1 < f_2$). Behalve in de gehoorgang, kunnen distorsie producten ook psychofysisch en neuraal gedetecteerd worden.

De cochlea, een opgerolde met vloeistof gevulde buis met daarin vele gespecialiseerde structuren, is het sensorische deel van het perifere auditief systeem waar de conversie van mechanische energie naar elektrische energie plaatsvindt. De cochlea is verdeeld in compartimenten die gescheiden zijn door het basilaire membraan. In respons op sinusoidale stimulatie zorgen de drukverschillen boven en onder het basilaire membraan voor een beweging van dit membraan, die beschreven kan worden als een lopende golf die zich voortplant van de basis van de cochlea richting de apex. De plaats waar de maximale excitatie van het basilaire membraan wordt bereikt noemt men de karakteristieke plaats, en die is afhankelijk van de frequentie. Hoge frequenties hebben hun karakteristieke plaats dicht bij de basis van de cochlea, terwijl de karakteristieke plaats van een lagere frequentie meer apicaal gelegen is. De excitatieprofielen van het basilaire membraan kunnen beïnvloed worden door de buitenste haarcellen (OHCs) die zich in het orgaan van Corti op het basilaire membraan bevinden. Deze OHCs fungeren als kleine motortjes, die energie kunnen toevoegen aan de beweging van het basilaire membraan. Dit actieve mechanisme is bovendien niet-lineair waardoor het de generatie van distorsie producten veroorzaakt die gedetecteerd kunnen worden in de gehoorgang als DPOAEs. Wanneer het oor gestimuleerd wordt met twee sinusoidale tonen met frequenties f_1 en f_2 hebben de distorsie producten frequenties

$f_{dp} = (n+1)f_1 - nf_2$. De emissie met frequentie $2f_1 - f_2$ is doorgaans de sterkste. Hetzelfde mechanisme dat de DPOAEs veroorzaakt is onmisbaar voor het goed functioneren van het binnenoor. De DPOAE amplitudes van mensen met een cochleaire gehoorafwijking zijn in het algemeen lager dan die van normaal horenden of zelfs afwezig, waardoor DPOAEs bruikbaar kunnen zijn om via een objectieve meting informatie te verkrijgen over eventuele beschadigingen van het binnenoor.

Het doel van het onderzoeksproject waarvan de resultaten in dit proefschrift beschreven staan, was het vergroten van de kennis van de perifere auditieve mechanismen die betrokken zijn bij de generatie van DPOAEs. Daartoe zijn het amplitude- en het fasegedrag van DPOAEs zowel experimenteel als theoretisch bestudeerd.

Voor een beter begrip van de cochleaire mechanica en voor de interpretatie van klinische DPOAE resultaten is het belangrijk te weten welke frequentiegebieden in de cochlea een rol spelen in het generatieproces van DPOAEs. De distorsie producten met frequenties die lager zijn dan die van de stimulustonen (de zogenaamde *lower sideband* DPOAEs, bijvoorbeeld $2f_1 - f_2$) worden gegenereerd in het gebied waar de excitatieprofielen van de stimuli de grootste overlap hebben, in de buurt van de karakteristieke plaats van de frequentie f_2 . Deze distorsie producten geven echter ook een respons op hun eigen karakteristieke plaats, apicaal gelegen ten opzichte van het generatiegebied, die eveneens een bijdrage levert aan de DPOAE in de gehoorgang. *Lower sideband* DPOAEs worden daarom ook wel apicale DPOAEs genoemd. Er zijn aanwijzingen dat de distorsie producten met frequenties hoger dan die van de stimuli (de basale of *upper sideband* DPOAEs, bijvoorbeeld $2f_2 - f_1$) voornamelijk worden gegenereerd in een gebied basaal ten opzichte van de karakteristieke plaatsen van de stimulusfrequenties.

Het bestuderen van cochleaire *delays* is een manier om meer informatie over generatieplaatsen van de DPOAEs te vergaren. Een veel gebruikte methode is de fase-gradiënt methode, waarbij de DPOAE frequentie in opeenvolgende metingen steeds een beetje gevarieerd wordt met een variërende f_1 en vaste f_2 of een variërende f_2 en vaste f_1 frequentie (respectievelijk het f_1 -sweep en het f_2 -sweep paradigma). Dit resulteert in een fase-frequentie curve, die bij benadering lineair is voor kleine frequentieveranderingen. De helling van deze curve, vaak de *group delay* genoemd, geeft een schatting van de looptijd van de stimulustonen van gehoorgang naar de generatieplaats plus de looptijd van het distorsie product van generatieplaats terug naar de gehoorgang. Er blijkt een verschil te zijn tussen *group delays* gemeten met het f_1 -sweep paradigma en *group delays* gemeten met het f_2 -sweep paradigma. Bij aanvang van dit onderzoeksproject bestond hiervoor nog geen goede verklaring.

Hoofdstuk 1 van dit proefschrift geeft achtergrondinformatie over de anatomie van het oor en de mechanica van het binnenoor, evenals een inleiding over distorsie product otoakoestische emissies en uitleg over het principe van de grootte *group delay*.

In hoofdstuk 2 van dit proefschrift is een uitgebreid experimenteel onderzoek naar *group delays* van DPOAEs in de cavia beschreven. De verschillen tussen *group delays* gemeten met het f_1 -sweep en het f_2 -sweep paradigma zijn onderzocht, alsmede de verschillen in *group delay* tussen de DPOAEs $2f_1 - f_2$, $3f_1 - 2f_2$, $4f_1 - 3f_2$ en $2f_2 - f_1$. Het blijkt dat de f_2 -sweep *group delays* groter zijn dan de f_1 -sweep *group delays*, maar alleen voor de apicale

DPOAEs (met $f_{dp} < f_1, f_2$). Voor de basale DPOAE $2f_2 - f_1$ is geen significant verschil gevonden tussen de twee paradigma's, behalve voor de hoogste en laagste f_2 -frequenties. Bij het vergelijken van de *group delays* van de verschillende DPOAEs blijkt dat alle vier de onderzochte distorsie producten gelijke *group delays* hebben wanneer deze met f_1 -sweep worden gemeten. Met het f_2 -sweep paradigma echter, zijn de *delays* van de apicale DPOAEs groter en bovendien afhankelijk van de orde van het distorsie product.

In hoofdstuk 3 is een theoretische analyse gepresenteerd van DPOAE *group delays*, met als doel de experimenteel gevonden verschillen tussen f_1 - en f_2 -sweep en de afhankelijkheid van de DPOAE orde te verklaren. Twee modellen voor DPOAE generatie zijn uitgewerkt, het *place-fixed* en het *wave-fixed* model. In het eerste model wordt aangenomen dat de plaats van generatie vast is voor kleine frequentie veranderingen. In het tweede model is rekening gehouden met de verschuiving van de veronderstelde generatieplaats X_2 in het f_2 -sweep paradigma. Door een lokale benadering van de schalingssymmetrie van de cochlea te gebruiken, is een mathematische conversie van fase-plaats naar fase-frequentie gradiënten in het *wave-fixed* model mogelijk. Onder de aanname dat de DPOAE (bepaald bij de optimale frequentie verhouding f_2/f_1) gedomineerd wordt door de bijdrage van de generatieplaats en niet door bijvoorbeeld reflectiecomponenten, leidt de analyse tot een eenvoudige uitdrukking voor de verhouding tussen de f_1 - en f_2 -sweep *group delays* die direct vergeleken kan worden met de experimentele resultaten. Validatie van de modellen met de experimentele data uit hoofdstuk 2 geeft aan dat de resultaten van de apicale DPOAEs ($2f_1 - f_2$, $3f_1 - 2f_2$ en $4f_1 - 3f_2$) het meest consistent zijn met het *wave-fixed* model van DPOAE generatie. Het verschil tussen de *group delays* verkregen met f_1 - en f_2 -sweeps wordt volledig verklaard door het verschuiven van de X_2 generatieplaats in het f_2 -sweep paradigma. De resultaten van de basale DPOAE $2f_2 - f_1$ komen met geen van beide modellen, *place*- of *wave-fixed*, goed overeen.

Het onderzoeksproject beschreven in dit proefschrift maakt deel uit van een samenwerkingsverband met de afdeling Biofysica van de Universiteit van Groningen, waar in het verleden een niet-lineair mathematisch cochlea model is ontwikkeld. Dit model is gebruikt om de DPOAE experimenten in de cavia zoals beschreven in hoofdstuk 2 te simuleren. De resultaten van deze simulaties worden in hoofdstuk 4 gegeven, waar ze vergeleken worden met de experimentele data en met de resultaten van het *wave-fixed* model voor DPOAE generatie uit hoofdstuk 3. De door het cochlea model gegenereerde apicale DPOAEs hebben *group delays* die zowel kwalitatief als kwantitatief redelijk goed overeenkomen met de experimentele data. Verschillende kenmerken van de experimentele resultaten worden gereproduceerd door het model. De *group delay* waarden nemen af met toenemende f_2 ; de f_1 -sweep *group delays* zijn gelijk voor alle vier de DPOAEs; de f_2 -sweep *group delays* zijn groter dan de f_1 -sweep *group delays*; en de f_2 -sweep *group delays* zijn groter voor kleinere DPOAE orde. De verhouding van f_2 - en f_1 -sweep *group delays* komt overeen met de experimentele resultaten en de theoretische *wave-fixed* voorspelling. Het cochlea model is niet in staat de experimentele resultaten voor de basale DPOAE $2f_2 - f_1$ te reproduceren.

Behalve van de status van de cochlea hangt de DPOAE amplitude ook af van stimulusparameters zoals de frequentieverhouding f_2/f_1 . In hoofdstuk 5 worden een aantal eigenschappen met betrekking tot de amplitude van cavia DPOAEs beschreven. De amplitude-

frequentie functies van de apicale DPOAEs hebben een *bandpass* vorm. De verhouding van de stimulusfrequenties f_2/f_1 waarbij de DPOAE amplitude maximaal is is bepaald. Deze verhouding als functie van f_2 blijkt bij de cavia een ander patroon te hebben dan bij de mens. Vooral bij een f_2 van ongeveer 4 kHz is de optimale frequentieverhouding bij de cavia erg groot. De breedte van de amplitude-frequentie functies is bestudeerd, alsmede de oplijning van de maxima van de drie verschillende apicale DPOAEs $2f_1 - f_2$, $3f_1 - 2f_2$ en $4f_1 - 3f_2$. De verschillen in deze eigenschappen tussen de DPOAE componenten en tussen de twee *sweep* paradigma's geven aan dat de DPOAE amplitude het best beschreven kan worden als functie van f_{dp}/f_2 .

Hoofdstuk 6 beschrijft een gedetailleerde twee-dimensionale DPOAE studie in het (f_1, f_2) vlak. Bij vele combinaties van f_1 en f_2 zijn de amplitude en fase van verschillende distorsie producten gemeten in de cavia. Fase-frequentie hellingen in de richting van constante f_1 , constante f_2 en constante f_2/f_1 zijn bepaald voor alle (f_1, f_2) combinaties, waaruit de *group delays* volgen die overeenkomen met respectievelijk *f₂-sweep*, *f₁-sweep* en constante f_2/f_1 . Deze experimentele delay waarden zijn vergeleken met de voorspellingen uit de *place*- en *wave-fixed* theorieën, waardoor we in staat zijn te bepalen bij welke frequentie verhoudingen (of afstand tussen de karakteristieke plaatsen van de stimulustonen) het fase-gedrag van de DPOAE *wave-fixed* is. Voor de apicale DPOAE blijkt dit zo te zijn bij de middelste frequentieverhoudingen (rond 1.2–1.3 voor de $2f_1 - f_2$ DPOAE). In die gevallen is de bijdrage aan de DPOAE die rechtstreeks van het generatiegebied rond X_2 komt dominant. Dit is belangrijk voor de interpretatie van klinische DPOAE data, die gewoonlijk gemeten worden bij deze middelste frequentieverhoudingen. Voor frequentieverhoudingen in de buurt van één is de *place-fixed* reflectiecomponent afkomstig van de DP resonantieplaats dominant. Bij grote verhoudingen kan het gedrag niet verklaard worden door dominantie van één van beide componenten.

Samenvattend, heeft dit onderzoeksproject een bijna volledig begrip van *lower sideband* DPOAE generatie opgeleverd. De combinatie van experimenteel en theoretisch onderzoek naar de DPOAE fase heeft geleid tot inzicht in de frequentieverhoudingen waarbij de DPOAE gedomineerd wordt door de *wave-fixed* component, gegenereerd rond de X_2 plaats, en de frequentieverhoudingen waarbij de *place-fixed* component (van de X_{dp} plaats) dominant is. We kennen de relaties tussen de verschillende *group delays* en kunnen het verschil tussen *f₁-sweep* en *f₂-sweep group delays*, gemeten bij de optimale frequentieverhouding, volledig verklaren. Daarnaast kon uit onderzoek naar de amplitudekarakteristieken van de *lower sideband* DPOAEs geconcludeerd worden dat DPOAE amplitude het best beschreven kan worden als functie van f_{dp}/f_2 , ofwel de afstand tussen de generatieplaats X_2 en de reflectieplaats X_{dp} in de cochlea.

Aan het eind van dit project, blijven een aantal vragen onbeantwoord. Het raadselachtige feit dat we ontdekten tijdens de experimenten die beschreven staan in hoofdstuk 5, de verhoogde optimale stimulusfrequentieverhouding in het 4 kHz gebied in de cavia cochlea, blijft onverklaard. Daarnaast kan het gedrag van de basale DPOAE $2f_2 - f_1$, dat in vele opzichten verschilt van dat van de apicale DPOAEs, nog steeds niet bevredigend verklaard worden. Hopelijk zullen de amplitude- en fasekenmerken van $2f_2 - f_1$ die te vinden zijn in dit proefschrift in de toekomst bijdragen aan het begrip van de generatie en

voortplanting van basale distorsie producten.

Curriculum Vitae

Op 17 maart 1972 ben ik geboren te Tilburg. Na het behalen van het VWO-diploma aan het Maurick-college te Vught, begon ik in 1990 met de studie natuurkunde aan de Katholieke Universiteit Nijmegen. Naast mijn studie gaf ik bijles wiskunde aan middelbare scholieren en was ik docent exacte vakken op een huiswerkbegeleidingsinstituut. In september 1994 begon ik met mijn afstudeerstage in de vakgroep Medische- en Biofysica, begeleid door Bart Melis en Jan van Gisbergen. Het onderzoek betrof oogbewegingen in drie dimensies. De wet van Listing, welke de 3D oogbewegingen beschrijft, werd bestudeerd in een aantal verschillende situaties. Mijn afstudeerscriptie getiteld 'Modifications of Listing's law' was het resultaat van dit onderzoek. De laatste anderhalf jaar van mijn studie was ik werkzaam als studentassistent bij de practica biofysica en neurofysiologie voor biologiëstudenten, geneeskundestudenten en studenten gezondheidswetenschappen. In januari 1996 behaalde ik het doctoraaldiploma experimentele natuurkunde. Aansluitend trad ik in dienst als onderzoeker in opleiding bij de stichting Aard- en Levenswetenschappen van de Nederlandse Organisatie van Wetenschappelijk Onderzoek (NWO). Mijn promotieonderzoek vond plaats op de afdeling Audiologie van het Leids Universitair Medisch Centrum, onder begeleiding van Vera Prijs en Ruurd Schoonhoven. Het onderzoek was onderdeel van een samenwerkingsprogramma met de afdeling KNO/Audiologie van het Academisch Ziekenhuis in Groningen en de vakgroep Biofysica van de Rijks Universiteit Groningen, getiteld 'Biophysics of otoacoustic emissions and essential nonlinearities of the inner ear'. Het Leidse deelproject betrof met name distorsie product otoakoestische emissies, welke werden gemeten bij cavia's. Op 21 januari 2004 hoop ik te promoveren op de resultaten van het onderzoek, beschreven in dit proefschrift. In januari 2001 begon ik op het IVLOS van de Universiteit Utrecht aan de lerarenopleiding tot eerstegraads docent natuurkunde, en tegelijkertijd kwam ik in dienst van de gemeente Breukelen als natuurkunde docent op RSG Brokdele, waar ik op dit moment nog steeds werk. In december 2001 behaalde ik de eerstegraads lesbevoegdheid voor het vak natuurkunde.

Sandra Schneider, november 2003

Publications

- Group delays of distortion product otoacoustic emissions in the guinea pig.
S. Schneider, V.F. Prijs, and R. Schoonhoven, *J. Acoust. Soc. Am.* **105** (1999) 2722-2730.
- f_1 - versus f_2 -sweep group delays of distortion product otoacoustic emissions in the guinea pig; experimental results and theoretical predictions.
S. Schneider, V.F. Prijs, R. Schoonhoven, and P.W.J. van Hengel, *In: Recent developments in auditory mechanics*, eds. H. Wada, T. Takasaka, K. Ikeda, K. Ohyama, and T. Koike, (2000) 360-366.
- Amplitude of distortion product otoacoustic emissions in the guinea pig in f_1 - and f_2 -sweep paradigms.
S. Schneider, R. Schoonhoven, and V.F. Prijs, *Hearing Research* **155** (2001) 21-31.
- Amplitude and phase of distortion product otoacoustic emissions in the guinea pig in an (f_1, f_2) area study.
S. Schneider, V.F. Prijs, and R. Schoonhoven, *J. Acoust. Soc. Am.* **113** (2003) 3285-3296.
- Group delays of distortion product otoacoustic emissions: Relating delays measured with f_1 - and f_2 -sweep paradigms.
V.F. Prijs, S. Schneider, and R. Schoonhoven, *J. Acoust. Soc. Am.* **107** (2000) 3298-3307.
- DPOAE group delays versus electrophysiological measures of cochlear delay in normal human ears.
R. Schoonhoven, V.F. Prijs, and S. Schneider, *J. Acoust. Soc. Am.* **109** (2001) 1503-1512.

